To the Graduate Council:

I am submitting herewith a thesis written by Lan Huang entitled "Microstructural Evolution of TiAl-Intermetallic Alloys Containing W and B". I have examined the final electronic copy of this thesis for form and content and recommend that it be accepted in partial fulfillment of the requirements for the degree of Master of Science, with a major in Materials Science and Engineering.

Dr. Peter K. Liaw

Major Professor

We have read this thesis
and recommend its acceptance:

Dr. Chain T. Liu

Dr. Raymond A. Buchanan

Accepted for the Council:

Dr. Anne Mayhew

Vice Chancellor and Dean of
Graduate Studies

(Original signatures are on file with official student records)

Microstructural Evolution of TiAl-Intermetallic Alloys Containing W and B

A Thesis
Presented for the
Master of Science Degree
The University of Tennessee

Lan Huang
August 2005

Acknowledgement

I would like to thank many of those who have help, advised, and cared for me during my master-degree study. If it were not because of them, I would not have been able to experience the exciting world of materials science, and enjoy the journey of gaining goals after hard working. My advisor, Dr. Peter K. Liaw, has always been a great guidance through my research work. Not only has he created an environment for me to extend my intellectual skills, but also inspired me to make full use of my potentials, so as to build up a "rich and famous" dream in the scientific world. Dr. C. T. Liu of the Oak Ridge National Laboratory and at the University of Tennessee has given precious instructions on my research work, providing all the necessary materials for my project, and transferring sparkles of wisdom into my research study. Dr. Raymond A. Buchanan, who kindly agreed to be on my committee, has been giving all kinds of help to me, making it possible for me to finish my master-degree study. They have been encouraging me on my research work and on every step of my progress.

Many thanks to Mr. Douglas E. Fielden at the machine shop of the Materials Sciences & Engineering Department, Dr. Gongyao Wang, Dr. Yulin Lu, Mr. Fengxiao Liu, Mr. Jiawan Tian, Ms. Migri Stoica, Ms. Dongchun Qiao, Ms. Julia Sun, and Ms. Yinghong Lin for their kind helps.

Many thanks to my family who has always been of great support to me, never letting me down and standing by me at all times.

Acknowledgements are due to the financial support of the Oak Ridge National Laboratory (ORNL), and the United States National Science Foundation (NSF), the

Combined Research-Curriculum Development (CRCD) Program, with Ms. Mary Poats as the Program Director, under the contract number of DGE 0203415.

Abstract

The TiAl alloys have been considered as promising candidates for structural-materials applications at around 800^0C. In this work, new TiAl alloys, containing tungsten (W) and boron (B), have been developed. Using the scanning-electron microscopy (SEM), electron-microprobe, and transmission-electron microscopy (TEM), the effects of W and B on the microstructural evolution of TiAl alloys, including the colony size and lamellar spacing, were analyzed. It is important to point out that fine uniform microstructures (with the colony size smaller than 50 μm) can be conveniently developed after Hot-Isostatic Pressing (HIP) the as-cast alloys at $1{,}250^0$C and 150 MPa for 4 h without the deformation process. It was found that tungsten prefers to react with boron to form borides, and disperses mainly along grain boundaries, and occasionally inside grains. With the increase of the tungsten content, the microstructure can be further refined. Heat treatments at temperatures ranging from 900^0C to $1{,}310^0$C were conducted. The addition of tungsten can restrain the grain coarsening and stabilize the microstructure up to $1{,}280^0$C by hindering the migration of grain boundaries at high temperatures. It is also noteworthy that the beta phase, a high-temperature ductile phase, forms when the tungsten content exceeds 0.4 atomic percent (at.%). The α phase transus temperature, T_α, has been determined through differential-thermal analyses (DTA) and further proved by the investigation of the microstructural changes during various heat treatments. Different microstructures meeting desirable needs can be developed through heat treatments beyond and below the α phase transus temperature. Mechanical testing, such as hardness experiments, has been conducted on the alloys. The addition of the

alloying element, tungsten, increases the hardness of TiAl alloys by the solution strengthening and refinement of grain sizes.

Table of Contents

1.	Introduction	1
2.	Literature Review	3
2.1	Development of the TiAl-based Intermetallic Alloys	3
2.2	Microstructures of the TiAl-based Alloys	4
2.2.1	Crystal Structures	4
2.2.2	Microstructures of the TiAl-based Alloys	6
2.2.3	The β phase of the TiAl-based Alloys	10
2.3	Mechanical Properties of the TiAl-based Alloys	12
2.3.1	Tensile Ductility	12
2.3.2	Fracture Toughness of the TiAl-based Alloys	16
2.3.3	Creep Resistance of the TiAl-based Alloys	18
2.3.4	Fatigue Behavior of the TiAl-based Alloys	18
2.3.5	Superplasticity of the TiAl-based Alloys	20
2.4	Preparation and Processing of TiAl-based Alloys	21
2.4.1	Composition Design of the TiAl-based Alloys	22
2.4.1.1	Nb in TiAl-based Alloys	24
2.4.1.2	W in TiAl-based Alloys	24
2.4.1.3	B in TiAl-based Alloys	25
2.4.1.4	Si in TiAl-based Alloys	25
2.4.2	Heat-treatment Techniques	25

2.4.3	Thermal-Mechanical Techniques	26
2.4.4	Powder-Metallurgy Technique	28
2.4.5	Surface Treatment of the TiAl-based Alloys	29
2.5	Refinement of the Microstructure of the TiAl-based Alloys	31
3.	Experimental Procedures	34
3.1	Alloy Preparation	34
3.2	Nondestructive Detection	35
3.3	Hot Isostatic Pressing (HIP) and Homogenization Treatments	35
3.4	Differential Thermal Analyses (DTA)	35
3.5	Heat Treatments	36
3.6	Measurements of the Grain Size and Lamellar Spacing of the Heat-treated Samples	36
3.7	Hardness Measurements	37
3.8	X-ray Diffraction Analyses (XRD)	37
3.9	Metallographic Analyses	37
3.10	Scanning-Electron Microscope (SEM) and Electron Microprobe	37
3.11	Transmission-Electron Microscopy (TEM)	38
3.12	Field-Emission-Electron Microscopy	38
4.	Experimental Results	39
4.1	As-cast Structures of the Alloys	39

4.2	Microstructures of the Alloys after HIPing and Homogenization	40
4.3	Microstructures of the Alloys after Heat Treatments	43
4.4	Differential-Thermal Analyses (DTA)	45
4.5	X-ray Diffraction Analyses (XRD)	45
4.6	TEM Analyses	46
4.7	Mechanical Property	46
5.	Discussion	47
5.1	Microstructures of the Alloys	47
5.1.1	Effect of HIPing and Homogenization on the Microstructures of the As-cast Alloys	47
5.1.2	Effect of Heat Treatments on the Microstructures of the Alloys	48
5.2	Determination of the α Transus Temperature	50
5.3	β phase in the Alloys	51
5.4	Effect of Alloying Elements on the Microstructure and Mechanical Properties of the Alloys	53
5.4.1	Effect of Nb on the Microstructure and Mechanical Properties of the Alloys	53
5.4.2	Effect of W on the Microstructure and Mechanical Properties of the Alloys	55

5.4.3 Effect of B on the Microstructure and Mechanical Properties of the Alloys 56

5.5 Hardness of the Alloys 59

6. Conclusions 60

7. Future Work 63

References Cited 64

Appendices 74

Appendix A - Tables 75

Appendix B - Figures 78

Vita 111

List of Tables

TABLE:		Page
Table 1	Development of the γ-TiAl-based Alloys (at.%) [5]	76
Table 2	Mechanical Properties of the γ-TiAl-based Alloys Manufactured through Power Metallurgy [22]	76
Table 3	Microstructural Evolution of the TiAl-based Alloys	77

List of Figures

Figure		Page
Figure 1	Binary phase diagram of the Ti-Al alloys	79
Figure 2	Crystal structures	80
Figure 3	Four typical microstructures of the γ-TiAl-based alloys after post-hot work heat treatments, (a) Near-gamma structure, (b) Duplex structure, (c) Nearly lamellar structure, and (d) Fully lamellar structure	81
Figure 4	Three typical heat-treating techniques of the γ-TiAl alloys (Type I, Π, Ш)	82
Figure 5	Creep curves of different TiAl alloys with different microstructures	83
Figure 6	Manufacturing of the engineering TiAl-based alloys	84
Figure 7	Optical microstructures of the as-cast Ti-Al-Nb-W-B alloys (The arrows indicate the dendrites.), (a) Ti-45Al-7Nb-0.15B, (b) Ti-45Al-7Nb-0.15B-0.2W, (c) Ti-45Al-7Nb-0.15B-0.4W, and (d) Ti-45Al-7Nb-0.15B-0.7W	85
Figure 8	Backscattered images of the as-cast Ti-Al-Nb-W-B alloys (The arrows show the porosities. Point A shows the needle-shaped Ti-B boride phase.), (a) Ti-45Al-7Nb-0.15B, (b) Ti-45Al-7Nb-0.15B-0.2W, (c) Ti-45Al-7Nb-0.15B-0.4W, and (d) Ti-45Al-7Nb-0.15B-	86

0.7W

Figure 9 Secondary electronic images of the Ti-Al-Nb-W-B alloys after HIPing and homogenization, (a) Ti-45Al-7Nb-0.15B, (b) Ti-45Al-7Nb-0.15B-0.2W, (c) Ti-45Al-7Nb-0.15B-0.4W, and (d) Ti-45Al-7Nb-0.15B-0.7W 87

Figure 10 Backscattered images of the Ti-Al-Nb-W-B alloys after HIPing and homogenization (Point A shows the γ phase), (a) Ti-45Al-7Nb-0.15B, (b) Ti-45Al-7Nb-0.15B-0.2W, (c) Ti-45Al-7Nb-0.15B-0.4W, and (d) Ti-45Al-7Nb-0.15B-0.7W 88

Figure 11 Effect of W on the (a) grain size, and (b) lamellar spacing of the Ti-Al-Nb-W-B alloys after HIPing and homogenization 89

Figure 12 Energy-Dispersive X-ray Spectroscopy (EDS) of the γ phase in the Ti-45Al-7Nb-0.15B-0.7W alloy after HIPing and homogenization 91

Figure 13 EDS of the α_2 phase in the Ti-45Al-7Nb-0.15B-0.7W alloy after HIPing and homogenization 92

Figure 14 Backscattered images of the Ti-45Al-7Nb-0.15B-0.7W alloy after HIPing and homogenization, (a) Lower magnification, (b) Higher magnification 93

Figure 15 Backscattered images of the Ti-45Al-7Nb-0.15B-0.7W alloy after HIPing and homogenization, (a) TiB_2 needles, (b) γ-phase, and (c) formation of γ-twin caused by TiB_2 (shown in area A) 95

Figure 16	Topograph and composition analyses of the β phase	97
Figure 17	Microstructure of the Ti-45Al-7Nb-0.15B-0.7W alloy after HIPing and homogenization	98
Figure 18	Microstructures of the Ti-Al-Nb-W-B alloys heat treated at 900^0C / 360 h, (a) Ti-45Al-7Nb-0.15B, (b) Ti-45Al-7Nb-0.15B-0.2W, (c) Ti-45Al-7Nb-0.15B-0.4W, and (d) Ti-45Al-7Nb-0.15B-0.7W	99
Figure 19	Microstructures of the Ti-Al-Nb-W-B alloys heat treated at $1{,}265^0$C / 18 h, (a) Ti-45Al-7Nb-0.15B, (b) Ti-45Al-7Nb-0.15B-0.2W, (c) Ti-45Al-7Nb-0.15B-0.4W, and (d) Ti-45Al-7Nb-0.15B-0.7W	100
Figure 20	Microstructures of the Ti-Al-Nb-W-B alloys heat treated at $1{,}280^0$C / 14 h, (a) Ti-45Al-7Nb-0.15, b) Ti-45Al-7Nb-0.15B-0.2W, (c) Ti-45Al-7Nb-0.15B-0.4W, and (d) Ti-45Al-7Nb-0.15B-0.7W	101
Figure 21	Microstructures of the Ti-Al-Nb-W-B alloys heat treated at $1{,}295^0$C / 10 h, (a) Ti-45Al-7Nb-0.15B, (b) Ti-45Al-7Nb-0.15B-0.2W, (c) Ti-45Al-7Nb-0.15B-0.4W, and (d) Ti-45Al-7Nb-0.15B-0.7W	102
Figure 22	Microstructures of the Ti-Al-Nb-W-B alloys heat treated at $1{,}310^0$C / 5 h, (a) Ti-45Al-7Nb-0.15, (b) Ti-45Al-7Nb-0.15B-0.2W, (c) Ti-45Al-7Nb-0.15B-0.4W, and (d) Ti-45Al-7Nb-0.15B-0.7W	103

Figure 23	Differential-Thermal Analyses (DTA) of the Ti-45Al-7Nb-1.5B-0.4W alloy after HIPing and homogenization	104
Figure 24	X-ray diffraction patterns of the Ti-45Al-7Nb-0.15B-0.7W alloy after HIPing and homogenization	105
Figure 25	TEM analyses of the Ti-Al-Nb-W-B alloys after HIPing and homogenization, (a) Ti-45Al-7Nb-0.15B-0.2W, (b) Ti-45Al-7Nb-0.15B-0.4W, and (c) Ti-45Al-7Nb-0.15B-0.7W	106
Figure 26	TEM analyses of the Ti-45Al-7Nb-0.15B-0.4W alloy after HIPing and homogenization, (a) γ-twin separated from the α_2/γ lamellae (shown in area A), (b) TiB_2 and γ-twin (shown in area B and area C)	108
Figure 27	Effect of W content on the hardness of the Ti-Al-Nb-W-B alloys after heat treating at 1280^0C / 4 h	109
Figure 28	Effect of interlamellar spacing on the hardness of the Ti-Al-Nb-W-B alloys after heat treating at 1280^0C / 4 h	110

1. Introduction

Two-phase TiAl alloys have been receiving considerable attentions because of their attractive properties, such as low density, excellent high-temperature strength, and good oxidation resistance. However, TiAl alloys are quite brittle at room temperature and have relatively low fracture toughness. The mechanical properties of the TiAl-based alloys with lamellar structures depend on three factors: the colony size, interlamellar spacing, and alloying addition. The tensile elongation at room temperature is strongly dependent on the lamellar colony size, showing the increased ductility with decreasing the colony size. The strength at room and elevated temperatures is sensitive to the interlamellar spacing, showing the increased strength with decreasing the interlamellar spacing [1].

The as-cast TiAl-based alloys are usually coarse in the grain size. A refinement in the microstructures is necessary to meet the desirable applications. Additional elements, such as W, B etc., added into the base alloy can help refine the grain size. Related heat treatments can facilitate the development of the desirable microstructures. In general, the fully lamellar (FL) structure has a better overall property than the other microstructures. But it has the low room-temperature tensile ductility. The duplex structure (DP) tends to have the good room-temperature tensile ductility, but its fracture toughness is low. This dilemma has not been satisfactorily solved recently. For the DP structure, it is hard to enhance its fracture toughness and creep resistance. On the other hand, the room-temperature ductility can be enhanced by refining the grain size of the FL structure. A fine fully lamellar microstructure has both good ductilities and fracture

strengths, and the fracture toughness and creep resistance are also better than the duplex microstructure.

For deformed TiAl-based alloys, the most optimal combination of the "composition-microstructure-property" can be obtained by different kinds of deformation techniques for the microstructural control, and by additional heat treatments for the microstructural rearrangement. Some deformation methods, such as isothermal forging, may initiate small cracks. Since most deformation techniques are costly, optimal solutions are in the search.

With the understanding of the relationship among the fabrication technique, the microstructure, and the related mechanical properties, optimal processing methods can be developed so as to control the microstructures of the TiAl intermetallics, and to improve the associated mechanical behaviors.

In this research, a refinement in the colony size of the TiAl-based alloy is obtained by alloying, and heat treatment. An investigation regarding the effect of the tungsten addition on the phase formation, the microstructural features, and the stability of both lamellar structures and beta phases is conducted. Mechanical properties related to the microstructures are studied through the hardness measurements of the alloys. The optimal composition of the TiAl-based alloy has been suggested.

2. Literature Review

2.1 Development of the TiAl-based Intermetallic Alloys

In the early 1950's, as the uses of titanium alloys in jet-turbine engines for their excellent properties, such as the low density, high strength, high-temperature resistance, and high corrosion resistance, increase research efforts on the phase diagram, phase composition, phase relationships of TiAl-based alloys, and their mechanical properties, oxidation resistances, had been conducted. Ti-50Al alloys had been studied first, but were abandoned for their low ductility at room temperature. Fifteen years later, 1975 ~ 1982, the Pratt & Whitney (P&W) lab in the United States found Ti-48A1-1V-0.3C (atomic percent, at.%), which was the first generation of TiAl-based alloys, to have the best properties, after investigating nearly one hundred other TiAl-based alloy compositions. The room-temperature ductility of this alloy can reach 2%. By the end of the 1980's, the second generation of TiAl-based alloys, Ti-48Al-2 Cr-2Nb (at.%) [2], was developed by Dr. S. C. Huang at the General Electric Company. For nearly ten years, the relationship among the alloy composition-processing-microstructure-mechanical properties had been investigated. A complete study of the overall properties of this alloy, such as the physical, mechanical, and chemical properties, had been conducted. The room-temperature ductility of the alloy can reach 2%, which is still not enough for engineering applications. The fracture toughness and the high-temperature creep resistance are low. However, the results had still drawn a worldwide interest in the research of TiAl-based alloys. The Pacific Western Airlines (PWA) developed the 47XD TiAl-based alloy for the high-pressure F119 engine [3]. One outstanding

characteristic of this alloy is that it has a great fatigue-crack-propagation resistance. It has a superior creep strength than the IN100, but the room-temperature ductility reaches only 1.2%.

Based on the COST 501 Round project, Europe developed Ti-47 at.% Al-2 at.% W-0.5 at.% Si [4], a TiAl-based alloy with a high creep resistance, which exceeds the nickel-based alloy IN738LC. But Ti-47 at.% Al-2 at.% W-0.5 at.% Si has a low tensile ductility of 0.5%. Following the research work of many investigators, there is a great improvement in the understanding of fundamental principles, fabrication techniques, microstructures, and overall properties of the γ-TiAl alloys [5]. The first three generations of the γ-TiAl alloys are listed in Table 1*.

2.2 Microstructures of the TiAl-based Alloys

2.2.1 Crystal Structures

The binary phase diagram of the γ-TiAl alloy is shown in Fig. 1*, with the range of Al from 45 to 52 at.%. The basic phase is the γ-TiAl, and the second phase is the α_2-Ti_3Al. γ-TiAl belongs to the Berthollide type of intermetallics. This type of structure remains ordered at any temperature, and its compositions can change within a specific range. γ-TiAl has the Ll_0 crystal structure, with a Pearson sign of TP4, and a lattice space of P4/mmm. Its lattice structure is shown in Fig. 2(a), composed of alternative atomic planes piling between each other, with either only Al or Ti atoms in the [001]

* All tables are located in Appendix A
* All figures are located in Appendix B

direction. The lattice constant in the [100] and [010] directions is different from that in the [001] direction. The crystal structure of the γ-TiAl is face centered tetragonal (FCT), and its lattice constant changes with the content of Al and compositions, in the range of: a = 0.397 - 0.401 nm, c = 0.404 - 0.408 nm, and c/a = 1.01 - 1.05 [6] (a and c represent, respectively, the short and long unit-cell dimensions). The ratio of the axis constant (c/a) can affect the dislocation movement of the crystal. With the addition of V, Mn, and Cr, the value of the ratio can be lowered, and the ductility of the alloy can be enhanced. For those non-stoichiometric γ phases**,** the additional Ti or Al atoms occupy the position of each other, and no vacancy is formed.

Even though in the early stages, the research concerning the ductility of the γ-TiAl-based alloy focused on the high Al-containing single-phase range. It was shown that the lower amount the Al content, the better the tensile ductility of the two phase alloy would be [7]. Up to now, the most practical TiAl-based alloy in progress consists of the two phases of the α_2-Ti_3Al and γ-TiAl. When there is a small amount of the α_2 phase, oxygen and carbon impurities dissolve in it, thus enhancing the purity of the γ phase, which leads to an increase in the tensile ductility of the γ-TiAl-based alloy. The α_2-Ti_3Al is a Kurnakov type of intermetallic, and the order-to-disorder temperature is about $1{,}125^0$C. Above this critical temperature, the α_2-Ti_3Al is of the disordered hexagonal close-packed (HCP) structure, while below this critical temperature, it is of the ordered $D0_{19}$ structure, and the lattice constants are a = 0.5782 nm, and c = 0.4629 nm. The crystal structure is shown in Fig. 2(b).

Generally speaking, the Ti-rich two-phase alloy is composed of two phases, the $\gamma+\alpha_2$ lamellae. In the lamellar structure, the γ-TiAl and α_2-Ti_3Al laths are alternatively arranged, and they have an orientation relationship as: $(111)_\gamma//(0001)\alpha_2,[110]_\gamma//<11\bar{2}0>\alpha_2$. The hexagonal $D0_{19}$ structure of the Ti_3Al phase is equivalent in three $<11\bar{2}0>$ directions; but as for the cubic structure of the TiAl phase, its [110] and [011] directions on the (111) plane are not equivalent. There are three different orientation relationships in the γ lamellae, twins (180^0 rotation axis), 120^0 rotation axis, and the pseudo twins (60^0 rotation axis).

2.2.2 Microstructures of the TiAl-based Alloys

Four important microstructures of TiAl-based alloys [7], as shown in Fig. 3, are: near-gamma (NG) microstructures, γ [Fig. 3(a)]; duplex microstructures (DP), $\alpha_2+\gamma$ and γ [Fig. 3(b)]; near-lamellar microstructures (NL) [Fig.3(c)]; and fully lamellar (FL) microstructures, $\alpha_2+\gamma$ [Fig. 3(d)]. NG are generally inhomogeneous microstructures, it is composed of bulk γ crystals, and fine γ crystals, which are restrained by small α_2 phases. DP is usually the most refined microstructure compared to the other three microstructures, and it is composed of the lamellar colony and equiaxed γ phase, which are of the same volume proportion. NL is composed of the bulk lamellar colony, which occupies most of the volume fraction, and a very small amount of the γ phase. FL is composed of completely bulk lamellar structures.

Fully lamellar structures are generally observed in cast conditions, and duplex structures are formed in thermomechanically-treated conditions. The FL microstructure

consists of equiaxed polycrystalline grains with densely packed lamellae, which are always called lamellar colonies. The lamellar colonies are composed of α_2 and γ laths. The DP microstructure, however, is made up of lamellar colonies with single-phase γ grains distributed around them.

The coarse FL structures with a grain size (d), $d > 500$ μm, exhibit adequate fracture toughnesses, but are usually brittle at room temperature. On the other hand, the DP structures with fine grain sizes ($d < 50$μm) show adequate tensile ductilities but poor fracture toughnesses, and more importantly, worse high-temperature strengths and creep resistances, as compared with the FL materials. The room-temperature tensile yield strength (σ_y), fracture strength (σ_f), and ductility (δ) of TiAl-based alloys increase with decreasing the colony size of the fully lamellar structure. Based on these results, a material with fine fully lamellar (FFL) microstructures would be expected to have balanced mechanical properties.

After heat treating the TiAl-based alloys at a temperature above $1{,}000^0$C, three phase transformations may take place: $\alpha_2+\gamma \rightarrow \alpha+\gamma \rightarrow \alpha$, and the single α phase region extends to $1{,}470^0$C. Thus, different microstructures can be obtained through different kinds of heat-treatments.

(1) As-cast microstructure:

The as-cast microstructure is a structure formed when the liquid metal solidifies in the casting mold. Thus, the grain size is usually large and non-uniform in the compositions. Columnar crystals and cellular structures are found to grow toward the center of the casting mold.

(2) Equaixed near-gamma microstructure:

Following heat treating the TiAl-based alloy in the α+γ two-phase region, at a temperature slightly above the eutectoid temperature (T_e), an equaixed near-gamma microstructure with a small amount of α_2-phase grains can be obtained. With a combination of heat-treatment, the microstructure can be refined.

(3) Duplex microstructure:

After heat treating the TiAl-based alloy in a temperature range (temperatures slightly below T_α, T_α-60^0C), where the volume fraction of the two phases in the α+γ region are almost equal, the duplex structure can be developed. At the heat-treatment temperature, the equiaxed α and γ phase are formed. The α phase is a high-temperature disordered structure, which can transform into a α_2/γ lamellar structure through the eutectic reaction after air or furnace cooling. Since the α and γ phases restrict each other during the heat treatments, the grain growth is very slow, thus leading to small colony sizes (10 μm -50 μm).

(4) Near-lamellar microstructure:

Following heat treating the TiAl-based alloys at a temperature range slightly below the α trasnsus temperature, T_α-10^0C, in the α+γ two phase region, a α_2/γ lamellar structure and a small amount of the equiaxed γ phase can be developed after air or furnace cooling. Since the amount of the γ phase is small, its effect on restraining the α phase is hindered. The colony size is larger than the DP microstructure (200 μm ~ 500 μm). The γ crystal is usually smaller than 20 μm. The larger the temperature far from Tα, the smaller the colony size, but the more the amount of γ crystals.

(5) Fully lamellar microstructure:

Following heat treating the TiAl-based alloy at a temperature slightly higher than the T_α, $T_\alpha+20^0C$, the high-temperature α phase can completely turn into a α_2/γ lamellar structure after furnace cooling. Since the heat-treatment temperature is high, and there is no γ phase restraining at the grain boundaries, the α phase grows very fast. Thus, the colony size of the FL microstructure is coarse. For the as-cast fully lamellar microstructure, the grain size is normally 600 ~ 1,000 μm. With additional heat-treatments and thermo-mechanical processing, the grain size of the FL microstructure can be refined.

The heat treatments of TiAl alloys can be divided into three categories, as shown in Fig. 4. Processes I and II consist of annealing, at a temperature slightly above T_α, and aging afterwards, while Process III contains only aging. The heat-treatment temperature, holding time, heating rate, cooling rate, and final properties are determined by the alloy compositions and the desired microstructures. In Process I, alloys are usually annealed at high temperatures for 0.5 ~ 5 h, cooled to room temperature at a rate of 30 ~ 150°C/min, reheated to an aging temperature, then aged for 4 ~ 100 h. In Process II, alloys are either furnace cooled after annealing, or moved directly from the annealing furnace to the aging furnace. In order to obtain refined and uniformed grains, a fast heating rate is preferred; while in order to avoid crack initiation and supersaturation in phases, a slow cooling rate is preferred. Two-step heat treatments (I and II) are for heat-treating non-lamellar structural alloys. Process III heats the alloy directly to the aging temperature without annealing. This process is used for alloys,

which do not need to change their as-cast structures, or alloys with stabilized microstructures (fully lamellar), which only needs the aging control. The aging temperature in Fig. 4 can be chosen either above T_e or below T_e.

For different TiAl alloys, the general principles for the heat treatment are the same, but since there are differences in the compositions, specific heat-treatment schedules can be designed to develop the best overall properties.

2.2.3 The β phase of the TiAl-based Alloys

Adding a β phase stabilizer, such as Cr, Nb, W, and Mo, to γ-TiAl-based alloys can form a β_2 (B_2) phase, which usually appears to be a bulk structure or contains small precipitates. Generally, the B_2 phases, which grow along the grain boundary, decrease the creep resistance of the alloy; while those dispersing in the alloy can enhance the creep resistance. The β phase commonly exists in the TiAl alloys. Research had been conducted on Ti-49Al-2W (at.%), and small particles had been found at the grain boundaries between the equiaxed γ phases and α_2+γ lamellar microstructures [9]. Since W is a beta-phase stabilizer, these small precipitates are determined as the β phase. A discontinuous β phase was found to be rich in W and Si in Ti-47Al-2W-0.5Si [10].

The orientation relationships among the B_2, α_2, and γ phases are: $(0001)\alpha_2$ // $\{111\}\gamma$ // $\{110\}\beta_2$ and $\langle 1120\rangle\ \alpha_2$// $\langle 110\rangle\ \gamma$ // $\langle 111\rangle\ \beta_2$. The B_2 phase has a cubic structure with 8 atoms as its nearest neighbors, which are all different atoms. The lattice constant at 900^0C is $a_0 = 0.33065$ nm. Its crystal structure is shown in Fig. 2(c). The β phase cannot exist at room temperature without alloying the intermetallics.

Experiments [11] on the ABB-23 alloy showed that when there are beta-phase stabilizers, such as W, in the TiAl-based alloy, the B_2 phase tends to precipitate with the dissolution of the α_2 phase, which is rich in W, during heat-treatments and creep deformations. The lamellar microstructures of the TiAl-based alloys are grown through ledges [12]. Since the α_2 phase has a higher amount of W than the γ phase, the excessive amount of W formed during the dissolving process of the α_2 lamellae (the growth of the γ lamellae) would go into the undissolved α_2 lamellae, especially at the α_2/γ boundaries and between the α_2/γ ledges. Once the amount of W at these places outgrows a critical value, B_2 would precipitate, since it is more stable than the γ phase. Thus, the α_2/γ boundaries and phase ledges are the favorable locations for the B_2 phase nucleation. Research on the Ti-Al-W-Mo-Si alloy showed that between 760^0C-$1{,}050^0$C, there is a three phase ($\alpha_2+\gamma+\beta$) region, where W, Si, Mo will be rich in lamellar boundaries, there is a phase-transformation action of $\alpha_2 + \gamma \rightarrow \alpha_2 + \gamma + \beta$ [13].

The morphology of the β phase may vary with the alloy compositions and the processing states. The β phase formed at the interface of the α_2/γ lamellae may be of an oval sphere shape [13]. In the ABB-23 alloy after the hot isostatic pressing (HIP) and heat treatment, discontinuous bar-shaped and massive Ti (Al, W) phases with the B_2 crystal structure were found [14]. For the TiAl-Cr alloy, β phases appear at grain boundaries and dendrites of the as-cast conditions as disk shapes, long ribbon shapes, or plate shapes. During heat treatments, the β phase precipitates even more and tends to coarse as the temperature increases.

With the calculations and analyses of the dielectric structure and phase structure factors of the alloy with β-stabilizing elements, W is the best β-stabilizer, V, Mo, and Nb are the next, and Ta, Hf, and Zr are the weakest. W can form a continuous solid solution with the β phase, but at a solid state, there is a single-phase segregation. Mn, Fe, and Cr are β phase eutectoid elements, which can easily form compounds through the eutectoid reaction. These compounds tend to make the alloy brittle. Even though Zr and Hf can stabilize the β phase, they are also α phase stabilizer, so they are not very effective in extending the β phase region. In this case, V, Mo, and Nb are more often chosen as alloying elements. Controlling the heat-treatment temperature and processing steps, a small addition of W is an effective way to stabilize the β phase.

2.3 Mechanical Properties of the TiAl-based Alloys

2.3.1 Tensile Ductility

At room temperature, the yield strength of the TiAl-based alloy is usually between 250 ~ 600 MPa, the fracture strength is around 300 ~ 700 MPa [17]. These values are affected by the grain size, lamellar spacing, and microstructures. For the FL microstructure, when the lamellar colony size refines from 1,200 μm to 300 μm, the yield strength changes from 300 MPa to 500 MPa [18]. This trend can be explained by the Hall-Patch equation: $\sigma_{0.2} = \sigma_0 + k_\lambda \lambda^{-1/2}$, where $\sigma_{0.2}$ is the 0.2% offset yield strength, σ_0 and k_λ are material constants, and λ is the lamellar spacing. For the PST single crystal, its yield strength is related to the tensile angle, ϕ (the angle between the lamellar interface and the tensile hard direction). Since the deformation appears on the {111}

plane, $\phi = 45^o$ is the deforming direction (soft direction), the yield strength is approximately 90 MPa. At $\phi = 0^o$ and $\phi = 90^o$, which is known as the hard direction, the yield strengths are 290 MPa and 500 MPa, respectively [18].

To increase the room-temperature ductility, the microstructures of the binary-phase intermetallic alloy should have a uniformed fine grain size. With the thermo-mechanical processing (TMP), and additional heat treatments, the grain size can be refined to 20 ~ 30 μm, the room-temperature ductility can reach 4.7%, which is much higher than the original as-cast alloys that have a large grain size and are usually difficult to refine through heat treatments. The tensile ductility of the FL microstructure, which is usually low, together with its yield strength, can be increased, when the grain size is refined. For PST crystals, its tensile ductility is related to the tensile angle. The tensile ductility reaches the highest point at the soft direction ($\phi = 30^o$), since in this direction, the shearing deformation is not subjected to the lamellar interface, thus exceeding the ductility of the fully lamellar structure. Moreover, the γ/α_2 dual phase alloy has a better tensile ductility, which is related to the transferring of the oxygen from the γ phase into the α_2 phase, since the solubility of oxygen in the α_2 phase is much higher than that in the γ phase [20].

There is a significant brittle-ductile transition point in the dual-phase intermetallic alloys. For a typical tensile strain rate of 1×10^{-4} s^{-1}, the brittle-ductile transition temperature (BDTT) is around 620 ~ 800^0C, and is related to the microstructure. Below the BDTT, the elongation is kept as a constant. The elongation increases significantly, as the temperature goes beyond BDTT. For PST crystals, when

the tensile orientation angle is $\phi = 0^o$ or $\phi = 30^o$, there is also a brittle-ductile transition point, but for $\phi = 30^o$, the transition is not so obvious. When $\phi = 90^o$, the tensile ductility of the PST is small, and there is no brittle-ductile transition found even when the temperature is raised to $1{,}100^0$C [21]. This is similar to the polycrystalline intermetallic alloy with the FL structure. Under the BDTT temperature, no matter what the microstructure or additional element is, there is little influence of temperature on the yield strength of the TiAl-based alloy. Above the BDTT temperature, the yield strength drops dramatically with the increase of the temperature.

The room-temperature ductility is always low, which is generally an obstacle to the application of the TiAl-based alloys. Recently, methods used to improve the ductility of the intermetallic alloys are:

1. Control the composition of the alloy, so that the atomic percent of the Al is between 46% ~ 49%. Induce a small amount of the α_2-Ti_3Al phase to form the binary-phase TiAl-based alloy. The fine microstructure of the alloy has the better ductility.
2. Alloy the TiAl-based intermetallic with elements, such as Cr, V, Mn, Si, C, and B, to increase the room-temperature ductility.
3. Improve the processing techniques of the alloying procedure. Combining high-temperature mechanical processing, such as isothermal forging and hot extrusion, with a heat treatment, the final microstructures of the alloy can be controlled. With the use of the directional-solidification method, the rapid solidification technique, and HIP, microstructures of the alloy can be improved.
4. Refine the colony size of the alloys.

5. Reducing the ratio of c/a in a single-phase γ-TiAl can increase the tensile ductility. But for the dual-phase alloy, reports have shown that there is a little relation between the c/a value and the ductility [21].

6. Improving the purity of the alloy can be an effective way to enhance the tensile ductility at room temperature.

7. Adding ductile particles or fibers into the intermetallic alloy can increase the tensile ductility.

8. Improve the environmental brittleness of the TiAl-based alloy.

The powder metallurgy is one of the important methods to produce γ-TiAl-based alloys. But for a long term, the TiAl-based alloys produced by the powder metallurgy showed poor mechanical properties. This trend is caused by the porosity, impurity, and oxygen content in the alloy. Recently, with the production of high-quality powders and highly-condensed techniques, the γ-TiAl-based alloys processed by the powder metallurgy showed better mechanical properties than the as-cast alloys in some aspects, and exhibited properties close to the forged alloys. The mechanical properties of the γ-TiAl-based alloys are shown in Table 2. From the table, we can conclude that the room-temperature tensile ductility of the γ-TiAl-based alloys, produced from the powder metallurgy, has been effectively improved, and the fracture strength can reach a value of 1,000 MPa [22]. The high-temperature oxidation resistance of the powder-metallurgy-produced γ-TiAl-based alloy is better than the as-cast TiAl-based alloy; but its high-temperature superplasticity is lower than the as-cast alloy, since there are impurities and porosities in the powder-metallurgy alloys.

2.3.2 Fracture Toughness of the TiAl-based Alloys

The microstructure of the TiAl-based alloy has a great effect on the fracture toughness of the material. It has been concluded that, as the volume fraction of the lamellar colony increases, the fracture toughness of the TiAl-based alloy increases. For the four typical microstructures of the TiAl-based alloy, the fully lamellar structure has the best fracture toughness. The duplex structure has a better fracture toughness than the equiaxed single-phase γ-TiAl alloy. The reason that the FL structure has the best fracture toughness is as follows:

(1) a fully lamellar structure can initiate a large plastic strain at crack tips, and can increase the resistance to the crack propagation;

(2) the difference in the the structure and the orientation between the neighboring lamellae can restrain the slip bands and the cleavage cracks to cross the interface, thus detering the crack from propagation;

(3) when the crack is stopped at the interface, there is a resolving shear stress along the interface, which causes the interface to slip and, thus, passivate the major crack tip;

(4) microcracks are initiated at the tip of the main crack, which causes a formation of a shear zone between the main crack and the microcracks. These shear zones restrain the expansion of the cracks. Only when the shear zone is deformed and broken down, the major crack could, then, propagate through. In this case, the deformation and rupture of the shear zone enhanced the toughness.

Decreasing the lamellar spacing of the TiAl-based alloy can enhance the crack-initiation toughness, K_{IC}, and the crack-growth toughness, K_S. But for the grain size, it

has a more complicated influence on K_{IC} and K_S. Based on the research of Ti-46.8at.%A1-2.3 at.%Nb-1.6 at.%Cr-0.9at.%V [23], when the colony size is smaller than 600 μm, both K_{IC} and K_S increase with increasing the colony size; when the colony size increases to 600 μm, the fracture toughness is no longer dependant on the colony size; when the colony size exceeds 600 μm, the fracture toughness is related to the size of the shear zone, which is influenced by the lamellar spacing and the orientation of the lamellar colony.

Additional alloying elements and adjusting processing techniques can change the microstructure, thus influencing the fracture toughness. The addition of Cr into the TiAl-based alloy can obviously increase the amount of the lamellar structures, which can lead to the formation of the lamellar fracture zone in order to increase the resistance of the fracture propagation, thus, increasing the fracture toughness [24]. The addition of Nb deters the fracture toughness, and this trend might be caused by the influence of Nb on the grain boundaries. With the addition of Nb, deposits have been found at the grain boundaries. The failure of the TiAl-based alloy is related to the microcracks, which are nucleated, propagated, and gathered at the grain boundaries or phase boundaries. Depositions along the grain boundaries can weaken the bonding strength between the grains. On the other hand, they can facilitate the nucleation of the microcracks, which can increase the possibility of the fracture along the grain boundaries. The effect of processing techniques and heat treatments on the fracture toughness of the TiAl-based alloy lies in the influence of these procedures on the microstructures [25].

2.3.3 Creep Resistance of the TiAl-based Alloys

The fully lamellar structure does not only have the best toughness, but also the highest creep resistance among the other three microstructures (shown in Fig. 5) [26]. Its transient-creep and steady-state creep rates are both lower than the other microstructures. The time needed for the FL structure alloy to reach the 0.2% strain is two magnitudes longer than the duplex structure. For high creep-resistant TiAl-based alloys, they either are a fully lamellar structure or contain a large fraction of the lamellar structure [27]. Research indicates that during creep, deformation twins occur in the γ phase and, then, refines the grain. For the α_2 lamellae, it tends to dissolve and spheroidize, which leads to an increase in the lamellar spacing.

2.3.4 Fatigue Behavior of the TiAl-based Alloys

At a temperature below 850^0C, the DP structure has a better low-cycle-fatigue life (LCF) than the FL structure, and shows a good high-cycle-fatigue life (HCF). But at a higher temperature, the FL structure has a longer fatigue life. The process of deformation and fracture during creep is similar to that of the tensile stress test loaded under low stresses. Below the BDTT, the deformation mechanism is planar, and along the lamellar direction, the fracture mechanism is mainly transgranular. Above the BDTT, cracking along the crystals, and spalling inside the lamellae increase. In the DP structure, cracks are formed at the surface of the alloy. For the FL structure, cracks are usually developed inside the alloy, and these cracks go through a propagation stage. Just

like the effect on the tensile ductility, the non-uniformed microstructures hinder the fatigue behavior.

Since γ-TiAl-based alloys have been intended to be used in the aviation industry, they should satisfy some necessary reliabilities, and meet some requests on abrasion limits. Due to these reasons, the research regarding the microstructural influence on the fatigue performance has become important.

The research on TiAl-based-alloy plates showed that fatigue cracks first nucleate at the shear zones and the grain boundaries, which are impacted by the shear bands [23]. But due to cyclic hardening, most microcracks are in a closed state, and are unable to move. At room temperature, microcracks are more likely to nucleate in the FL structure than in the equiaxed γ structure. But just like fracture toughness, the propagation and gathering of microcracks is much faster in the equiaxed γ structure than in the FL structure [28]. In the FL structure, the initiation of microcracks is a continuous procedure, but the newly formed microcracks are separated by the shear band, and the already existing expanding or non-expanding microcracks. The shear zone between the microcracks can stop the cracks from propagating, only when the alloy is under a quasi-static load. When the alloy is under the cyclic load, the shear zone is destructed by fatigue, and loses its protection from the crack propagation. In the FL structure, expanding microcracks, stable microcracks, and newly nucleated microcracks form up the macrocracks of the alloy.

2.3.5 Superplasticity of the TiAl-based Alloys

Starting in the 1990's, researchers have become interested in the superplasticity of the TiAl-based alloys. The superplasticity of the TiAl-based alloy usually occurs at a temperature above $1{,}000^0$C. At this high temperature, expensive mold materials are needed, and the alloy oxidizes severely. Thus, finding a way to lower the superplasticity temperature has become a critical issue. Now, the superplasticity temperature has been lowered to $700 \sim 900^0$C [29], or even lower. Usually, equiaxed fine microstructures are needed to obtain the superplasticity. But to transform as-cast bulk TiAl-based alloys into fine equiaxed structures needs complicated thermo-mechanical processing, which causes a dramatic increase in the cost. This trend leads to another critical issue, how to develop the superplasticity under the condition of large TiAl-based alloy grains [30]. Research has been conducted, and the superplasticity has been found in TiAl-based alloys with a grain size of $20 \sim 95$ μm [31].

The un-equiaxed thermally-deformed microstructure (including deformed metastable structures) also shows a good superplasticity. Besides lowering the superplasticity temperature of the alloy, enhancing the rate of the superplasticity can also enhance the mechanical property of the alloy. This not only reduces the oxidation resistance of the alloy, which sensitively influences the mechanical property of the TiAl-based alloy; but also enhances the production efficiency, which is very much of practical use. The strain rate of the TiAl-based alloy under superplasticity is in the range of $10^{-2} \sim 10^{-5}s^{-1}$, there are rates, which are higher than 10^{-2} that is close to the practical use.

Two applications of the superplasticity are: (1) shaping the parts; and (2) solid-state welding. At the temperature of $1{,}150^0$C [32], hemisphere-shaped, arc-shaped, and wave-shaped parts were obtained from a 1 mm sheet of Ti-48 at.% Al-2 at.% Cr. At the temperature of $1{,}000^0$C, a box shape was obtained from Ti-47 at.% Al- 2 at.% Cr- 0.2 at.% Si and Ti-48 at.% Al-3.5 at.% (Cr, Mn, Nb, Si, B); more complicated shapes were obtained from the Ti-47 at.% Al-2 at.% Cr-0.2 at.% Si sheet. The application of the superplasticity in the TiAl-based alloy is rising. We can predict that the superplasticity is a useful technique, which can overcome the difficulty of metal working of the TiAl-based alloy, and it will turn into an essential technique in processing the alloy.

2.4 Preparation and Processing of TiAl-based Alloys

The techniques for producing the TiAl-based alloy can be divided into three typical methods [33]: (1) Near Net Shape Casting; (2) Ingot Metallurgy (IM); and (3) Powder Metallurgy (PM). Each method involves one or multiple processing. Figure 6 presents the flow chart of the processing paths.

The casting method is a low-cost production, and is able to produce complicatedly shaped samples. Due to these reasons, it is one of the most useful methods, which are often used in aircraft and automobile industries. But cast alloys usually have coarse crystal structures, even though they have high fracture toughness and creep resistivity, and the room-temperature ductility is low. Cast alloys are aeolotropism, and have porosities. How to refine the microstructure of the as-cast alloys, and enhance their ductility and density, has become a critical issue.

The ingot metallurgy (IM) first casts samples into large ingots, then homogenizes the samples through HIP, and the final step is the thermal machining process, such as the iso-thermal forging and hot extrusion. Through subsequent heat treatments, various microstructures can be developed to meet different needs [7]. Mechanical properties of the TiAl alloys using this procedure are good, but the cost is also high, and the production rate is low.

The powder Metallurgy (PM) includes "sintering + thermo-mechanical processing" and "sintering into a near-net shape". Since the original grain size of this method is small, the heat-treatment temperature is not as high as the IM procedure, and its final grain size is much smaller. But since the impurities of the TiAl-based alloys produced by this method are hard to control, the use of PM is limited.

The rolling process of the TiAl alloy is multiply-stepped. But since the ductility of this alloy is limited, the machining process is difficult. But with the advancement of the technology, now equiaxed $\gamma+\alpha_2$ microstructures [34], which are reliable for the superplasticity formation, can be obtained. This feature made the TiAl-based alloy plate useful for the aviation industry, which has high requests for the specific strength and damage limitation.

2.4.1 Composition Design of the TiAl-based Alloys

The first step in designing the TiAl-based alloys is to control the Al content. The amount of Al has to be less than 53 at.% in order to obtain a two-phase alloy.

Experimental results show that, the best ductility lies in the region of 45 ~ 47 at.% Al [35].

Recently, researches have been focused on the alloying of the intermetallic, in order to enhance the properties of the alloy. Major points are on the improvement in the ductility and oxidation resistance. Generally, alloying elements can affect the alloys through the intrinsic and extrinsic effects. The intrinsic effect changes the properties of the alloy directly, while the extrinsic effect affects the alloy indirectly through the change of microstructures. The objects of the following additional elements are [7, 36]:

(1) enhance the ductility and oxidation resistance: Nb, Ta, W, Mo, etc.;

(2) enhance the ductility but decrease the oxidation resistance: Cr, V, Mn, etc.;

(3) enhance the strength: Cr, V, Mn, Mo, Ta, Hf, Sn, W, Ca, Sb, La, B, C, N, etc.;

(4) enhance the ductility: Si, C, B, N, P, Se, Fe, Ni, Ca, Sb, La, Mo, Fe, etc.;

Since there are differences in production methods, machining techniques, and heat-treatments, different effects can be obtained even if the same kind of element is added [35], and the explanation may vary. But the effects of niobium (Nb), boron (B), tungsten (W), and silicon (Si) are clear: Nb is a beta-phase stabilizer, and it can enhance the ductility and oxidation resistance of the alloy [37]; B forms borides in the TiAl-based alloy, and it tends to refine the grain size, and enhance the mechanical properties [38, 39]; W can stabilize the beta phase, and a small amount of W can enhance the strength and creep resistances of the TiAl-based alloy [40, 41]; Si can notably strengthen the creep and oxidation resistances of the alloy. The distribution and existing arrangements of the Nb, B, W, and Si are controlled by processing procedures,

machining techniques, and heat treatments. They are very important in changing the properties of the intermetallic alloys [42]. Below is a summarization of the effects of alloying elements in TiAl-based alloys:

2.4.1.1 Nb in TiAl-based Alloys

Nb has a high melting point (2,468°C), and good resistance to oxidation. The addition of Nb in the TiAl alloy can increase its high-temperature strength and oxidation resistance [47]. Depending on the amount of Nb, there are high-Nb TiAl alloys (~ 23 at.% Nb and ~ 20 at.% Al), medium-Nb TiAl alloys (17 ~ 18 at.%Nb and 20 ~ 30 at.% Al), low-Nb TiAl alloys (10 at.% Nb and 40 at.% Al), and less-Nb TiAl alloys (~ 2 at.% Nb).

Moreover, the addition of Nb will increase the ductility of the TiAl alloy by stabilizing the β phase, and increase the ambient-temperature strength by solution strengthening [43-46].

2.4.1.2 W in TiAl-based Alloys

The addition of W may increase the room-temperature strength and high-temperature strengths of the TiAl alloy [48-49], but may decrease the room-temperature ductility [50]. Furthermore, the addition of W improves the oxidation resistance [47] and enhances the creep resistance [52].

2.4.1.3 B in TiAl-based Alloys

B has a significant effect on the grain refinement of TiAl alloys [54, 57]. Also the addition of B can strengthen the alloy by forming secondary TiB_2 particles [58]. The morphology of TiB_2 particles has a great influence on the microstructure and mechanical properties of the TiAl alloy [55, 56, 59, 60].

2.4.1.4 Si in TiAl-based Alloys

Si can increase the oxidation resistance of the TiAl-based alloy. With the addition of Si, the fine condensed oxidation film can be formed on the surface of the TiAl-based alloy. The oxidation film is composed of alternated TiO_2 and Al_2O_3 layers, and the Al_2O_3 layer is condensed. These layers made the diffusion rate of the oxygen into the alloy slow, and, thus, lowered the oxidation rate [61]. High Nb containing alloys can form condensed Al_2O_3 films, and the TiO_2 particles in the oxidation film are fine and uniform. Si tends to refine these TiO_2 particles. The more Si added, the more refined these particles are. Si can lower the oxidation rate of alloys. However, as the concentration of Nb increases, the beneficial effect of Si decreases. In this case, Si is more effective in binary alloys and low Nb alloys.

2.4.2 Heat-treatment Techniques

Recent heat-treatment techniques are: quench-temper/aging heat-treatment and cyclic heat-treatment. For quench-temper/aging heat treatments, it is separated into two

steps: first quench the alloy at a temperature above T_α, and then let the alloy slow cool at a temperature above T_α, in the $\gamma+\alpha$ two-phase region or the $\gamma+\alpha_2$ two-phase region. In this technique, microstructures obtained during quenching are essential to the refinement of the alloy, and the non-continuous coarsening of microstructures during slow cooling is also important to the refinement.

The cyclic heat treatment of the TiAl-based alloy refers to the cyclic heat-treatment of the steel, and it is based on the phase transformation during heating and cooling. In the TiAl-based alloy, the cyclic heat-treatment temperature is chosen at the transformation temperature, T_α, or eutectic temperature, T_e. γ-TiAl has a FCT structure, α_2-Ti_3Al and α-TiAl have HCP structures. During the heat treatment, the HCP structures, α_2, and the α phase precipitate from the four faces of the FCT γ phase. Since the growth of the α_2 and α phases are different in the directions, the growth is restricted, and thus, the α_2 and α particles from the γ phase are refined. During cooling, the γ phase precipitates from the α_2 and α phases, with a refined grain size than before. When heat-treated afterwards, the α_2 and α phases will, then, again precipitate from the γ phase in four favorable directions. The grain size is, then, refined. So, as the cycle goes on, the more refined the alloy will be.

2.4.3 Thermal-Mechanical Techniques

In thermal-mechanical techniques, alloy crystals are refined through the dynamic recrystallization. The original ingots can be the as-cast or powder-metallurgy

sintered ones. Thermal-mechanical methods are the most commonly used techniques in grain refinements. It mainly includes iso-thermal forging and hot extrusion.

Before any thermal-mechanical treatments, the ingots must be HIPed for the homogenization. The homogenization is usually processed in the α phase region or the α+β region. HIPing conditions typically needed are: $1{,}260^{0}$C/175 MPa/4 h. For the Al content smaller than 46 at.%, the HIPing temperature can be lowered.

The iso-thermal forging is the most commonly used thermal-mechanical method. For TiAl-based alloys, iso-thermal forging parameters are: the compression ratio of 4:1 ~ 6:1; the temperature range of $1{,}065 \sim 1{,}157^{0}$C; the deforming rate of $10^{-3} \sim 10^{-4}s^{-1}$. To obtain uniform microstructures, multiple forging processes in different directions are adopted. As-cast ingots needed more procedures in iso-thermal forging than powder-metallurgy ingots. The previous ones need 15 ~ 20 times of forging, while the later ones need only 3 ~ 5 times.

In TiAl-based alloys, the temperature for hot extrusion is usually higher than the temperature used for iso-thermal forging. The parameters for hot extrusion are: a handspike speed of 15 ~ 50 mm/s; a compression ratio of 4:1 ~ 12:1; a preheated temperature of $1{,}050 \sim 1{,}450^{0}$C. The research group of Dr. C. T. Liu has found that hot-extruded CTI-8 alloy has a better strength and ductility than other lamellar or duplex structured alloys. At the same time, it also bears a better high-temperature creep resistance than other lamellar or duplex structured alloys [60]. The greatest problem of the hot extrusion technique is that the microstructure of the alloy is not uniform. This trend leads to an uneven distribution of grains. With the use of coating, this tend can be

reduced, but not eliminated. Equal-angle pressing is a newly developed technique, which is useful to refine the grain size of the TiAl-based alloy. But through this technique, the extent of cracking of alloys is severe, and the improvements need to be conducted.

2.4.4 Powder-Metallurgy Technique

The powder metallurgy technique is a near net shaping method. It is also an important technique to produce alloys of refined microstructures. It is suitable for various materials, especially the brittle materials, which are difficult to deform, such as the ceramics, sintered-carbides, and intermetallics.

The powder-metallurgy (PM) technique includes the powder production and consolidation. The source of the powders for TiAl-based alloys includes: the mixture of the Ti and Al powders, mechanical-alloying powders, the rapid solidification of pre-alloy powders, rotation-electrode-atomization powders, and other additional elemental powders. The consolidation of the TiAl-based alloys includes: the sinter-reaction method, the high-temperature exploding method, the hot-pressing method, and the hot iso-thermal pressing, etc. Usually, the smaller the original powder, the more refined the TiAl-based alloy microstructures are. Consolidated alloys can be hot forged, hot extruded, and hot rolled. With the use of PM, sub-micron crystalline TiAl-based alloys can be obtained.

2.4.5 Surface Treatment of the TiAl-based Alloys

After decades of developments, many surface-treatment methods of TiAl-based alloys have been found. They are mainly: gas carburization; iso-ionic carburization; carbon-laser-surface alloying; alumetizing; gas nirtiding; ionic nitriding; nitrogen-laser-surface alloying; ionic infuse of B, C, N, and O acidation; coating; and boriding, etc.

After alumetizing, the surface of the TiAl-based alloy is mainly the $TiAl_3$ phase, a small amount of the TiAl, and the Ti_3Al phase with low Al contents. After the high-temperature alumetizing, the surface of the TiAl-based alloy is composed of condensed Al_2O_3 films, which can protect Ti from being oxidated, and greatly enhance the oxidation resistance of the alloy. But since there is a difference in the hot-expanding coefficient, between the base alloy and the surface layer, the crack may be initiated. How to eliminate the cracks has been a major problem to be solved.

Research has been conducted, regarding the influence of phosphoric and sulfuric acids on the high-temperature oxidation resistance of the TiAl-based alloys, after air drying and calcinations. After the phosphoric treatment, the oxidation rate is ten times less in the TiAl-based alloy at 800 ~ 900^0C, and there is no oxide film peeling off through the cyclic heat treatment at 850^0C after 200 h. The phosphoric treatment can enhance the oxidation resistance of the alloy through the formation of the Al_2O_3 -rich film, which has a condensed structure and adheres closely to the base alloy. Compared with other techniques, the phosphoric treatment is easy to perform, inexpensive in cost, and suitable to complex shaped alloys [61].

The low-partial-pressure oxidation is to oxidize the TiAl-based alloy at high temperatures for a short period of time, under low oxygen pressures. This procedure forms an Al_2O_3 film on the surface of the alloy, which can enhance the oxidation resistance. The thickness of the film formed through this procedure is limited, it cannot restrict the out diffusion of Ti, and thus, impairs the oxidation resistance of the alloy.

The infiltration of B can enhance both the oxidation and abrasion resistances of the TiAl-based alloy. Research on boriding the alloy at 900 ~ 1,100^{0}C for 5 ~ 11 h shows that, after 900^{0}C/11h, the hardness of the sample is 2,720 Vickers-hardness, which greatly increased the abrasion resistance of the alloy [62]. Samples also showed a good oxidation resistance at 1,000 and 1,050^{0}C.

Carburizing the TiAl-based alloy can enhance the oxidation resistance of the alloy. This trend is due to the formation of the Al_2Ti_4C and Al_4C phases after 2 h of carbonization at 900^{0}C [63]. These phases are tightly combined with the base alloy, prevent oxygen from contacting with the alloy, and, hence, improve the high-temperature oxidation resistance.

The iso-ionic carburization of the TiAl-based alloy for 1 hr can form a 3 μm Ti_2AlC film, which can protect the alloy from oxidation. Its hardness exceeds HV836 [64].

Gas nirtiding is an effective way to improve the abradability of the TiAl-based alloy [65]. With the use of the x-ray spectroscopy, TiN, $TiN_{0.90}$, and Ti_2AlN have been determined. For alloy MJ47, after gas nirtiding at 927^{0}C for 100 h, its hardness can

reach 1,391.3 kg/mm^{-2}. The hardness increases, as the time of nitrizing increases. The abrasion test shows that the abrasion width deceases for 99.84% after gas nirtiding.

The surface treatment of the TiAl-based alloy can enhance the high-temperature oxidation and abrasion resistances. Besides the techniques listed above, coating is another preferable method. The most optimal coating material is the Ti_2Al-based alloy. It has the best chemical and mechanical compatibility with the γ basis, and can form continuously Al_2O_3 films, which can prevent the oxygen/nitrogen embrittlement. The Ti-Al-Cr-based coating has gained the approval. But the optimal composition, which has a good mechanical property and remains a good fatigue life, is still in search.

2.5 Refinement of the Microstructure of the TiAl-based Alloys

The most practically used TiAl-based alloys are the as-cast ones. But since as-cast alloys usually have large grain sizes, refining the intermetallic alloy is an essential subject. There are mainly three methods used in the refinement of the TiAl alloys.

One of the methods is to alloy the TiAl intermetallics with additional elements, which could be an effective way to refine the microstructures. The cyclic heat treatment (CHT) is another method used. It is well known that the uniform fine grain duplex γ-TiAl alloys exhibit an adequate tensile ductility. Fine fully lamellar (FFL) microstructures could be obtained by the method of the cyclic heat treatment in the α+γ phase field. But its difficulty in controlling the tendency to form cracks has impeded its wide industrial applications. Using the improved cyclic heat-treatment technology, a series of fine duplex microstructures with grain diameters about 20 μm were obtained.

With the increase of the number of heat-treatment cycles, the uniformity and the spheroidicity of the materials were largely improved, and a duplex microstructure of the γ-TiAl alloy with varied fractions of lamellar structures could be obtained by changing the time and temperature of the cyclic heat treatment [65, 66]. The third method employed is to deform the TiAl intermetallic alloy in order to refine the grain size, using techniques, such as iso-thermal forging, rapid forging, or hot extrusion. Iso-thermal forging is a dynamic-processing procedure to refine the grain size, which is conducted at a static high temperature. The shear strain and heavy bending in the lamellar structure of the γ-TiAl alloy can be induced by the heavy deformation during hot working. The shear strain, which is parallel to the boundaries of the lamellar structure, can make the lamellar structure produce a great amount of dynamic recrystallization structures.

The mechanism of the cyclic heat treatment is: (1) For each cycle of the heat treatment, the concentration of the two phases, the α and γ phases, will change. This kind of change depends on the nucleation and growth of the new grains, so as to be subjected to the new phase balance. (2) Dislocations, twins, and stacking faults, which were trapped in the α+γ phases through the heating and cooling procedures, are the nucleation spots for new grains. As the new grains are generated, the number of grains per unit volume will increase, thus, refining the grain size of the alloy. The merits of CHT are: this procedure of refinement does not need any mechanical process, so that the usage of the material is more efficient. Since the alloys used in CHT are the as-cast material, the shape of the alloys can be complex, and the casting equipments could be

simple. The disadvantages of CHT are: cyclic procedures can cause the over-consumption of the energy; the multiple procedures can lead to crack initiation; and since the alloys are usually large in size, the homogenization of microstructures in the alloys is hard to obtain [68, 69].

For the isothermal forging, the grain size of the TiAl alloys is refined through the dynamical recrystallization. The merit of this procedure is: it is a preferable way to process brittle materials, since the alloy is kept at a higher temperature, and the speed of pressing is kept even. But the iso-thermal forging will initiate small cracks, and microstructures are not homogenized [70].

The rapid canned forging of TiAl alloys is a repeated treatment of the rapid forging and heat treatment. It can refine the grain size and obtain different kinds of microstructures at the same time. With the use of this method, the grain size can be efficiently reduced from thousands of micrometers to ten micrometers. The microstructures of the alloy can be homogenized. Because of the coating, there is no crack initiated [71].

Alloying the TiAl intermetallics with different kinds of elements can refine the grain size. With the combination of heat-treatments, different microstructures with desirable mechanical properties can be obtained. In this research, niobium, tungsten, and boron are added to the TiAl alloy, and with scheduled heat treatments, the related microstructure and mechanical property changes are being investigated.

3. Experimental Procedures

3.1 Alloy Preparation

In order to strengthen TiAl alloys, reducing the Al concentration is effective in increasing the ratio of the α_2 phase composition. However, the toughness deteriorates, if the Al concentration is reduced too much. More than 45 at.% Al is required in order to secure toughness. The strength of the TiAl alloy is improved with the increase of the Nb concentration, but the elongation decreases. The oxidation resistance of TiAl-Nb alloys is improved up to 7.5 at.% Nb. It is accordingly concluded that 7.5 at.% is an optimal concentration of Nb. The B addition alone refines the lamellar structure, but causes fragmental and discontinuous α_2 lamellae. In contrast, the W + B addition refines the lamellar structure and produces more uniform and continuous α_2 lamellae.[46] In this research, the base TiAl intermetallic alloy is Ti-45at.%Al-7at.%Nb- χ at.%W-0.15at.%B (χ = 0, 0.2, 0.4, 0.7, 1.1, and 1.5). TiAl-based samples fabricated at the Oak Ridge National Laboratory (ORNL) by Dr. C. T. Liu are labeled as:

#52 Ti-45at.%Al-7at.%Nb-0.2at.%W-0.15at.%B

#53 Ti-45at.%Al-7at.%Nb-0.4at.%W-0.15at.%B

#54 Ti-45at.%Al-7at.%Nb-0.7at.%W-0.15at.%B

#55 Ti-45at.%Al-7at.%Nb-0.15at.%B

#56 Ti-45at.%Al-7at.%Nb-1.1at.%W-0.15at.%B

#57 Ti-45at.%Al-7at.%Nb-1.5at.%W-0.15at.%B

All alloys were prepared by arc melting and drop casting, using pure Ti, Al, W, and Nb metal lumps together with the semiconductor-grade boron. Alloy buttons were

melted at least 5 times and then drop cast into a copper mold with an ingot size of 12.7 x 12.7 x 76.2 mm.

3.2 Nondestructive Detection

γ-ray nondestructive detection has been conducted to study the inner defects of the samples. Ts-1A type γ-rays are in use for the detection. The diameter of the beam spot is 3 mm.

3.3 Hot Isostatic Pressing (HIP) and Homogenization Treatments

The equipment used for HIPing is QIF-6 produced by the ABB company. Samples are HIPed under the conditions of: argon atmosphere, $1{,}250^0$C, 150 MPa, 4 h, and furnace cooling. After HIPing, a homogenization treatment is conducted at $1{,}250^0$C for 16 h in air, followed by furnace cool to room temperature.

3.4 Differential Thermal Analyses (DTA)

Based on the differential thermal analyses (DTA), the phase-transformation temperatures were roughly estimated. Combining the microstructure with the desirable grain size, proper heat-treatment temperatures can be determined. With the comparison of microstructures after each heat treatment, a more accurate phase-transformation temperature, such as T_α, can be obtained. The DTA & DSC machine is used for the test. The experimental conditions are: a heating rate of 20^0C/min. with an argon atmosphere, and the reference sample is an Al_2O_3 powder.

3.5 Heat Treatments

The TiAl-based sample alloys are hot-isostatic pressed (HIPed) at 1,250^{0}C, for 4 h at a pressure of 150 MPa, and then, heat-treated at 1,250^{0}C for 16 h for homogenization. The heat-treatment temperatures for the sample alloys have been scheduled as: at 900^{0}C for 360 h; at 1,265^{0}C for 18 h; at 1,280^{0}C for 14 h; at 1,295^{0}C for 10 h; and at 1,310^{0}C for 5 h. Most alloy samples were encapsulated in quartz tubes at a low inert-gas pressure. A small group of samples were heat treated in a vacuum furnace (10^{-6} torr). Some specimens were cooled in air after heat treatments, and others were quenched by immersing capsules in water.

3.6 Measurements of the Grain Size and Lamellar Spacing of the Heat-treated Samples

As the concentration of the W changes, the grain size and alloy phases (such as the β phase) will change accordingly. With the use of a linear intercept method, the grain size of the alloys will be measured. The colony size has a major effect on the tensile ductility of the alloy. The smaller the colony size, the better the ductility is expected. The tensile strength and fracture toughness are related more to the lamellar spacing. The smaller the interlamellar spacing, the better the tensile strength and the fracture toughness are.

3.7 Hardness Measurements

Hardnesses of the metallographically-mounted specimens were measured, using a diamond-pyramid hardness tester under a 10 Kg load.

3.8 X-ray Diffraction Analyses (XRD)

For powder samples, small smashed alloy pieces are chosen to grind into powders for the X-ray diffraction analyses. But for bulk samples, they are just grinded and polished. The Rigaku D/max 2550VB+X X-ray diffraction machine is employed for the analyses. Testing conditions are: Cu Kα radiation; nickel filter; voltage 40 KV; electrical current 300 mA; scanning rate 8^0/min.

3.9 Metallographic Analyses

Specimens were prepared for optical microscopy by conventional grinding and polishing, using a 0.5 μm diamond paste, followed by etching with Kroll solution, 1%HNO_3+1%HF +98%H_2O (vol.%). Metallography was done on the REICHERT MeF3A optical microscope.

3.10 Scanning-Electron Microscope (SEM) and Electron Microprobe

The SEM and electron microprobe are used for more detailed analyses of the specimens. The preparation for the specimens is the same as that for the metallography. For the backscattering detection, specimens do not need any etching. For the secondary-electron detection, a Kroll solution is used for etching. JSM-5600LV is employed for

the SEM analyses, with an acceleration voltage of 20 KV. The JCXA-733 Microprobe is used for more detailed microprobe analyses. The electron beam used is 2 μm in size, the electric current is 100 μA, and the working voltage is 20 KV.

3.11 Transmission-Electron Microscopy (TEM)

In order to obtain the more detailed structure information of the specimens, the TEM analyses are performed. Specimens are spark eroded into slices with a diameter of 3 mm, and a thickness of 0.3 mm, then mechanically thinned into 35 - 45 μm. Foils for TEM are prepared with a twin jet electropolishing, using a solution of a 30% nitric acid plus 70% methanol (volume percent), operating at -20^0C, 100 mA, and 30 V. Hitachi H-800 TEM (200 KV) is used for the TEM analyses.

3.12 Field-Emission-Electron Microscopy

For more detailed structure and composition analyses, a field-emission-scanning microscope, Sirion200 (20 KV), is used. The GENESIS 60S energy spectrometer is employed for the composition analyses. Specimens prepared for field-emission scanning are the same as those for metallography. Samples for the backscattering analyses are not etched.

4. Experimental Results

4.1 As-cast Structure of the Alloys

From the binary phase diagram of the TiAl-based alloy, two main phases, α_2 and γ, are formed under the equilibrium condition, and the microstructure contains the equiaxed γ phase and the lamellar structure. But for as-cast alloys, which are fast cooled, non-equilibrium structures, such as cellular structures and dendrites, are formed. As shown in Fig. 7, the as-cast Ti-Al-Nb-W-B contains cellular structures, lamellar structures, and dendrites.

Figure 8 presents the backscattered images of the as-cast Ti-Al-Nb-W-B alloys. Small amounts of casting defects and porosities are shown by the arrows. Under the backscattering condition, the contrast grade is in the positive correlation with the coordinate number of the elements. The greater the coordinate number, the brighter the image is. In Fig. 8, the boundary of the cellular structure is bright, which indicates that heavy metal elements, such as Nb and W, are enriched in this area. Furthermore, ribbon-shaped phases can be found in the structure of the alloys. These phases are consistent with the boride structures mentioned in references [46, 47]. They are the Ti-B boride phases, shown in the area A of Fig. 8 (b), as the ribbon shaped phase. Since these boride phases are bright, heavy metals must be present. Comparing the Figs. 8(a), (b), (c), and (d) as the amount of W differs, the structure of the as-cast alloys varies. In Fig. 8(a), when no W is added into the alloy, the cellular interfaces of the alloy are bright, indicating that there is a strong segregation of Nb at the grain boundaries. As the amount of W increases, cellular structures also tend to grow, and the brightness of the

interface increases. Since the composition of Nb is kept constant, W tends to segregate more in the dendrites, as its amount increases.

4.2 Microstructures of the Alloys after HIPing and Homogenization

The as-cast TiAl-based alloys contain defects, such as porosities and composition segregations. These defects can be eliminated after HIPing and homogenization. Figure 9 shows the secondary-electron image of the Ti-Al-Nb-W-B alloy after the treatments. A comparison of Figs. 8 and 9 shows that, porosities in the as-cast alloy disappear after HIPing and homogenization, indicating that the alloy is densified. Structure defects, such as cellular structures, dendrites, and composition segregations all have disappeared. From the above results, HIPing and homogenization are effective ways to eliminate the defects from casting. Figure 10 shows the backscattered electron images of the Ti-Al-Nb-W-B alloys after HIPing and homogenization. Microstructures presented in the figure is composed of the lamellar structures, which are composed of black and white ribbons; the white blocky structures, which have the β phases and distributed mainly at the ends of lamellar structures; and the bright needle-shaped structures, which are borides, distributed in the grains or at the grain boundaries.

As shown as in Figs. 10(a), (b), (c), and (d), as the content of W differs, the equilibrium structure of the TiAl-based alloys varies. Presented in Fig. 11, with the content of W increasing from 0 at.% to 0.2 at.%, 0.4 at.%, and 0.7 at.%, the colony sizes are 70 μm, 50 μm, 32 μm, and 25 μm, respectively; and the interlamellar spacings are

2.46 μm, 2.35 μm , 2.28 μm, and 2.08 μm, respectively. With the addition of W, the microstructure of the Ti-Al-Nb-W-B alloy refines. As the content of W increases, the grain size and the interlamellar spacing decrease. As the amount of W exceeds 0.4 at.%, the trend of the refinement slows down.

From Fig. 10, the colony size tends to change, as the amount of W varies. However, the size of the equiaxed γ phase does not change much. The difference in the W content leads to changes in the shapes of bright phases (later identified as the β phase and borides), especially in the amount of these phases. The volume fraction of these phases increases, as W increases.

To obtain more information of the phase compositions, the energy-dispersive X-ray spectroscopy (EDS) attached to SEM, the electron microprobe, and the field-emission microscope are employed. In the lamellar structure, the γ lamellae has a higher Al content and lower W content; the α_2 lamellae has a higher W content and a lower Al content (Figs. 12 and 13). For more accurate phase analyses, the electron-microprobe analyses are conducted in micro-areas (Fig. 14). Points 4 ~ 6 are γ phases (equiaxed γ and γ in the lamellae); Point 7 is the α_2 in the lamellae. The microstructure for a duplex structure, composed of the α_2/γ lamellae and primary equiaxed γ phases, which are dispersed along the colony boundaries. Furthermore, bright phases are detected at the grain boundaries and in the grains, Points 1 ~ 3 in Fig. 14. More accurate analyses in structure are conducted, using the field-emission scanning electron microscopy. In Fig. 15 (a), bright needle-shaped phases contain 7.74 at.% of Al, 20.27 at.% of Nb, and 6.79 at.% of W. From the shape and content, these phases could be borides. Beside these

needle-shaped phases is the hexagonal phase, which has the same composition as the boride, and, thus, could be the cross-section of the boride. The gray phase in Fig. 15(b) contains 49.54 at.% of Al, which exceeds the amount of 42.45 at.% of Ti, and the amount of other elements are the same as the base alloy. Small cracks are also observed. The gray phase is determined to be the γ phase. γ twin-phases can be triggered to form in regions beside the borides, as exhibited in Fig. 15(c). This trend might be caused by the capture of Ti by B, which can lead to a fast decrease of Ti in the boride-surrounding region, and trigger the formation of the high-Al, low-Ti γ twins. Bright ellipsoid-shaped phases are observed in the figure, which contain greater amounts of W (3.46 at.%) and Nb (12.95 at.%), a lower amount of Al (31.77 at.%), and about the same amount of Ti, relative to the base alloy. The shape of these phases differs from the borides (which are usually long in shape and have polygon cross sections). These phases contain more Al than in the borides, and, thus, identified as the β phases. Figure 17, using a more accurate electron superprobe (15 KV), with the alloy containing 0.7 at.% W (alloy #54), shows detailed compositions of the boride and β phase. The bright phase with compositions of Ti-1.0 at.% Al-9.6 at.% Nb-3.6 at.% W-51.9 at.% B can be determined as borides. The other bright blocky phases, which have different shapes, as compared with the boride, composed of Ti-35.7 at.% Al-8.5 at.% Nb-1.7 at.% W, can be determined as the β phase. No β phases with these characteristics are found in the samples containing 0.4 at.% W. Thus, the β phase tends to form at an amount above 0.4 at.% of W.

4.3 Microstructures of the Alloys after Heat Treatments

After HIPing and homogenization, Ti-Al-Nb-W-B alloys are heat-treated at scheduled temperatures of: 900^0C for 360 h; $1{,}265^0$C for 18 h; $1{,}280^0$C for 14 h; $1{,}295^0$C for 10 h; and $1{,}310^0$C for 5 h. Microstructures and their evolution are examined.

Microstructures of the Ti-Al-Nb-W-B alloys heat treated at 900^0C for 360 h after HIP and homogenization are shown in Fig. 18. Compared with microstructures before the heat treatment, there is not much difference. It is still mostly composed of lamellar structures. The γ phase in samples containing 0.7 at.% W tends to coarsen and congregate, compared with samples containing 0.2 at.% W.

After the heat treatment at $1{,}265^0$C for 18 h, Ti-Al-Nb-W- B alloys contain a less amount of γ lamellae structures (Fig. 19) as compared with that in Fig. 18. Since specimens are kept in the α+γ two-phase region for some time, the α_2 and γ phases tend to grow, and the lamellar structure coarsens. Note that there is no significant increase in the colony size by this heat treatment. The volume fractions of β phases and borides decrease.

Microstructures of the Ti-Al-Nb-W-B alloys, after the heat treatment at $1{,}280^0$C for 14 h, indicate that the lamellar structure tends to coarsen greatly, and the grain size also grows (Fig. 20). When the Ti-Al-Nb-W-B alloy is heat treated at $1{,}280^0$C, the microstructures are composed of mostly lamellae and a small amount of the equiaxed γ phase, which belong to a nearly fully lamellar structure. Even though the specimens are

annealed for a long time, there is not much change in the colony size of the alloys, but the lamellae tend to coarsen, and the interlamellar spacing increases.

Figure 21 presents the microstructures of the Ti-Al-Nb-W-B alloys after the heat treatment at $1{,}295^0$C for 10 h. Fine equiaxed γ phase almost disappeared, and the structure is mainly composed of the fully lamellae $\alpha_2+\gamma$. The colony size of the alloy coarsens significantly, and the average grain size reaches 400 μm. The segregation phases (β phases and borides) decrease and widely disperse along grain boundaries and in grains.

After the heat treatment at $1{,}310^0$C for 5 h, the microstructure of the alloy, composed of fully lamellae, further coarsens. The grain size reaches 500 μm, shown in Fig. 22. Segregation phases decrease even more.

From the above observations, the grain size of the Ti-Al-Nb-W-B alloy coarsens significantly, and the microstructure changes from the nearly fully lamellar to fully lamellar structures, between the temperatures of $1{,}280^0$C and $1{,}295^0$C. This observation indicates that the α transus temperature, T_α, is about $1{,}290 \pm 5^0$C, not sensitive to the W concentration.

In summary, the phase compositions of the TiAl alloys, related to the heat treatments and tungsten contents are listed in Table 3. Heat treating the TiAl-based alloys below the α transus temperature, T_α, the phase composition of the 0 to 0.4 at.% W alloys consist of the primary γ phase and $\alpha_2+\gamma$ lamellae. The 0.7 at.% W alloy contains the β phase, in addition to the primary γ phase and $\alpha_2+\gamma$ lamellae. When the alloys are heat treated at a temperature above T_α, the phase composition of the 0 to 0.4

at.% W alloys consist of fully lamellar structure $\alpha_2+\gamma$. The 0.7 at.% W alloy contains a small amount of the β phase which tends to decrease as the heat-treating temperature increases, in addition to the fully lamellar structure $\alpha_2+\gamma$.

4.4 Differential-Thermal Analyses (DTA)

In order to determine the α transus temperature, T_α, of the alloy, the heat treatments in the $\alpha+\gamma$ phase region and single-α phase region are previously conducted. Through the differential-thermal analyses (DTA), T_α, can be determined by the decalescence during the phase transformation of the alloy. Results are shown in Fig. 23. In the temperature range of $1,280^0$C ~ $1,295^0$C, a decalescence reaction is found. Thus, T_α, is estimated to be $1,290 \pm 5^0$C.

4.5 X-ray Diffraction Analyses (XRD)

Presented in Fig. 24 are the X-ray diffraction analyses (XRD) of the #54 sample (0.7 at. % W) after HIPing and homogenization. The diffraction pattern in Fig. 24 shows that the alloy is mainly composed of the γ-TiAl phase and α_2-Ti_3Al phase. Through EDS and EPMA, the substance similar to the β phase has been detected, but no (110) peak corresponding to the β (β_2) phase is found in the XRD. This result might be caused by the insufficient amount of the β phase (< 5 %), which cannot be shown in the XRD analyses.

4.6 TEM Analyses

The TEM structure of Ti-Al-Nb-W-B alloys after HIPing and homogenization is exhibited in Figure 25. The content of W has a great effect on the lamellar structure. As W increases, the interlamellar spacing decreases. This observation matches the results of Fig. 10.

Figure 26 indicates the segregation phases of the Ti-Al-Nb-W-B alloy. Figure 26(a) exhibits the γ twins segregated from the α/γ lamellae grains. Figure 26(b) shows the borides formed in the α/γ lamellae and the triggered γ twins. These results match those by the field-emission-electron microprobe.

4.7 Mechanical Property

Hardness tests have been conducted on the Ti-Al-Nb-W-B alloys with different W contents after the heat treatment at $1{,}280^{0}$C for 14 h. The results are presented in Fig. 27 (a). It is clearly shown that, as the amount of W increases, the hardness of the alloy also increases. This trend indicates that W can strengthen the alloy. Hardness of the alloy is also related to the microstructure of the alloy. Shown in Fig. 28, as the interlamellar spacing decreases in the TiAl-based alloys, the hardness of the alloys increases. This trend indicates that the hardness is sensitive to the changes in the interlamellar spacing of the alloys. Other mechanical experiments, such as the tensile test, will be performed on later.

5. Discussion

5.1 Microstructures of the Alloys

5.1.1 Effect of HIPing and Homogenization on the Microstructures of the As-cast Alloys

From the Ti-Al binary phase diagram (Fig. 1), the equilibrium condition of the TiAl-based alloy containing 45 at.% Al mainly consists of two phases, the α_2 and γ phases, resulting in the formation of the lamellar structure. In the as-cast condition, the TiAl-based alloy is composed of typical non-equilibrium structures. The addition of B in the TiAl-based alloy can cause the in-situ formation of TiB_2 in the melt. Since the melting temperature of TiB_2 is high ($3{,}253^0$C), it is surround by the TiAl melt during casting and can induce the heterogeneity nucleation during cooling. Under the condition of drop casting, the cooling rate of the Ti-Al-Nb-W-B alloy is very fast, and a peritectoid reaction is involved, as the TiAl alloy cools down. This trend made the compositions within the colony and between the colonies not uniform. Non-uniform as-cast structures, such as the cellular structures and dendrites, are formed. W and other solutes are enriched at the cellular boundaries and the peripheries of the dendrites.

The Ti-Al-Nb-W-B alloys are kept at a high temperature ($1{,}250^0$C) and high pressure (150 MPa) during HIPing. The diffusion process takes place, and the defects, such as porosities in the as-cast material, are eliminated. Comparing Figs. 8 and 10, after HIPing and homogenization, the microstructure of the Ti-Al-Nb-W-B alloy has changed greatly. The lamellar structure after the treatments is more continuous, and the colony size of the lamellae refines. As-cast microstructures are non-uniform, and Nb

and W are richly dispersed in the α_2 phase, the β_2 phase, and in the borides. During Hipping and homogenization, the α phase preferentially nucleates at the metastable lamellae-colony boundaries, thus refining the as-cast coarse microstructure. After the homogenization, the Ti-Al-Nb-W-B alloy is fast cooled. The high-temperature α phase turns into a lamellar structure, and this trend made the inhomogeneous as-cast microstructure develops into a fine lamellar structure.

5.1.2 Effect of Heat Treatments on the Microstructures of the Alloys

The microstructures of the as-cast Ti-Al-Nb-W-B alloy are developed in a non-equilibrium condition within a γ matrix. The heat-treatment temperatures for the TiAl alloys have been scheduled as: 900^0C for 360 h; $1{,}265^0$C for 18 h; $1{,}280^0$C for 14 h; $1{,}295^0$C for 10 h; and $1{,}310^0$C for 5 h. According to the binary phase diagram of the Ti-Al alloy, above the eutectoid temperature (T_e, approximately $1{,}175^0$C), as the heating temperature increases, the fraction of the γ phase tends to decrease, as the amount of the α phase increases in the Ti-45 at.% Al alloy. Heat treating the alloys below T_e, at 900^0C for 360 h, after the redistribution of the elements, the microstructure of the alloy is in an equilibrium condition. The microstructure of the alloy contains a blocky γ phase and α_2/γ lamellae, with the γ phase as the matrix. There is not much change in the grain size (Fig. 18).

After heat treating the alloy above T_e, at $1{,}265^0$C for 18 h, the matrix of the alloy tends to change from the γ matrix to α matrix. The microstructure of the alloy is made up of the blocky γ phase and α_2/γ lamellae. The grain size does not change much in the

alloy, but the interlamellar spacing tends to increase (Fig. 19). This is because above the eutectoid point, the concentration of the α (α_2) phase is higher than at room temperature. Since the γ phase is the $L1_0$ structure, it has four close-packed {111} planes. The α_2 phase has a $D0_{19}$ structure with only one close-packed plane (0001). At a heat treating temperature above the eutectoid point, the α phase tends to precipitate from the four close-packed planes of the γ phase. The lamellar structure is formed from the α phase at the eutectoid point of $1{,}175^0$C, $\alpha \rightarrow \alpha_2 + \gamma$, with an orientation relation of: $\{111\}_\gamma$ // $(0001)\alpha_2 <110>_\gamma$ // $<1120>\alpha_2$. Since the $\alpha \rightarrow \alpha_2$ change is an ordered transformation, the required degree of the supercooling and energy is small. But the γ phase has a different crystal structure from the α phase, and a large amount of supercooling and energy is needed for atoms to transfer and diffuse to nucleate and grow. In a large amount of supercooling, the γ phase does not have enough time to precipitate from the α phase, nor to grow. Thus the volume fraction of the α_2 phase increases. In a region approaching the single-α phase region, it is more difficult for the γ phase to grow, and a greater volume fraction of the α_2 phase forms. When heat-treating the alloy below T_α, there is little difference in the colony size, but as the α_2/γ lamellae inside the colony tend to be equiaxed, the lamellae coarsen.

After heat-treating the alloy at $1{,}280^0$C for 14 h, the amount of the γ phase starts to diminish. The grain size of the alloy tends to grow, and the interlamellar spacing increases (Fig. 20).

After heat-treating the alloy at $1{,}295^0$C for 10 h and at $1{,}310^0$C for 5 h (Figs. 21, and 22), the microstructure of the alloy is composed of only a fully lamellar structure.

No primary γ phase is found in the alloy. The grain size tends to grow fast. This is because when the heat-treatment temperature exceeds the α transus temperature, T_α, the alloy enters the single-α phase region. Since the reaction γ→α takes place, almost all of the γ phase transforms into the α phase, and the α crystals tend to grow rapidly. During cooling, the reactions, such as α→α+γ, and α→α_2+γ take place. The microstructure of the alloy, being heat treated at a temperature above T_α, depends mainly on the cooling rate of the alloy. When the alloy is being cooled very fast, the phase transformation has been suppressed, and no γ phase will form. The microstructure of the alloy is composed of the supersaturated α phase, which later on will tend to decompose into martensite structures. If the alloy is cooled down in a medium pace, fine fully lamellae of α_2/γ lamellae will be formed. When the alloy is cooled down slowly, the reaction, α→α_2+γ, takes place completely, and the α_2/γ lamellae is equiaxed, a fully lamellar structure will be formed.

5.2 Determination of the α Transus Temperature

From the differential thermal analyses (Fig. 23), the Ti-Al-Nb-W-B alloy shows an endothermic reaction around the temperature range of $1,280^0$C ~ $1,295^0$C, and the peak appears at a temperature around $1,290^0$C. This reaction indicates that, a phase transformation occurs at $1,290^0$C in the Ti-Al-Nb-W-B alloys. Comparing the microstructures in Figs. 9 to 13, obtained from different heat-treatment temperatures (900^0C, $1,265^0$C, $1,280^0$C, $1,295^0$C, $1,310^0$C), the grain size does not change much for the 900^0C, $1,265^0$C, and $1,280^0$C heat-treatments, but it coarsens significantly at

temperatures above 1,280^{0}C. Apparently, there is a phase transformation in the Ti-Al-Nb-W-B alloy at a temperature above 1,280^{0}C and below 1,295^{0}C, which involves $\alpha + \gamma \rightarrow \alpha$. Based on the results from the heat treatments and differential thermal analyses, the α phase transus temperature, T_α, of the Ti-Al-Nb-W-B alloy is around 1,290 $\pm$ 5^{0}C.

5.3 β phase in the Alloys

The composition and structure of the β phase differs as the alloy composition and heat treatment change in the alloy. Particles at the α_2/γ boundaries appear to be the β phase ellipsoids [12]. This is because, the α_2/γ interface, which is enriched in W, is a favorable nucleation site for the β_2 phase. The composition of the β_2 phase in the ABB-23 alloy is 48.9 at.% Ti, 36.4 at.% Al, and 14.7 at.% W. Compared with the nominal composition, nearly 1/3 of the Al has been substituted by W, while the amount of Ti is similar to that in the γ-TiAl. The β phase composition of the Ti-45Al-6Cr (at.%) alloy after the heat treatment at 1,200^{0}C for 168 h is: 46.7 at.% Ti, 39.3 at.% Al, and 13.9 at.% Cr. For Ti-46Al-2Cr- 2Mo-0.25Si-0.3B (at.%) after the heat treatment at 1,150^{0}C for 48 h, the composition of the β phase is: 52.16 at.% Ti, 37.58 at.% Al, 3.7 at.% Cr, and 5.19 at.% Mo. From the above results, the β phase has a low Al content, and high contents of alloying elements, such as W, etc [14]. Figure 16 exhibits microstructures of the Ti-45Al-7Nb-0.7W-0.15B (at.%) alloy after HIPing and homogenization. The bright non-uniform ellipsoid-shaped microstructure has high contents of W and Nb, a low content of Al, and a similar amount of Ti, relative to the base alloy. It is different from

the borides, but close to the characteristic of the β phase. Hence, the ellipsoids can be β phases.

The β phase is a high-temperature residual phase, which exists as the β_2 phase at room temperature. The orientation relationships among the α_2 phase, γ phase and β phase are: $(0001)\alpha_2$ // $\{111\}\gamma$ // $\{110\}\beta_2$, and 〈1120〉 α_2 // 〈110〉 γ // 〈111〉 β_2. Compared with the γ phase, the composition of the β phase is closer to that of the α phase. This trend assumes that, when the β phase precipitates from the α phase, the composition fluctuation requirement is easier to meet, which is the reason why the β phase precipitated more often from the ends of the α phase. The research regarding the effect of Ru on the Ti-47Al alloy showed that for the Ti-47Al-1Ru (at.%) heat treated at $1{,}200^0$C for 24 h, the formation of the β_2 phase relies on the consumption of the α_2 phase. In the region where the β_2 phase forms greatly, the α_2 phase decreases accordingly. When the heat-treatment temperature exceeds the α phase transus temperature, T_α, the reaction, $\gamma \rightarrow \alpha$, happens. The grain coarsens fast in the single-α phase region. When the β phase precipitates dispersedly, the atoms do not need to move and diffuse in the alloy, and the energy needed is small. This is why the β phase disperses separately in the alloy at high temperatures.

5.4 Effect of Alloying Elements on the Microstructure and Mechanical Properties of the Alloys

5.4.1 Effect of Nb on the Microstructure and Mechanical Properties of the Alloys

One important characteristic of the Ti-Al-Nb ternary system is the formation of the ordered β phase, marked as β_0. The other characteristic of the ternary system is the presence of the orthorhombically structured phase, marked as O, which exists in a region where Nb > 11 at.% [43]. After continuously cooling the alloy, the α_2 phase can precipitate inside the β phase or at the grain boundaries. This trend is important in developing the favorable microstructure and mechanical properties of the alloy.

With the method of the substitutional solid-solution strengthening, the moving Peierls-Nabarro (P-N) force of dislocations (the force required to move a dislocation through the crystal lattice), and the critical shear stress, τ_{CRSS} (the threshold value of the shearing stress on the slip plane in the slip direction when slip begins), of the γ-TiAl-based alloys have been enhanced [45]. The Nb content in the high Nb-containing TiAl-based alloys significantly increases the elevated-temperature strength. The main effect of high Nb contents on high-temperature strengths relies on the increase of the value of σ_0 in the Hall-Petch equation:

$$\sigma_{0.2} = \sigma_0 + k_\lambda \lambda^{-1/2}$$

where $\sigma_{0.2}$ is the 0.2% offset yield strength, σ_0 and k_λ are material constants, and λ is the lamellar spacing. It means that the friction stress of moving dislocations arises mainly from the Peierls stress of the lattice, and the interactions between dislocations are much stronger than those for TiAl-based alloys with less Nb contents. The high Nb content

also improves the elevated-temperature stability of microstructures of the TiAl-based alloys, resulting in the improvement of the high-temperature strength.

Nb can improve the ductility of the alloy [46]. With the addition of Nb, the high-temperature phase, $\beta/\beta_{2,}$ of the body-centered-cubic (BCC) structure, with a good ductility, can be formed. Nb is also a beta-phase stabilizer, which has a higher concentration in the β phase [44]. Since the beta phase has a good ductility, by adding Nb, the ductility of the TiAl alloy can be improved. By cooling the alloy from a temperature higher than $1{,}100^0$C, the β_2 phase can be partly transformed into a triangularly structured ω phase. At the temperature of 700^0C, it can be transformed into a hexagonal phase of a B_{82} structure. With the combination of alloying and mechanical heat treatments, the phase composition and microstructure of the intermetallics can be controlled in order to enhance the ductility of the alloy at room temperature.

Niobium can improve the oxidation resistance of the alloy, because Nb^{5+} can replace Ti^{4+} in TiO_2, reduce the amount of anions, improve the protection of TiO_2, and facilitate the formation of Al_2O_3 [47]. Nb can lower the solubility of oxygen in the alloy, which can restrain the interior oxidation and improve the structure of the Al_2O_3 in order to form an interlinked reticulate structure. The structure change of the inner Al_2O_3 and the stability change of the outer Al_2O_3, which is linked to the TiO_2 layer, can lead to a large decrease in the oxidation resistance of the alloy. The amount of Nb to be added is generally determined from the oxidation resistance required.

5.4.2 Effect of W on the Microstructure and Mechanical Properties of the Alloys

The W addition in the Ti-Al-Nb alloy tends to segregate between the dendrites and facilitate the formation of the β phase, which can refine the lamellar colony. After the heat treatment, W is enriched in the β_2 precipitated phase. The β_2 phase can precipitate either in the grain, or at the boundaries of the equiaxed γ crystals [50]. W segregates at the interface of the γ/γ and α_2/γ phase, and it stabilizes the α_2 lamellae from dissolving during aging [48]. A small amount of W can enhance the room-temperature and high-temperature strengths of the Ti-Al-Nb-W alloy [48, 49]. But the addition of W can lead to structural segregations in the alloy. These segregations, such as the dendrites structures formed in the alloy, can initiate cracks [50], which deter the ductility of the alloy. An increase in the brittle-ductile transition temperature does not have much influence on the room-temperature ductility of the alloy.

The mechanism of enhancing the high-temperature oxidation resistance by W is similar to that of Nb [47]. W can effectively improve the oxidation resistance of the TiAl-based alloy, especially at 900^0C. With the increasing amount of W, the oxidation mass decreases. The oxidization surface, from the outer to inner sides, of the TiAl-based alloy, with the W addition, is: TiO_2/Al_2O_3 (continuous)/Al_2O_3 (reticular) + TiO_2/Ti_3Al/TiAl base alloy. At 900^0C, there is no oxidization occuring inside the alloy. The inner reticular Al_2O_3 is combined with the outer Al_2O_3 layer. This extended Al_2O_3 screen enhances the oxidation resistance of the alloy. At $1{,}000^0$C, a small amount of oxides are found in the TiAl-2 at.% W alloy. The addition of W can reduce the amount of oxygen in the alloy. W represses the initial growth of TiO_2, and facilitates the

formation of the outer Al_2O_3 layer, especially the inner reticular Al_2O_3 layer, thus enhancing the oxidation resistance.

Tungsten was found to improve the creep properties significantly [52]. The dynamic deformation controlled by dispersion slowed down by the W solute, and the creep resistivity of the alloy increased.

In this work, W tends to segregate between the dendrites of the TiAl alloy. In the as-cast lamellar structure of the alloy, W is enriched at the phase interface. Since the lamellar structure grows in a surface-step-kink mechanism, W can deter the growth of the new phase and, thus, refine the colony size and the interlamellar spacing. As the content of W increases, this effect becomes more obvious. W is a beta-phase stabilizer, which is distributed mainly in the β phase. The segregation of the β phase increases with the increase of W. During heat treatments, the growth of the β phase mainly relies on the α_2 phase. Hence, the β_2 phase is usually formed at the ends of α_2 phases, hindering the growth of the grain size and reducing the interlamellar spacing. From the wave-spectrum analyses, the solubility of W in the α phase is high. W has little influence on the precipitation and growth of the γ phase. Thus, W does not affect the size of the equiaxed γ crystal.

5.4.3 Effect of B on the Microstructure and Mechanical Properties of the Alloys

B can evidently restrain the grain growth of the α phase at and above the α phase transus temperature. The addition of B has become an effective way to refine the grain size of the TiAl-based alloy. The mechanism of refining the alloy by B can be explained

in many ways. The most accepted explanation is that, as the alloy solidifies, the high melting-point borides formed in the alloy will become the grain nucleation nucleus, which facilitates the refinement of the alloy. Boron is added into the TiAl-based alloys as an in-situ ceramic phase. It exists as borides, such as TiB_2, TiB etc., and segregate along γ/γ or α_2/γ interfaces, in order to refine the grain size [54]. A small amount of boron tends to dissolve in the α_2 and γ phase as strengthening phases, which can enhance the properties of the alloy. In lamellar TiAl-based alloys, the effect of the boron addition on room-temperature tensile ductilities depends predominately on the size of titanium-boride precipitates [55, 56]. Alloys with fine titanium-boride precipitates have good ductilities. This trend is due to the refinement in the grain size induced by the boron addition in both wrought and cast conditions. Large titanium-boride precipitates proved to be detrimental to ductilities. Cracking along large titanium-boride precipitates can suppress the beneficial effect reflected from the grain refinement. Any refinement in titanium-boride precipitates, i.e., breaking down long titanium-boride precipitates by thermomechanical processing, or limiting the boride-precipitate growth by fast cooling during solidification, will increase the ductility significantly. There is a threshold for the amount of B added to the TiAl alloy. As the content of B increases, the grain size of the annealed alloy refines more [57]. Room-temperature mechanical properties are also very sensitive to the addition of B. The addition of > 0.5 at.% of boron refines grain sizes and improves strengths and workabilities.

Pu found that the TiB_2 phase can be easily formed in the TiAl-based alloys [58], and no typical grain-boundary segregation of B in the as-cast alloys was found. The thermal deformation can facilitate the grain-boundary segregation of B, which leads to a restraint in the growth of grains. If the boron segregates along the γ/γ or α_2/γ phases as TiB_2, TiB, etc. in order to refine the grain size, the restraint mechanism is due to the formation of the second phase. If B dissolves in the α_2 and γ phases in the atomic state, which refines the lamellar phase, and improves the properties of the alloy, the restraint mechanism is due to the atomic aggregation. The combination of B and W in TiAl-based alloys can refine the lamellar structure, homogenize the lamellar spacing, and effectively enhance the thermal stability [59]. The B addition has a great effect on the grain uniformity. The research in the CTI-8 alloy by Liu et al. showed that, B has an important control over the lamellar structure of the TiAl-based alloy [60]. The amount of 0.1 at.% of B can help develop uniform microstructures in the alloy. With a less amount of B, the abnormal growth of grains will occur during thermal processing. The tensile ductility of the sample with a uniform grain structure more than doubles that with an abnormal grain structure.

In this work, borides can be found in the grains of different TiAl-based alloys. They are usually added into the alloy as alternatives to refine the grains. Borides in the TiAl-based alloys might refine the grain size through a heterogeneous nucleation mechanism. In the present research, W can refine the microstructure of the alloy. However, as the content of W increases to 0.4 at.%, the effectiveness of the refinement slows down. W is enriched in the borides and tends to make borides locate at the grain

boundaries, hindering the growth of the grains. A small amount of W can effectively impede the grain growth, and it is found that 0.4 at.% is most effective in refining the microstructures of the alloy.

5.5 Hardness of the Alloys

The hardness of the TiAl-based alloys is related to three factors: the interlamellar spacing, the colony size, and the alloy addition. The essential factor lies in the interlamellar spacing of the microstructure. As shown in Hall-Petch equation, $\sigma_{0.2} = \sigma_0 + k_\lambda \lambda^{-1/2}$, where $\sigma_{0.2}$ is the 0.2% offset yield strength, σ_0 and k_λ are material constants, and λ is the lamellar spacing. The yield strength of the alloy increases, as the interlamellar spacing decreases. Exhibited in Fig. 28, the hardnesses of the TiAl-based alloys are very sensitive to the changes in the interlamellar spacing. As the interlamellar spacing of the alloys slightly decreases, the hardness of the alloys increases. Alloy additions, such as W, in the TiAl-based alloys can increase the hardness of the alloy, shown in Fig. 27(a). W can effectively refine the microstructure of the alloys. As the amount of W increases, the colony size of the alloy decreases, leading to an increase in the hardness of the alloy. Thus, W strengthens the alloy by solution strengthening and grain-size refinement.

6. Conclusions

1. Cellular structures and dendrites are formed in the as-cast Ti-Al-Nb-W-B alloys [Fig. 7]. This is because the addition of heavy metals, such as Nb and W, increased the undercooling of the liquid phase, which triggered the formation of the cellular structure and dendrite at the solid-liquid interface. Nb and W tend to segregate strongly at the interface of the cellular structure [Fig. 8].

2. Porosities in the as-cast Ti-Al-Nb-W-B alloys can be generally eliminated by HIPing at $1{,}250^0$C [Figs. 8 and 10]. The cellular structures, dendrites, and macro-segregation of the alloys can also be eliminated after the HIPing and long-term homogenization at $1{,}250^0$C [Fig. 10].

3. After HIPing and homogenization, microstructures of the Ti-Al-Nb-W-B alloys consist of the equiaxed γ phase and lamellar structure of α_2/γ. The γ grains form mainly along the lamellar colony boundaries [Fig. 10(d)].

4. After the HIPing and homogenization, Nb and W are enriched in the α_2 and β phases, but they are depleted in the γ phase [Figs. 12, 13, and 16].

5. Ti and B have a strong chemical affinity. Ti and B in as-cast TiAl alloys tend to form Ti-B compounds, which are ribbon-like [Fig. 8, Point A]. The addition of B can refine the microstructure.

6. After the HIPing and homogenization, the boride tends to be uniformly distributed in the alloy, and is needle-shaped with a hexagonal cross section [Fig. 15 (a)].

7. Borides in the TiAl-based alloys tend to capture Ti from the base alloy, resulting in a decrease amount of Ti in the surrounding area and triggering the γ-twin formation around the borides [Fig. 15(c)].

8. A small additional amount of W can refine the grain size of the Ti-Al-Nb-W-B alloys. The lamellar spacing also decreases with increasing the W concentration. But as the amount of W exceeds 0.4 at.%, its beneficial effect becomes small [Figs. 10, 11, and 25].

9. The hardness of the alloy increases with increasing the W concentration. This trend indicates that W strengthens the TiAl-based alloys by solution strengthening and grain-size refinement [Fig. 27].

10. The addition of W promotes the formation of the β phase. When the amount of W exceeds 0.4 at.%, the β phase precipitates. The β phase in the blocky form mainly distributes along the grain boundary. Its composition is close to the α_2 phase, but with a less amount of Al [Fig. 17].

11. As the heat-treatment temperature is below Tα, the colony size of the lamellar structure does not change much. However, the coarsening of the lamellar structure leads to an increase in the interlamellar spacing. When the heat treatment is above Tα, the grain size increases sharply [Figs. 18~22].

12. From the results of microstructural changes related to different kinds of heat treatments, and differential-thermal analyses (DTA), the α transus temperature, T_α, is estimated to be $1{,}290 \pm 5^0$C [Figs. 20, 21, and 23].

13. The Ti-45Al-7Nb-0.15B-0.4W alloy is a newly developed TiAl-based alloy,

which has good properties and promising applications. A fine grain size can be developed using this composition without any hot deformations or cyclic heat treatments.

14. Related heat treatments can be selected to obtain desirable microstructures for the Ti-45Al-7Nb-0.15B-0.4W alloy. Fine fully lamellae, with good overall properties, can be obtained through heat treatments at temperatures slightly below T_α (T_α - 10^0C). Duplex microstructures can be obtained through heat treatments at temperatures slightly above the eutectoid temperature, T_e (T_e + 10^0C).

7. Future Work

In order to have a complete understanding of the relationship between the microstructure and mechanical properties of the alloy, the future research work on the promising Ti-45Al-7Nb-0.15B-0.4W alloy has been planned as follow:

(1) Produce large ingots of this TiAl-based alloy.

(2) Characterize the microstructures and determine the optimal heat-treatment conditions.

(3) Conduct mechanical testing, including tensile, creep, and fatigue experiments on the alloys.

(4) Study mechanical behaviors and identify key factors that control the deformation and fracture behavior of the alloys.

(5) Investigate the oxidation and corrosion behavior of the alloy at elevated temperatures.

(6) Establish a theoretical model for predicting the relationship between the microstructure and mechanical behaviors of the alloy.

References Cited

1) C. T. Liu, J. H. Schneibel, P. J. Maziasz, J. L. Wright, and D. S. Easton, “Tensile Properties and Fracture Toughness of TiAl Alloys with Controlled Microstructures”, Intermetallics, 1996, 4, 429 ~ 440.

2) C. M. Austin and T. J. Kelly, “Gas Turbine Engine Implementation of Gamma Titanium Aluminide,” Superalloys, Pennsylvania, TMS, 1996, 539～548.

3) D. E. Davidson, “Designing with Gamma Titanium CAESAR Program Titanium Aluminide Component Application,” Superalloys, Pennsylvania, TMS, 1996, 545～557.

4) M. Nazmy and V. Lupinc, “Gamma TiAl Intermetallic for Gas Turbine Applications,” Materials for Advanced Power Engineering, 1998, 933～941.

5) G. L. Chen, and J. P. Lin, “Physical Metallurgy of the Ordered Structural Intermetallic Compounds,” Metallurgy Industry Publish. Co., 1999.

6) K. Hashimoto, H. Doi, and T. Tsujimoto, “Re-Examination of the Ti-Al-V Ternary Phase Diagram,” Transactions of the Japan Institute of Metals, 1986, 27(10), 741～749.

7) S. C. Huang, E. L. Hall, and M. F. Gigliotti, “Rapidly Solidified Binary TiAl Alloys,” High-Temperature Ordered Intermetallic Alloys II Symposium, 1987, 481～486.

8) Y. W. Kim, “Solidification Behavior of Pb Droplets Embedded in a Cu Matrix,” Acta Metallurgical Material, 1992, 40(12), 1121～1134.

9) P. L. Martin, M. G. Mendiratta, and H. A. Lipsitt, “Creep Deformation of TiAl and TiAl Plus W Alloys,” Metallurgical Transactions A, 1983(14), 2170～2174.

10) M. Nazmy, C. Noseda, M. Staubli, B. Phillipsen, N. S. Stoloff, and R. H. Jones eds. "Processing and Design Issues in High Temperature Materials," The Minerals, Metals Materials Society, Switzerland, 1997, 159.

11) R. Yua, L. L. Hea, Z. Y. Cheng, J. Zhu, and H. Q. Yea, "B_2 Precipitates and Distribution of W in a Ti-47Al-2W-0.5Si Alloy," Intermetallics, 2002, 10(7), 661～665.

12) G. H. Chen, A. Frefer, and F. H. Froes, "Structural Evolution of Mechanically Alloyed Ti-Al alloys," Materials Science & Engineering A, 1992, 158(1), 93～101.

13) W. R. Chen, L. Zhao, and J. Beddoes, "Precipitation Hardening of the Fully Lamellar Structure of Investment Cast Ti-47Al-2Nb-1Mn-0.5Mo-0.5W-0.2Si Alloy," Scripta Materialia, 1999, 41(6), 597～603.

14) W. M. Yin, J. T. Guo, "Microstructure Analyses on a New Creep Resistant TiAl Alloy," Acta Metallurgica Sinca, 1999, 35(1), 176~182.

15) Y. R. Zheng and X. P. Wang, "β_2 Phase in TiAl-Cr Alloy," Nonferrous Met. Soc., 1998, 18(1), 1～6.

16) W. D. Liu, "Valence Electronic Structure and Mechanical Properties of Ti_3Al and TiAl Alloy," Ph.D. Dissertation, North Western University, 2002.

17) Y. W. Kim, "Ordered Intermetallic Alloy, Gamma-Titanium Aluminides," JOM, 1994, 46(7), 30～39.

18) Y. W. Kim and D. M. Dimiduk, "Designing Gamma TiAl Alloys: Fundamentals, Strategy and Production," Proceedings of the Second International Symposium on Structural Internetallics. TMS, 1997, 531-543.

19) Y. W. Kim, “Effects of Microstructure on the Deformation and Fracture of γ-TiAl Alloys,” Materials Science & Engineering A, 1995, 192-193(2), 519～533.

20) A. Menand, A. Huguet, and A. N. Partaix, “Interstitial Solubility in γ and α_2 Phases of TiAl-Based Alloys,” Acta Materialia, 1996, 44(12), 4729～4737.

21) M. Yamaguchi, H. Inui, K. Kishida, M. Matsumuro, and Y. Shirai, “Gamma Titanium Aluminide Alloys,” Materials Research Society Symposium – Proceedings. 1995, 364(1), 3～16.

22) S. C. Huang, “Microstructure and Property Tradeoffs in Wrought TiAl-Base,” Metallurgical Transactions A (Physical Metallurgy and Materials Science), 1992, 23A (1), 375～377.

23) G. Wegmann and K. Maruyama, “On the Microstructure Stability of TiAl/Ti_3Al Polysynthetically Twinned Crystals under Creep Conditions,” Phil. Mag. A, 2000(80), 2283.

24) R. Gnanamoorthy, Y. Mutoh, N. Masahashi, and M. Matsuo, “High Temperature Strength and Fracture Toughness in γ-phase Titanium Aluminides,” Journal of Materials Science, 1993, 28(24), 6631～6638.

25) C. T. Liu, P. J. Maziasz, and J. L. Wright, “Key Microstructures Controlling the Mechanical Properties of Two Phase TiAl alloys with Lamellar Structures,” In MRS Procs., High Temperature Intermetallic Alloys VII, 1997, 460, 83~90.

26) D. A. Lukasak and D. A. Koss, “Flow and Fracture of a Ti_3Al-Nb Alloy,” Metallurgical Transactions A (Physical Metallurgy and Materials Science), 1990, 21A (1), 135～143.

27) S. C. Huang, “Microstructure and Property Tradeoffs in Wrought TiAl-Based Alloys,” Metall. Trans., 1992, 23A, 375.

28) G. Wegmann and K. Maruyama, “On the Microstructure Stability of TiAl/Ti_3Al Polysynthetically Twinned Crystals under Creep Conditions,” Phil. Mag. A, 2000, 80, 2283.

29) W. O. Soboyejo, J. E. Deffeyes, and P. B. Aswath, “Investigation of Room-and Elevated-Temperature Fatigue Crack Growth in Ti-48Al,” Materials Science & Engineering A (Structural Materials: Properties, Microstructure and Processing), 1991, 138 (1), 95～101.

30) L. M. Hsiung and T. G. Nieh, “Microstructures and Properties of Powder Metallurgy TiAl Alloys,” Materials Science and Engineering A, 2004, 364(1-2), 1～10.

31) M. R. Shagiev, O. N. Senkov, G. A. Salishehev, and F. H. Fores, “High Temperature Mechanical Properties of a Submicrocrystalline Ti-47Al-3Cr Alloy Produced by Mechanical Alloying and Hot Isostatic Pressing,” Journal of Alloy and Compounds, 2000, 313 (1-2), 201～208.

32) F. Sun and T. L. Lin, “Superplastic Phenomenon in a Large-grained TiAl Alloy,” Scripta. mater., 2001, 44 (4), 665～670.

33) H. Clemens, I. R. Umberg, and P. Schwantes, “Characterization of Ti-48Al-2Cr Sheet Material,” Intermetallics, 1994, 2(3), 179～184.

34) Y. W. Kim and D. M. Dimiduk, “Progress in the Understanding of Gamma Titanium Aluminides,” JOM, 1991, 43(8), 40～47.

35) Y. W. Kim, R. Wagner, M. Yamaguchi, H. lemens, W. Glatz, P. Schretter, C. Koeppe, A. Bartecs, R. Behr, and A.Wanner, in Gamma Titanium Aluminides and Alloys, eds., TMS, Warrendale, PA, 1995, 717～726.

36) Y. W. Kim and D. M. Dimiduk, "Progress in the Understanding of Gamma Titanium Aluminides," JOM, 1991, 43(8), 40～47.

37) C. Q. Peng, "Effects of Cyclic Heat Treatment on the Microstructure and Mechanical Properties of TiAl Base Alloy," Ph.D. Dissertation, Central South University, 2001.

38) R. Gerling, A. Bartels, H. Clemens, H. Kestler, and F. P. Schimansky, "Structural Characterization and Tensile Properties of a High Niobium Containing Gamma TiAl Sheet Obtained by Powder Metallurgical Processing," Intermetallics, 2004, 12(3), 275～280.

39) D. Hu, "Effect of Boron Addition on Tensile Ductility in Lamellar TiAl Alloys," Intermetallics, 2002, 10(9), 851～858.

40) T. T. Cheng, "The Mechanism of Grain Refinement in TiAl Alloys by Boron Addition - An Alternative Hypothesis," Intermetallics, 2000, 8(1), 29～37.

41) Y. Mizuhara, K. Hashimoto, and N. Masahashi, "Microstructure and Phase Stability of TiAl-W Ternary Alloy," Intermetallics, 2003, 11(8), 807～816.

42) R. Yu, L. L. He, Z. Y. Cheng, J. Zhu, and H. Q. Ye, "B_2 Precipitates and Distribution of W in a Ti-47Al-2W-0.5Si Alloy," Intermetallics, 2002, 10(7), 661～665.

43) F. Appel, M. Oehring, and R. Wagner, “Novel Design Concepts for Gamma-base Titanium Aluminide Alloys,” Intermetallics, 2000, 8(9-11), 1283～1312.

44) D. Arrel, H. M. Flower, and D. R. West, “Effect of Si on Microstructure of Ti_3Al Alloys Containing Niobium,” Mater. Sci. Techno., 1996,12(8), 617～622.

45) T. T. Cheng and M. H. Loretto, “The Decomposition of the Beta phase in Ti-44Al-8Nb and Ti-44Al-4Nb-4Zr-0.2Si Alloys,” Acta Metall. Mater., 1998, 46(13), 4801～4819.

46) Z. C. Liu, Y. W. Kim, S. J. Li, W. J. Zhang, J. P. Lin, and G. L. Chen, “Effect of Nb and Al on High Temperature Strength of γ-TiAl,” Chin. J. Nonferrous Met. Soc., 2000, 10(4), 470-475.

47) X. Y. Chen, X. J. Wan, and J. N. Shen, “Effect of Alloy Element Nb on High Temperature Oxidation Behavior of TiAl Alloy,” Corrosion and Protection, 2002, 22(2), 69~71.

48) Y. Shida and H. Anada, “Role of W, Mo, Nb and Si on Oxidation of TiAl in Air at High Temperature,” Mater Trans, JIM, 1994, 35(9), 623～631.

49) D. J. Larson, C. T. Liu, and M. K. Miller, “Tungsten Segregation in $\alpha_2 + \gamma$ Titanium Aluminides,” Intermetallics, 1997, 5(7), 497～500.

50) C. T. Liu, P. J. Maziasz, and D. J. Larson, “Effect of B and W Addition on Microstructures and Mechanical Properties of Dual Phase Lamellar TiAl Alloys,” In: Interstitial and Substitutional Solute Effects in Intermetallics, Eds, T. Baker, P. D. Noebe and E. P. George, TMS Publication, Warrendale, PA, 1998, 179~188.

51) J. Beddoes, L. Zhao, P. Au, and W. Wallace, “The Brittle-ductile Transition in HIP Consolidated Near γ-TiAl + W and TiAl + Cr Powder Alloys,” Materials Science and Engineering A, 1995, 192-193, 324～332.

52) V. Recina and B. Karlsson, “Tensile Properties and Microstructure of Ti-48Al-2W-0.5Si γ-titanium Aluminide at Temperature between Room Temperature and 800^0C,” Mater. Sci. Techno., 1999, 15(1), 57～66.

53) Y. W. Kim, “Gamma Titanium Aluminides: Their Status and Future,” JOM, 1995(7), 39～41.

54) H. Anada and Y. Shida, “Effect of W Addition on the Oxidation Behavior of TiAl Intermetallic Compound,” J. Japan Institute Metals, 1994, 58(9), 1036～1043.

55) D. J. Larson, C. T. Liu, and M. K. Miller, “Boron Solubility and Boride Compositions in α_2 + γ Titanium Aluminides,” Intermetallics, 1997, 5(6), 411～414.

56) W. L. Gao, H. Zhang, E. L. Zhang, and S. Y. Zeng, “Morphology of TiB_2 in TiAl-B Alloy,” Cast Tech., 2003, 24(3), 176~178.

57) W. L. Gao, H. Zhang, J. P. He, Y. X, Jin, and S. Y. Zeng, “Growth of Fine Rod-like TiB_2 Cross in TiAl-B Alloy,” Rare Met. Mater. Eng., 2003, 32(3), 179～182.

58) S. H. Kim, H. H. Chung, S. G. Pyo, S. J. Hwang, and N. J. Kim, “Effect of B on the Microstructure and Mechanical Properties of Mechanically Milled TiAl Alloys,” Metallurgical and Materials Transactions, 1998, 29A (9), 2273～2283.

59) Z. J. Pu and K. H. Wu, “Investigation on Boron Distribution in a TiAl-based Alloy Using Particle-Cracking,” Scripta. Metall. Mater., 1996, 34(1), 169～174.

60) P. J. Maziasz, R. V. Ramanujan, C. T. Liu, and J. L. Wright, “Effects of B and W Alloying Additions on the Formation and Stability of Lamellar Structures in Two-Phase γ-TiAl,” Intermetallics, 1997, 5(2), 83～95.

61) C. T. Liu, J. L. Wright, and S. C. Deevi, “Microstructures and Properties of a Hot-Extruded TiAl Containing no Cr ,” Materials Science and Engineering, 2002, 329A, 416～423.

62) L. M. Dong, Y. Y. Cui, R. Yang, and F. H. Yang, “Effect of Si Element on the Oxidation Resistance of TiAl Alloy,” Acta Metallurgica Sinca, 2004, 40(4), 383~387.

63) R. A. Perkins and F. Smith, Proceedings of the Industry University Advanced materials Conference Ⅱ. Golden, Co., Advanced Materials Institute, 1989.

64) Y. H. He, B. Y. Huang, X. H. Qu et.al., “Effect of Carburization on Enhancing the High-Temperature Oxidation Resistance of the TiAl-Based Alloys,” J. Mater. Res., 1996, 10(6), 603~607.

65) T. Nado, M. Okabe, and S. Isobe, “Hard Surfacing of TiAl Intermetallic Compound by Plasma Carburization,” Metarials Science & Engineering A, 1996, 213(1-2), 157～161.

66) S. Thongtem, T. Thongtem, and M. J. McNallan, “High-Temperature Nitridation of the Intermetallic Compound TiAl at 1000-1200K,” Surface and Interface analysis, 1999, 28(1), 61～64.

67) C. T. Liu, “Recent Advances in Ordered Intermetallics,” Materials Chemistry and Physics, 1995, 42(2), 77-86.

68) F. Appel, M. Oehring, and R. Wagner, “Novel Design Concepts for Gamma-base Titanium Aluminide Alloys,” Intermetallics, 2000, 8(9-11), 1283-1312.

69) R. T. Zheng, Y. G. Zhang, and C. Q. Chen, “Effect of Circle Heat Treatment on Microstructure of Duplex γ-TiAl Alloys,” Heat-treatments of Metals, 2002, 31(6), 472-475.

70) Z. C. Liu, H. J. Li, G. P. Lin, and G. L. Chen, “Refinement Mechanism of Cyclic Heat Treatment on Ti-46Al-8.5Nb-0.2W,” Rare Metals, 2000, 24(4), 251-255.

71) Z. Q. Pan, C. X. Han, “Effects of Iso-thermal Forging on Microstructures of Ti-47Al-5 (Cr + V + Mo + Nb) Intermetallics,” Rare Materials and Engineering, 1996, 25(3), 22-25.

72) S. J. Li, Z. C. Liu, and G. L. Chen, “Refinement of Microstructures of Forged Ti-46Al-8.5Nb-0.2W,” Material Science and Technology, 2000, 8(3), 46-49.

Appendices

Appendix A

Tables

Table 1 Development of the γ-TiAl-based Alloys (at.%) [5]

Generation	Compositions (at.%)	Processing
1st	Ti-48Al-1V-0.3C	Exploratory
2nd	Ti-47Al-2(Cr,Mn)-Nb Ti-(45-47)Al-2Nb-2Mn-0.8 TiB_2 Ti-47Al-2W-0.5Si	Cast Cast XD Cast
3rd	Ti-47Al-5(Cr,Nb,Ta) Alloy K5 (Ti-46.2Al-2Cr-3Nb-0.2W) Ti-(45-47)Al-(1-2)Cr-(1-5)Nb-(0-2)(W,Ta,Hf,Mo,Zr)-(0.02)B-(0-2)(W,Ta,Hf,Mo,Zr)-(0-0.2)B-(0.03-0.3)C-(0.03-0.2)Si-(0.15-0.25)O-X	Cast Wrought Wrought

Table 2 Mechanical Properties of the γ-TiAl-based Alloys

Manufactured through Power Metallurgy [22]

Composition/ at %	δ(R. T.) / %	σ_s(R. T.) / MPa	σ_b(R. T.) / MPa	σ_s(H. T., 800 ℃) / MPa
Ti-47Al-2Cr-2Nb	1.4	971	1005	841
Ti-48Al-2Cr-2Nb	2.3	370	488	-
Ti-46.6Al-1.4Mn-2Mo	3.1	548	606	478
Ti-45Al-1.6Mn	1.7	552	692	433
Ti-46.5Al-4(Cr,Nb,Ta,B)	>1.0	550	620	480

Table 3 Microstructural Evolution of the TiAl-based Alloys

	900^0C/ 360 h	$1,265^0$C/ 18 h	$1,280^0$C/ 14 h	$1,295^0$C/ 10 h	$1,310^0$C/ 5 h
0 at.% W	γ, $\alpha_2 + \gamma$, boride	γ, $\alpha_2 + \gamma$, boride	γ, $\alpha_2 + \gamma$, boride	$\alpha_2 + \gamma$, boride	$\alpha_2 + \gamma$, boride
0.2 at.% W	γ, $\alpha_2 + \gamma$, boride	γ, $\alpha_2 + \gamma$, boride	γ, $\alpha_2 + \gamma$, boride	$\alpha_2 + \gamma$, boride	$\alpha_2 + \gamma$, boride
0.4 at.% W	γ, $\alpha_2 + \gamma$, boride	γ, $\alpha_2 + \gamma$, boride	γ, $\alpha_2 + \gamma$, boride	$\alpha_2 + \gamma$, boride	$\alpha_2 + \gamma$, boride
0.7 at.% W	γ, $\alpha_2 + \gamma$, β, boride	γ, $\alpha_2 + \gamma$, β, boride	γ, $\alpha_2 + \gamma$, β, boride	$\alpha_2 + \gamma$, β, boride	$\alpha_2 + \gamma$, boride

Appendix B

Figures

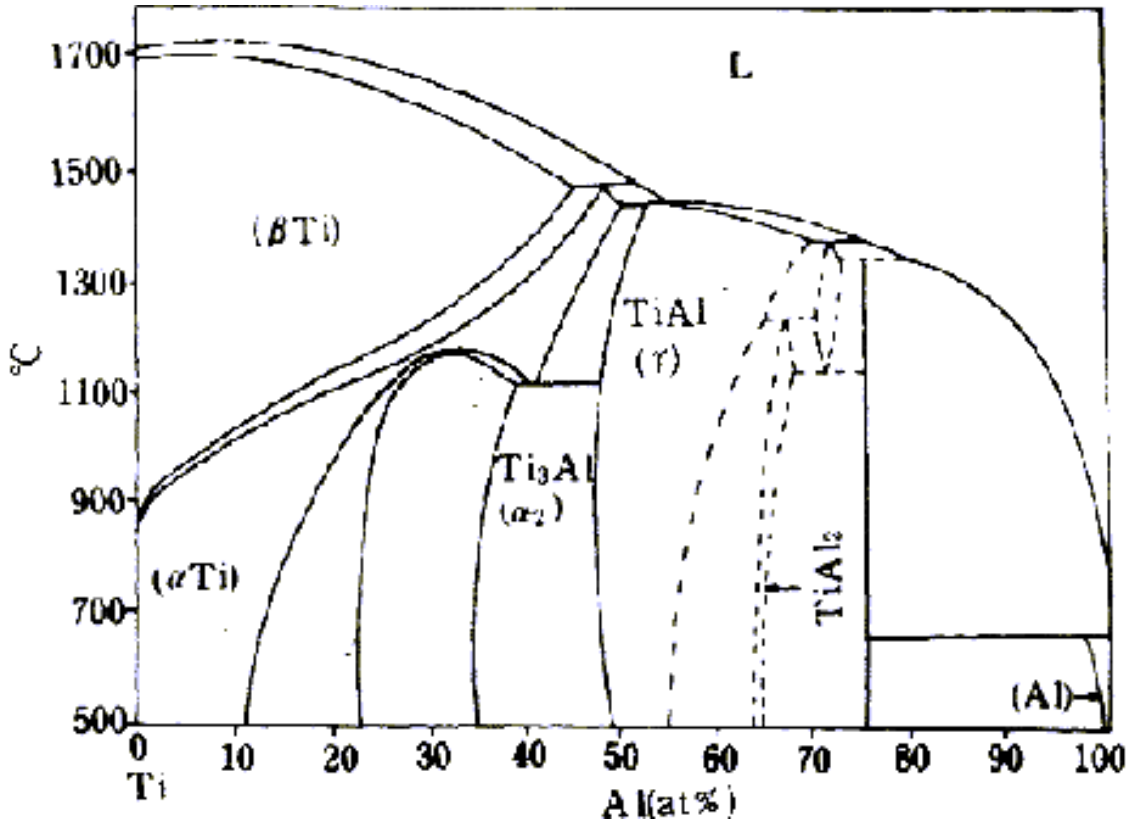

Figure 1 Binary phase diagram of the Ti-Al alloys

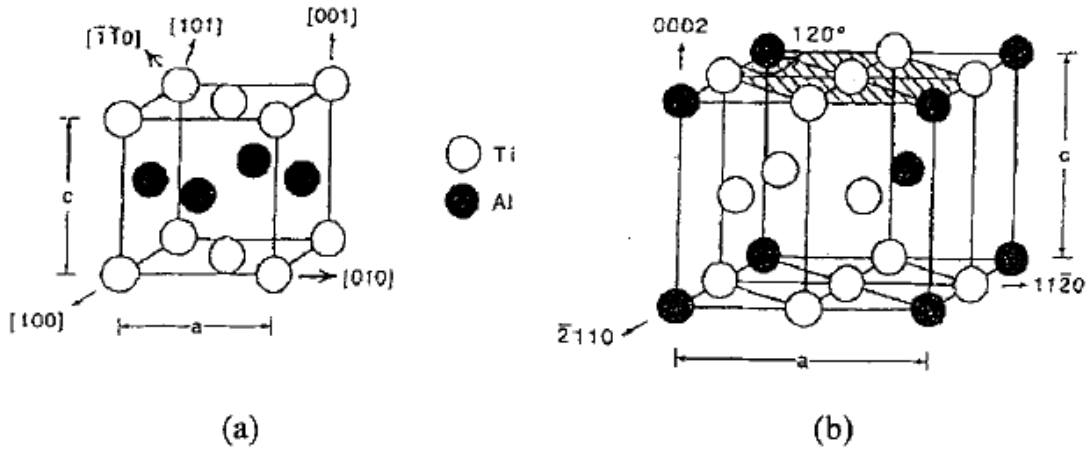

(a) γ phase (Ll_0) structure

(b) α_2 phase ($D0_{19}$) structure

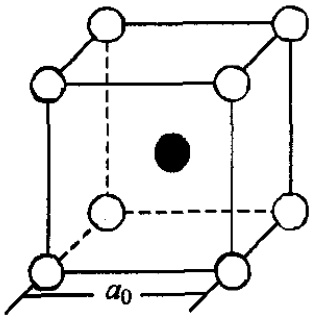

(C)

(c) B_2 phase BCC structure

Figure 2 Crystal structures

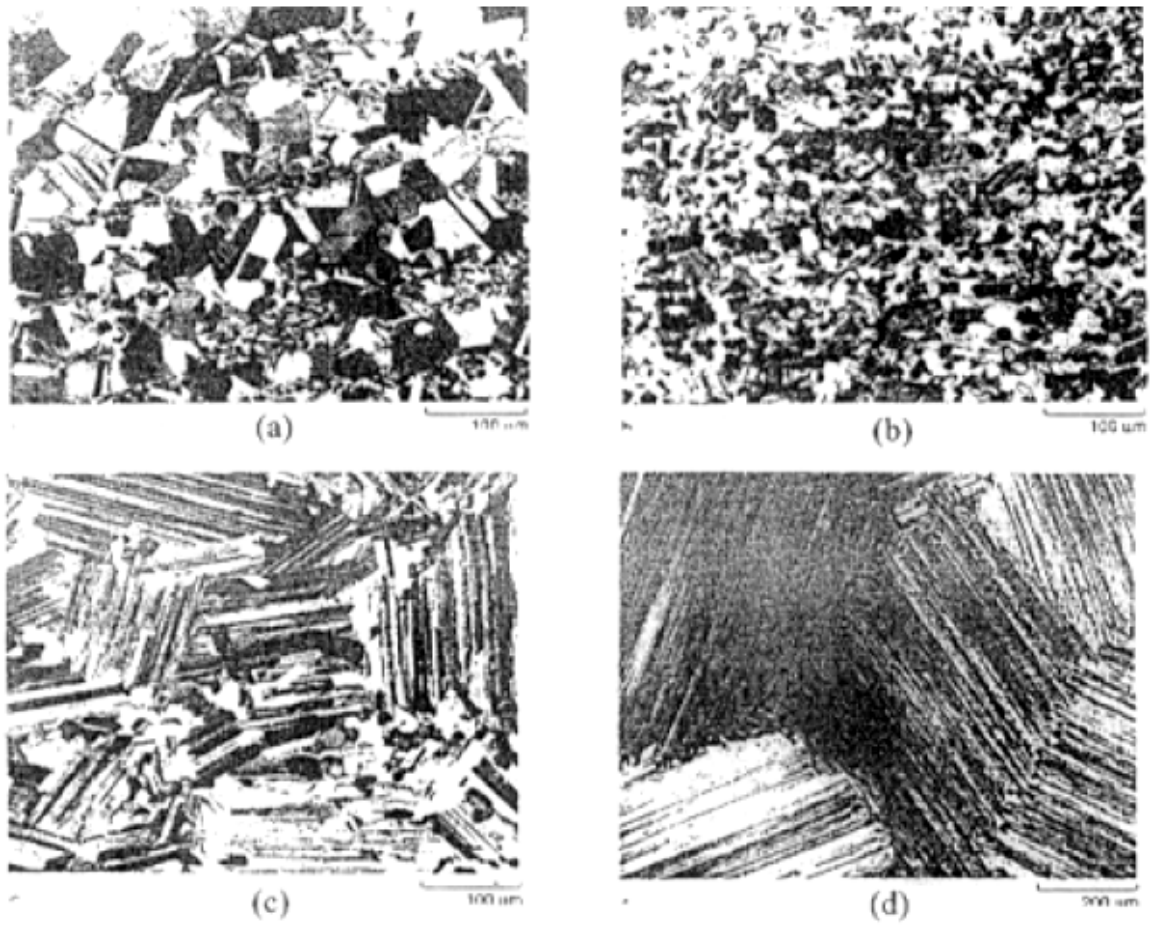

Figure 3 Four typical microstructures of the γ-TiAl-based alloys after post-hot work heat treatments, (a) Near-gamma structure, (b) Duplex structure, (c) Nearly lamellar structure, and (d) Fully lamellar structure

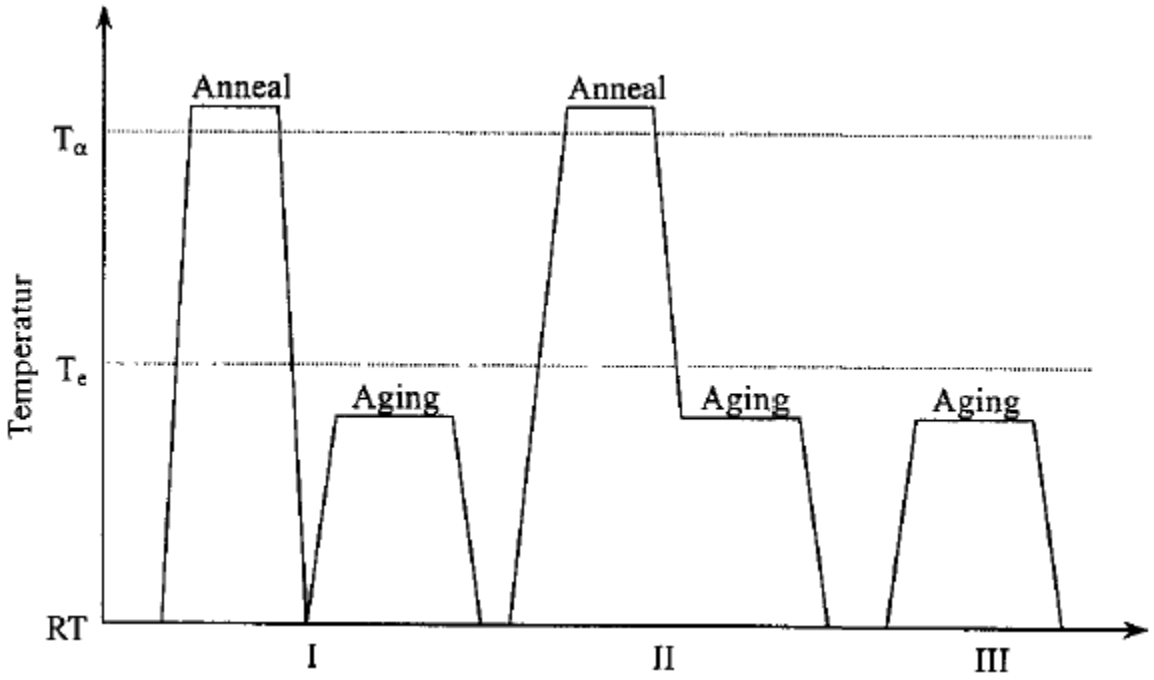

Figure 4 Three typical heat-treating techniques of the γ-TiAl alloys (Type I, II, III)

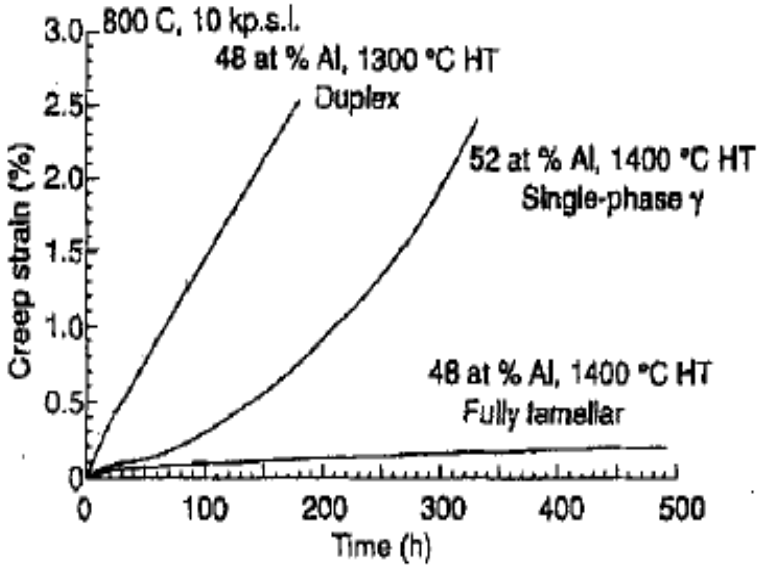

Figure 5 Creep curves of different TiAl alloys with different microstructures

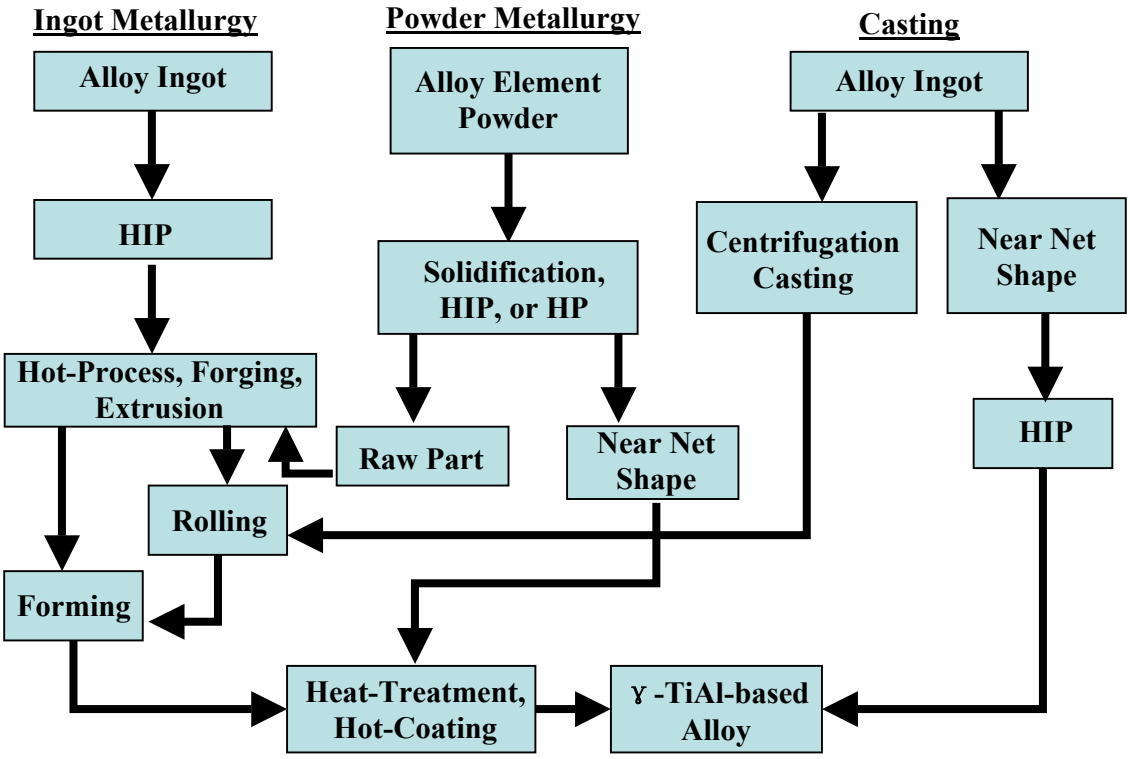

Figure 6 Manufacturing of the engineering TiAl-based alloys

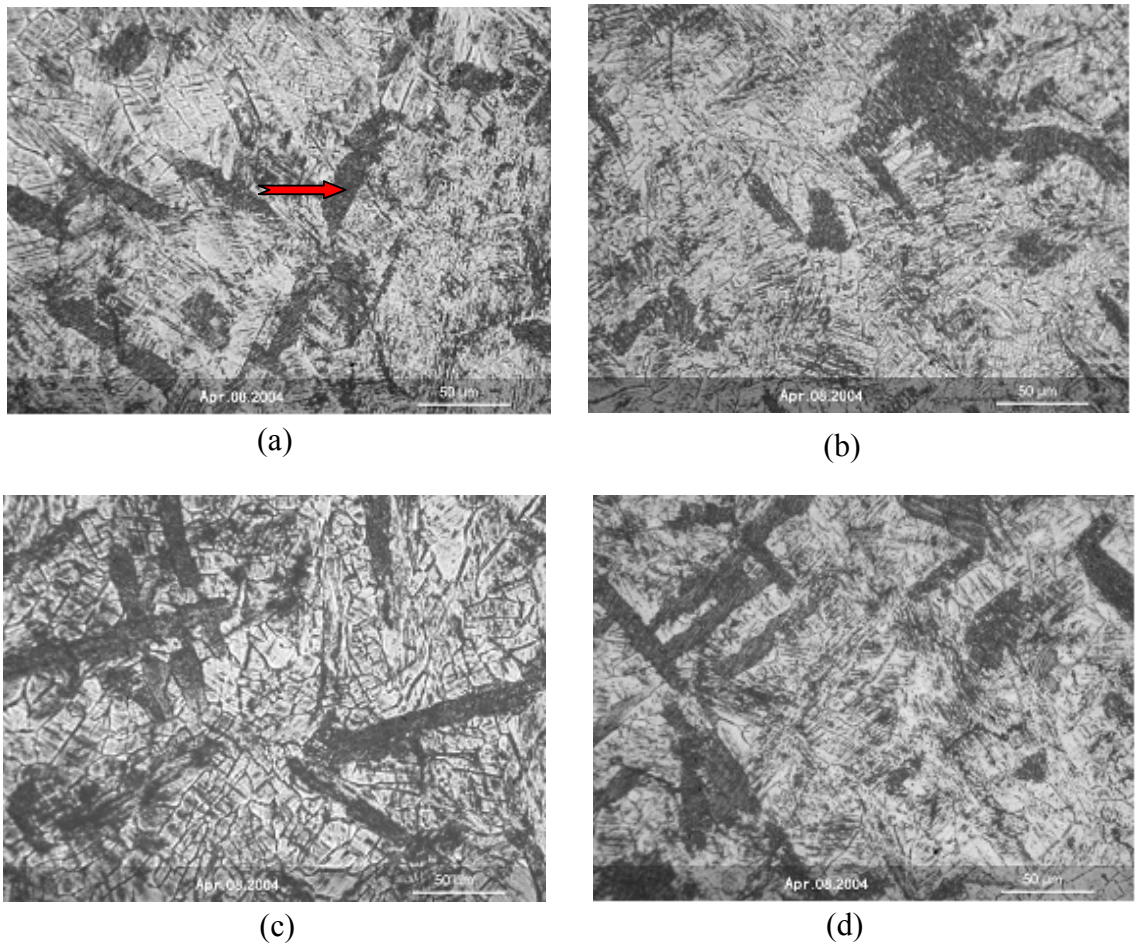

Figure 7 Optical microstructures of the as-cast Ti-Al-Nb-W-B alloys
(The arrows indicate the dendrites.)
(a) Ti-45Al-7Nb-0.15B, (b) Ti-45Al-7Nb-0.15B-0.2W, (c) Ti-45Al-7Nb-0.15B-0.4W, and (d) Ti-45 Al-7Nb-0.15B-0.7W

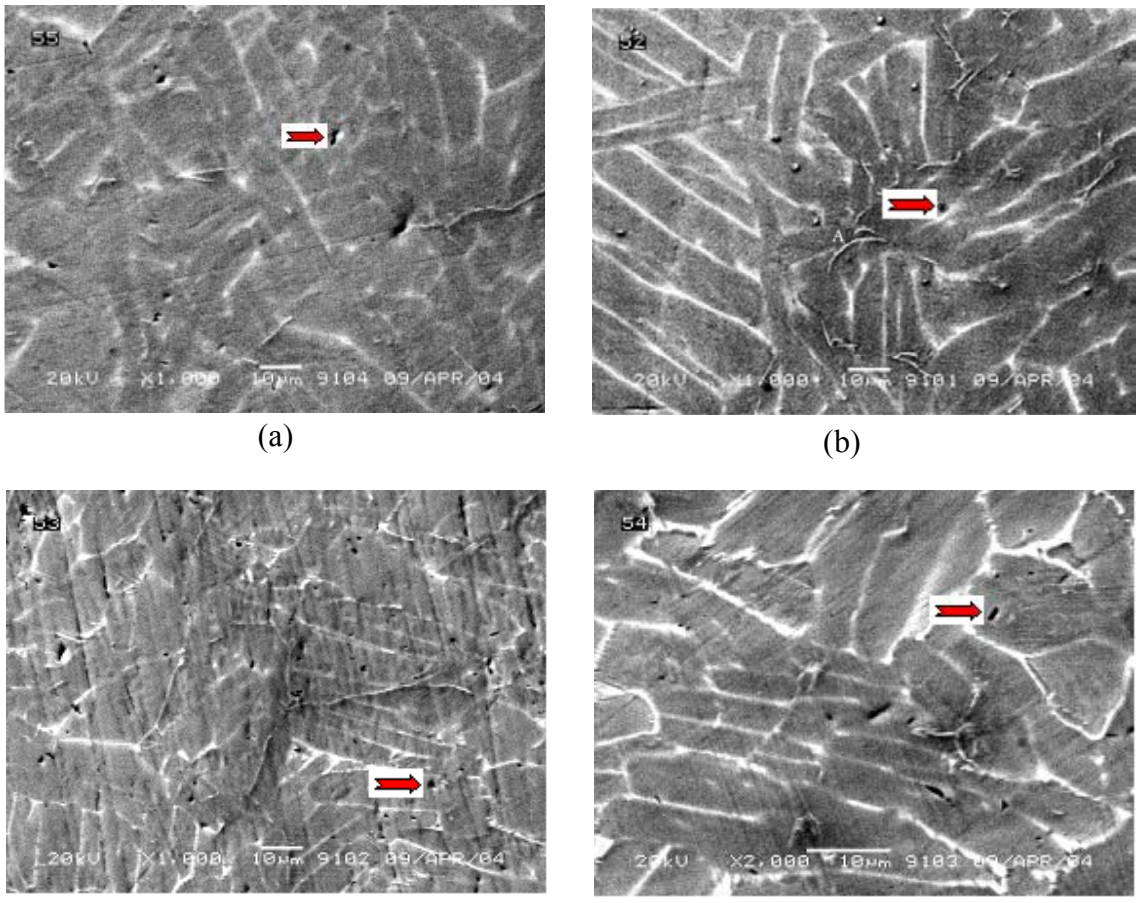

Figure 8 Backscattered images of the as-cast Ti-Al-Nb-W-B alloys
(The arrows show the porosities. Point A shows the needle-shaped Ti-B boride phase.)
(a) Ti-45Al-7Nb-0.15B, (b) Ti-45Al-7Nb-0.15B-0.2W, (c) Ti-45Al-7Nb -0.15B-0.4W, and (d) Ti-45Al-7Nb-0.15B-0.7W

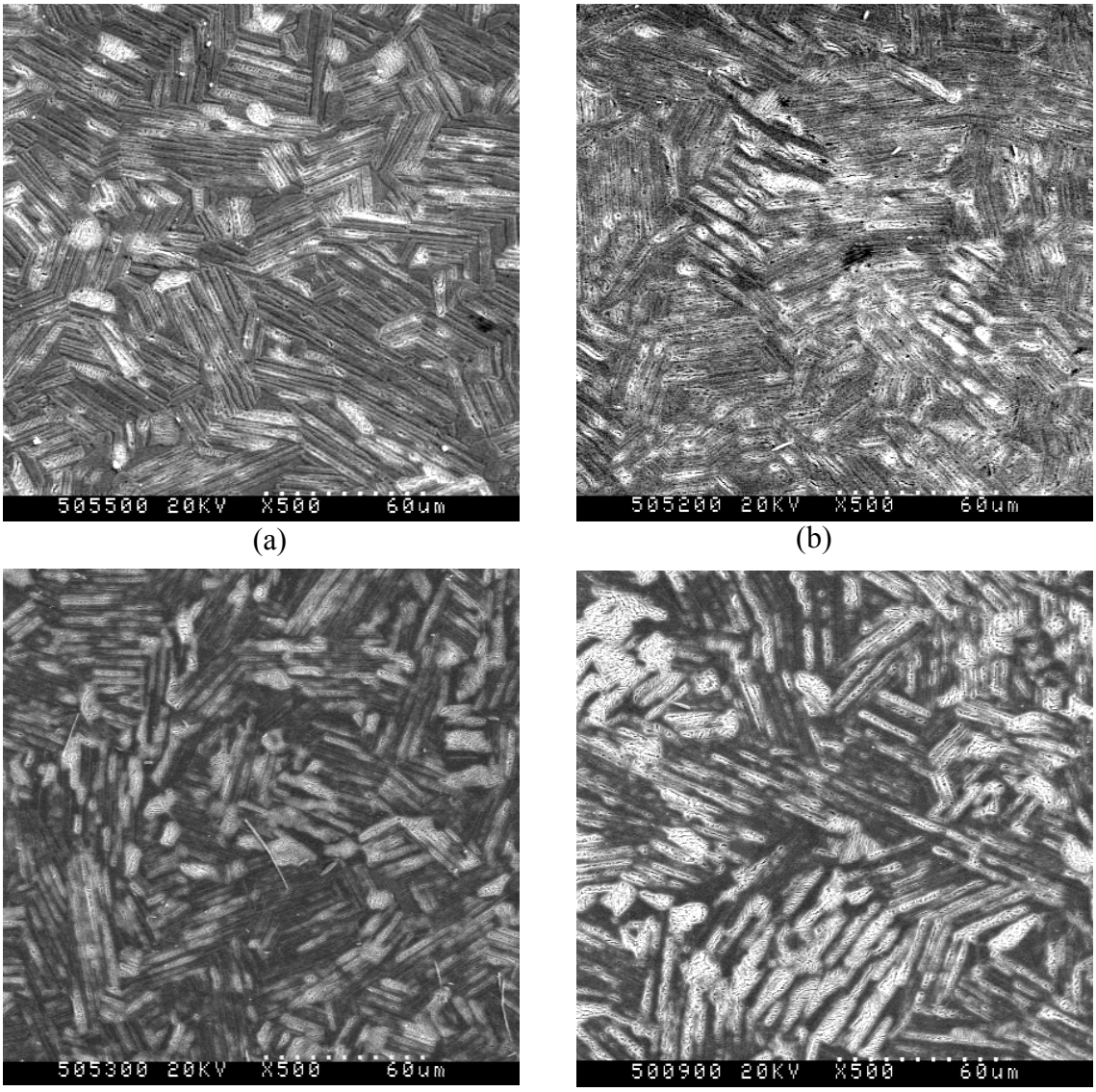

Figure 9 Secondary electronic images of the Ti-Al-Nb-W-B alloys after HIPing and homogenization, (a) Ti-45Al-7Nb-0.15B, (b) Ti-45Al-7Nb-0.15B-0.2W, (c) Ti-45Al-7Nb-0.15B-0.4W, and (d) Ti-45Al-7Nb-0.15B-0.7W

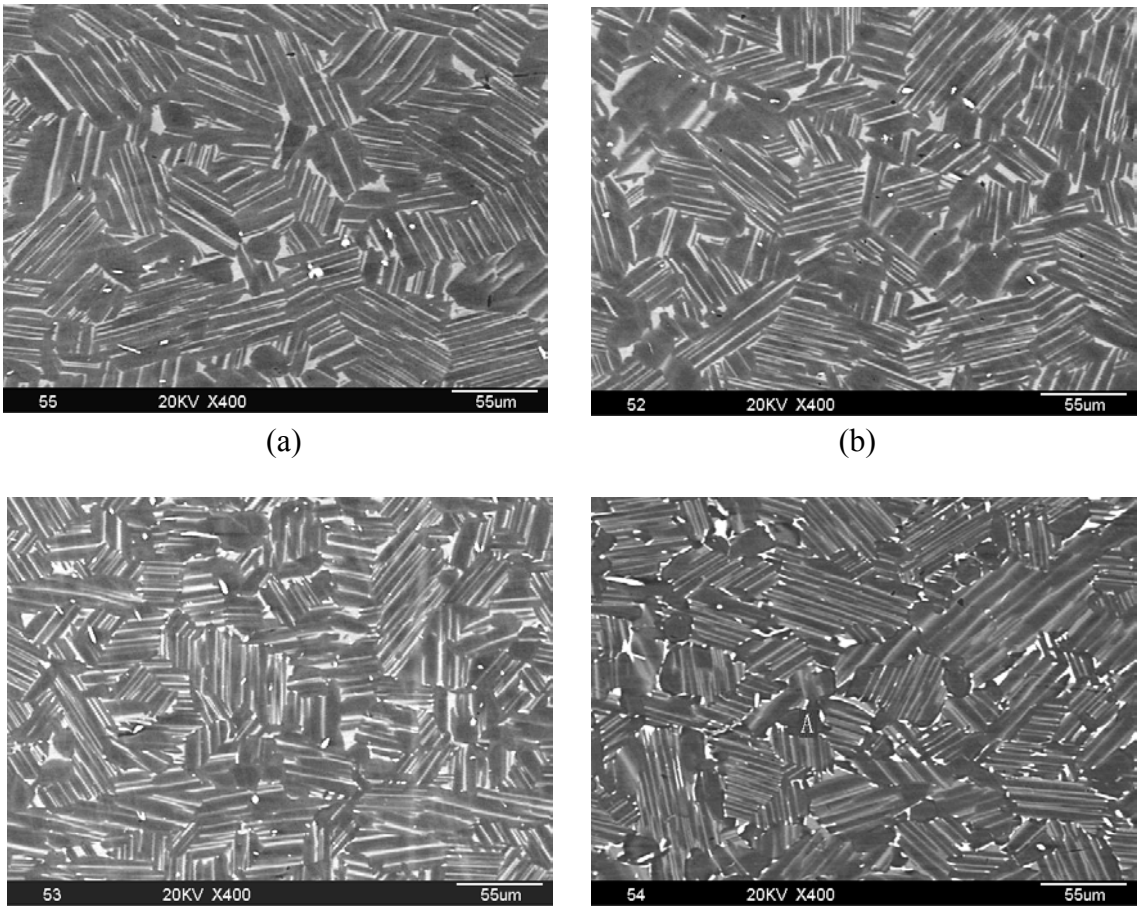

Figure 10 Backscattered images of the Ti-Al-Nb-W-B alloys after HIPing and homogenization (Point A shows the γ phase), (a) Ti-45Al-7Nb-0.15B, (b) Ti-45Al-7Nb-0.15B-0.2W, (c) Ti-45Al-7Nb-0.15B-0.4W, and (d) Ti-45Al-7Nb-0.15B-0.7W

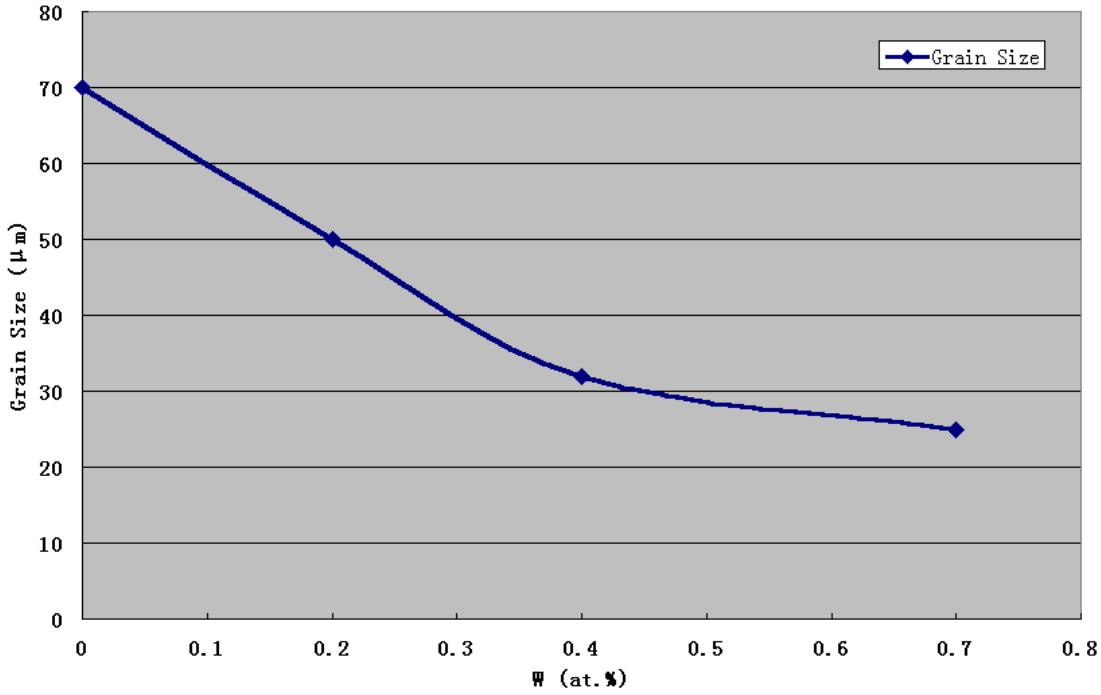

(a)

Figure 11 Effect of W on the (a) grain size, and (b) lamellar spacing of the Ti-Al-Nb-W-B alloys after HIPing and homogenization

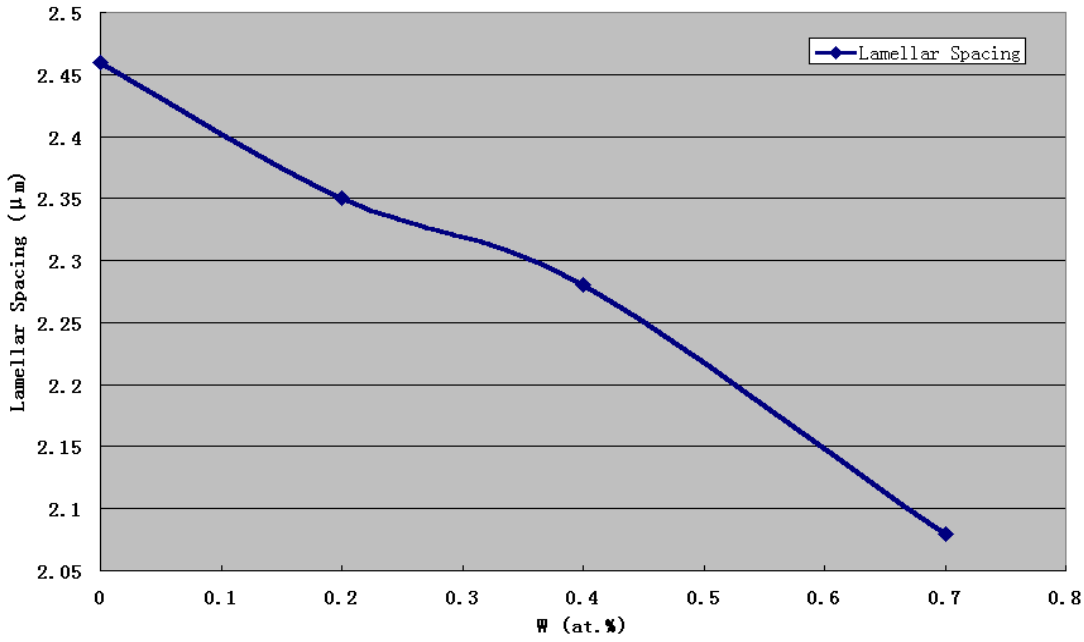

(b)

Figure 11 Continued

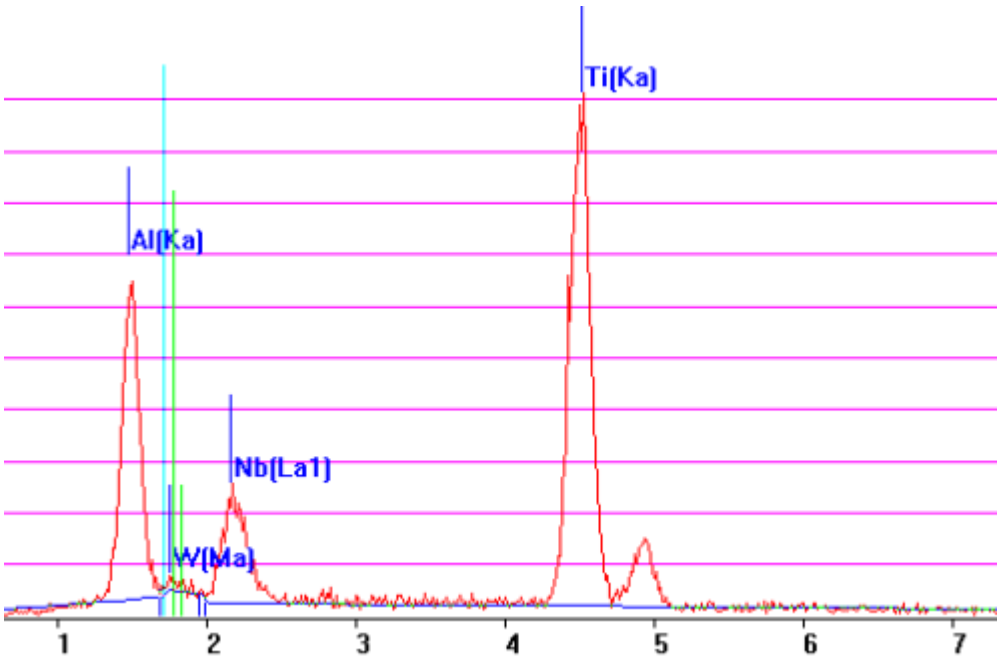

Figure 12 Energy-Dispersive X-ray Spectroscopy (EDS) of the γ phase in the Ti-45Al-7Nb-0.15B-0.7W alloy after HIPing and homogenization

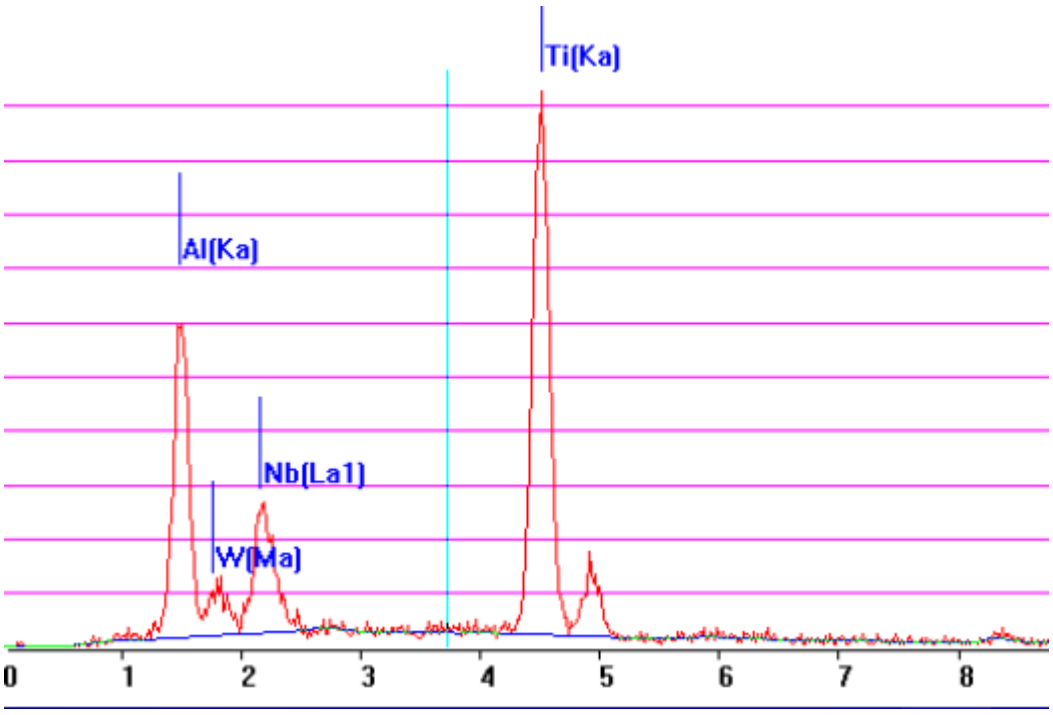

Figure 13 EDS of the α_2 phase in the Ti-45Al-7Nb-0.15B-0.7W alloy after HIPing and homogenization

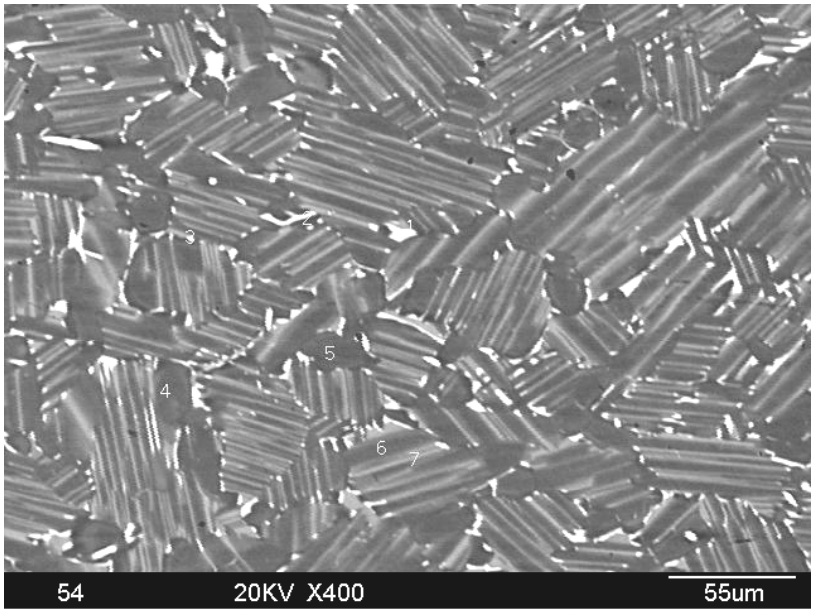

(a)

Figure 14 Backscattered images of the Ti-45Al-7Nb-0.15B-0.7W alloy after HIPing and homogenization, (a) Lower magnification, (b) Higher magnification

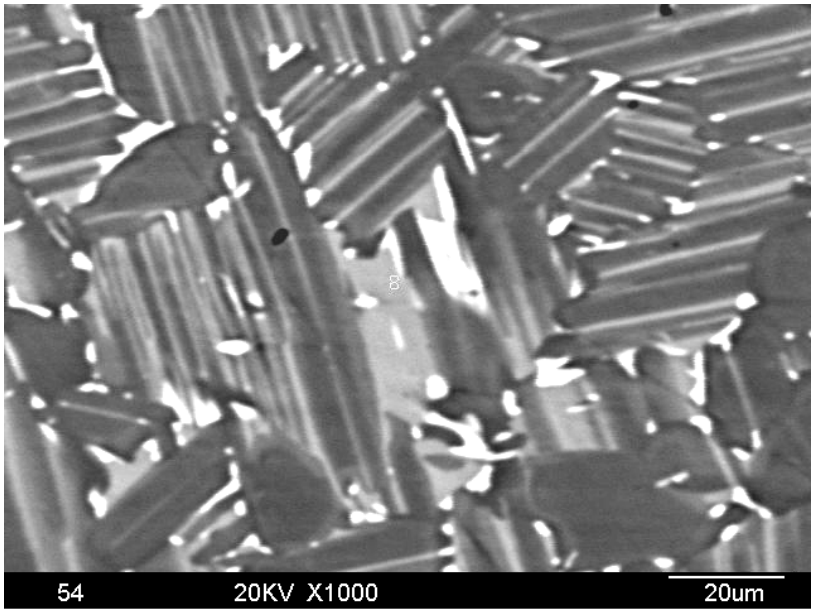

(b)

Figure 14 Continued

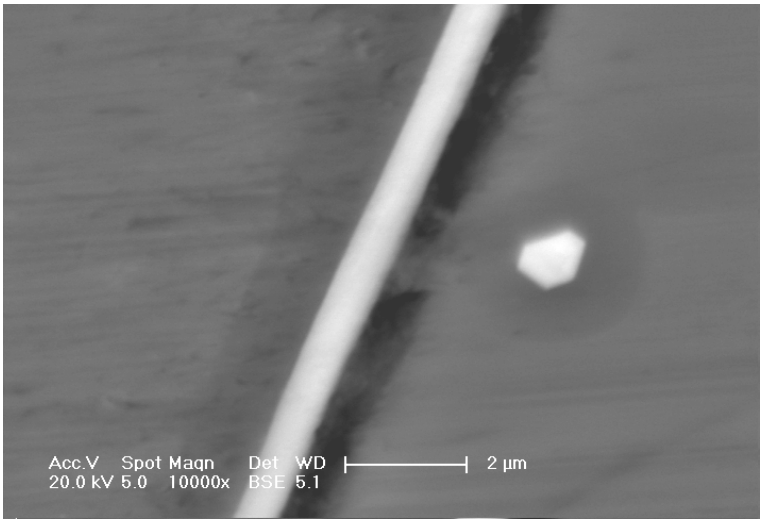

(a)

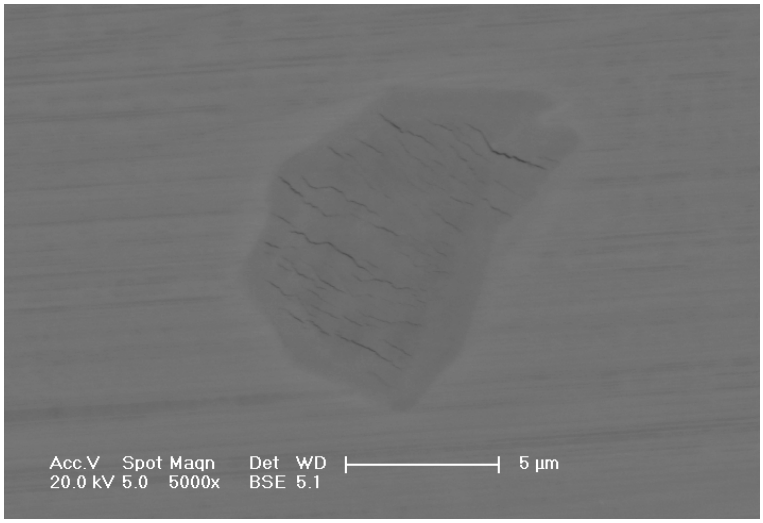

(b)

Figure 15 Backscattered images of the Ti-45Al-7Nb-0.15B-0.7W alloy after HIPing and homogenization, (a) TiB_2 needles, (b) γ-phase, and (c) formation of γ-twin caused by TiB_2 (shown in area A)

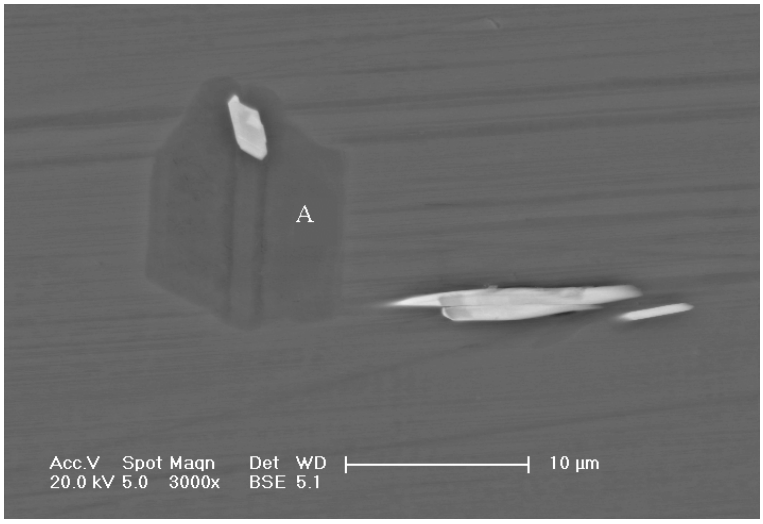

(c)

Figure 15 Continued

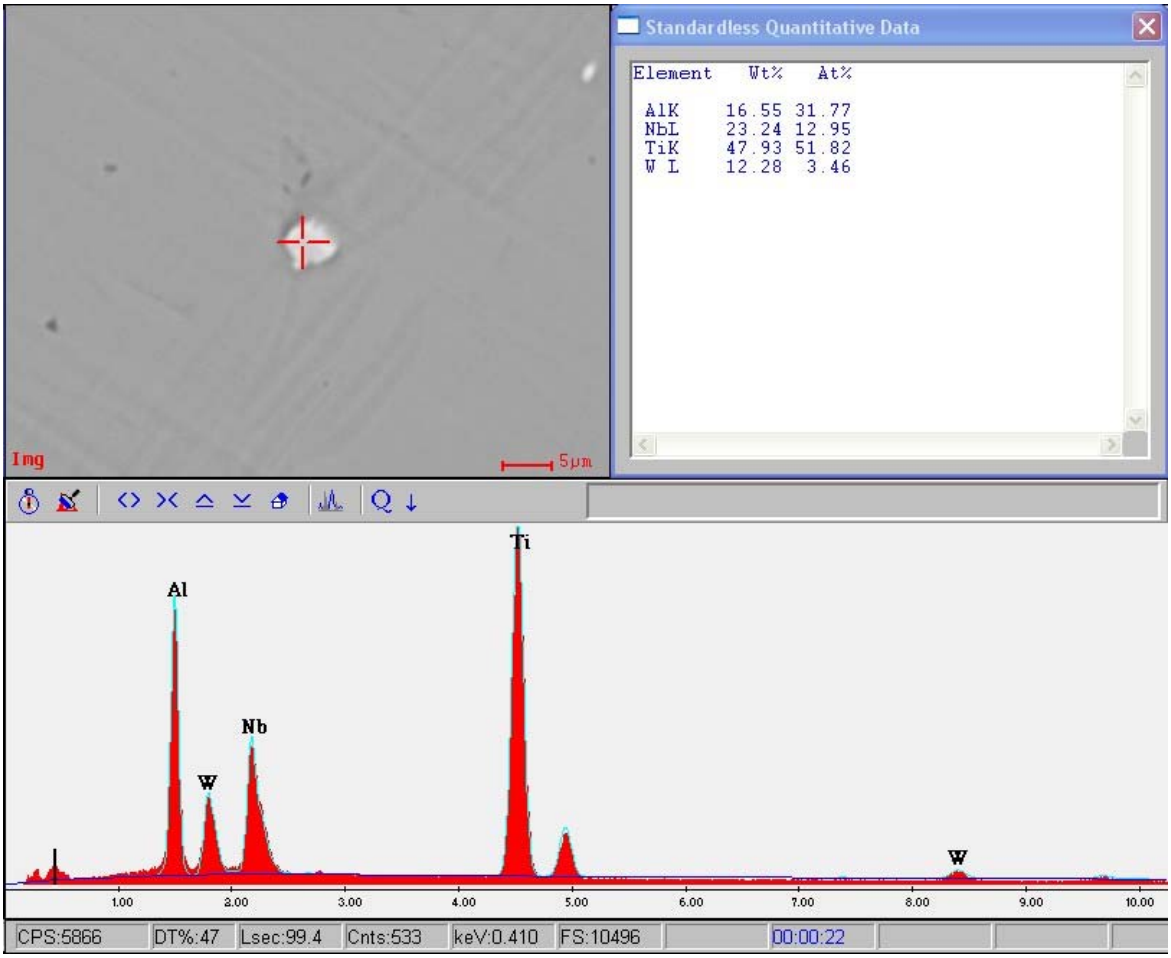

Figure 16 Topograph and composition analyses of the β phase

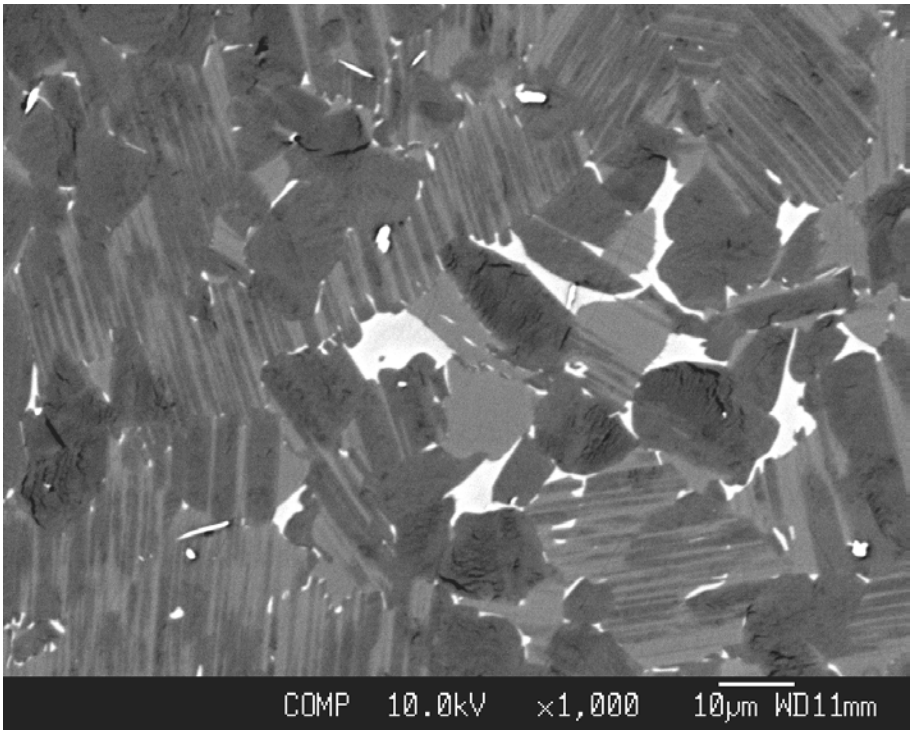

Figure 17 Microstructure of the Ti-45Al-7Nb-0.15B-0.7W alloy after HIPing and homogenization

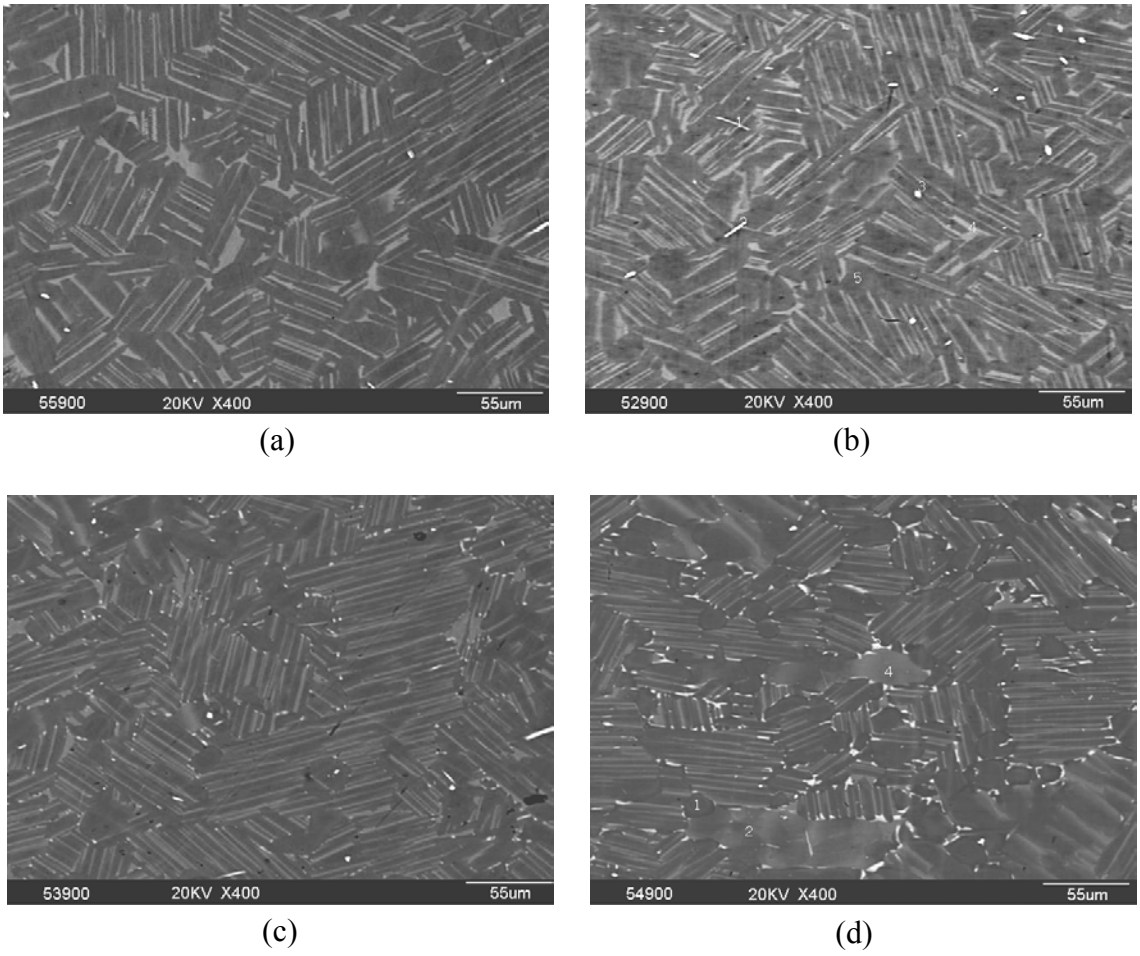

Figure 18 Microstructures of the Ti-Al-Nb-W-B alloys heat treated at 900^0C / 360 h, (a) Ti-45Al-7Nb-0.15B, (b) Ti-45Al-7Nb-0.15B-0.2W, (c) Ti-45Al-7Nb-0.15B-0.4W, and (d) Ti-45Al-7Nb-0.15B-0.7W

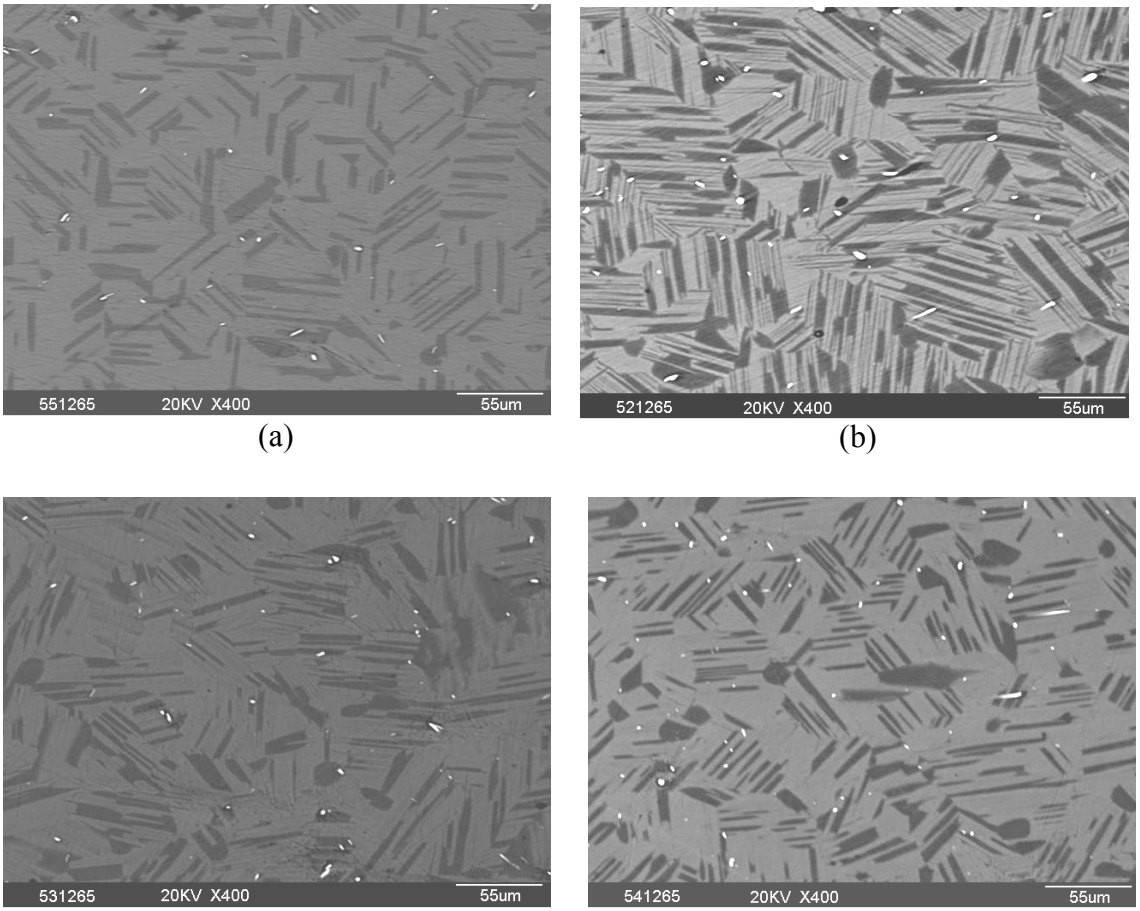

Figure 19 Microstructures of the Ti-Al-Nb-W-B alloys heat treated at $1{,}265^{0}$C / 18 h, (a) Ti-45Al-7Nb-0.15B, (b) Ti-45Al-7Nb-0.15B-0.2W, (c) Ti-45Al-7Nb-0.15B-0.4W, and (d) Ti-45Al-7Nb-0.15B-0.7W

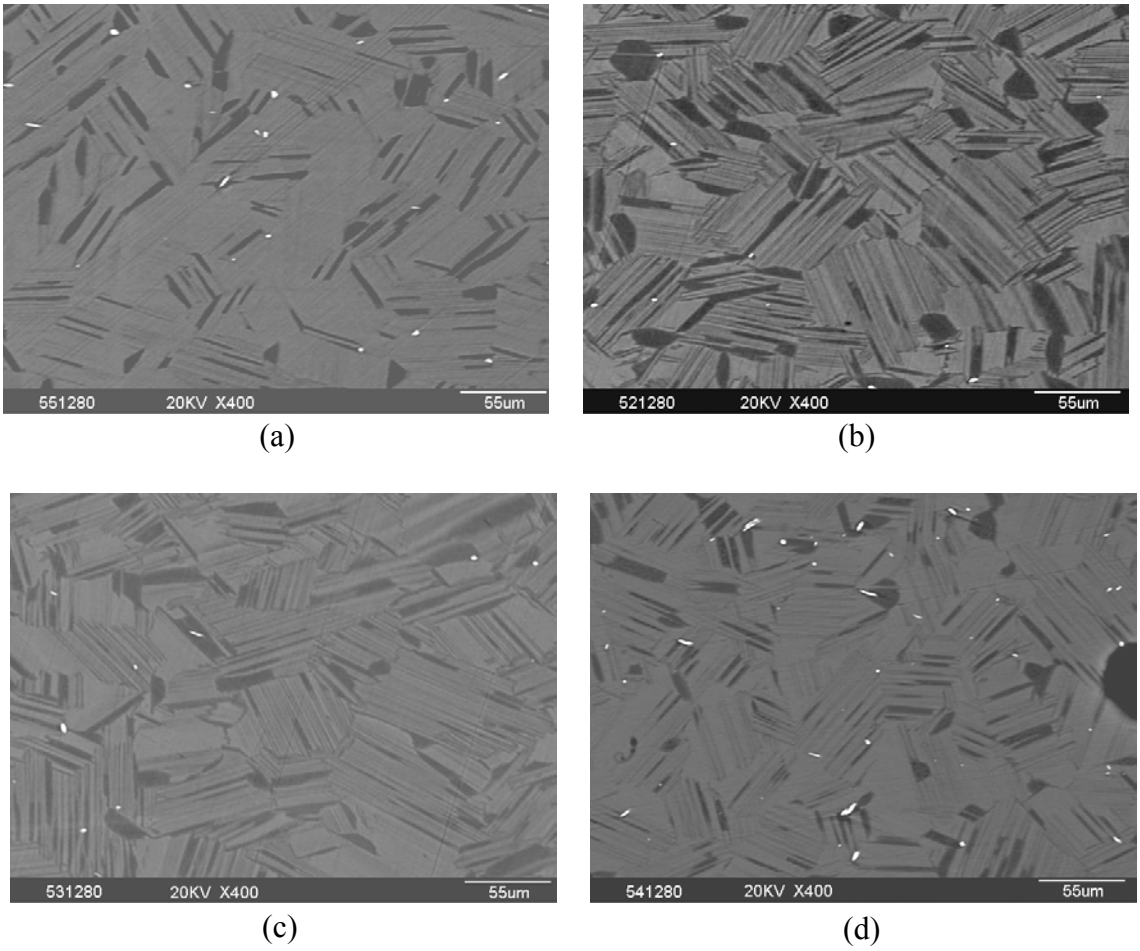

Figure 20 Microstructures of the Ti-Al-Nb-W-B alloys heat treated at 1,280^{0}C / 14 h, (a) Ti-45Al-7Nb-0.15, b) Ti-45Al-7Nb-0.15B-0.2W, (c) Ti-45Al-7Nb-0.15B-0.4W, and (d) Ti-45Al-7Nb-0.15B-0.7W

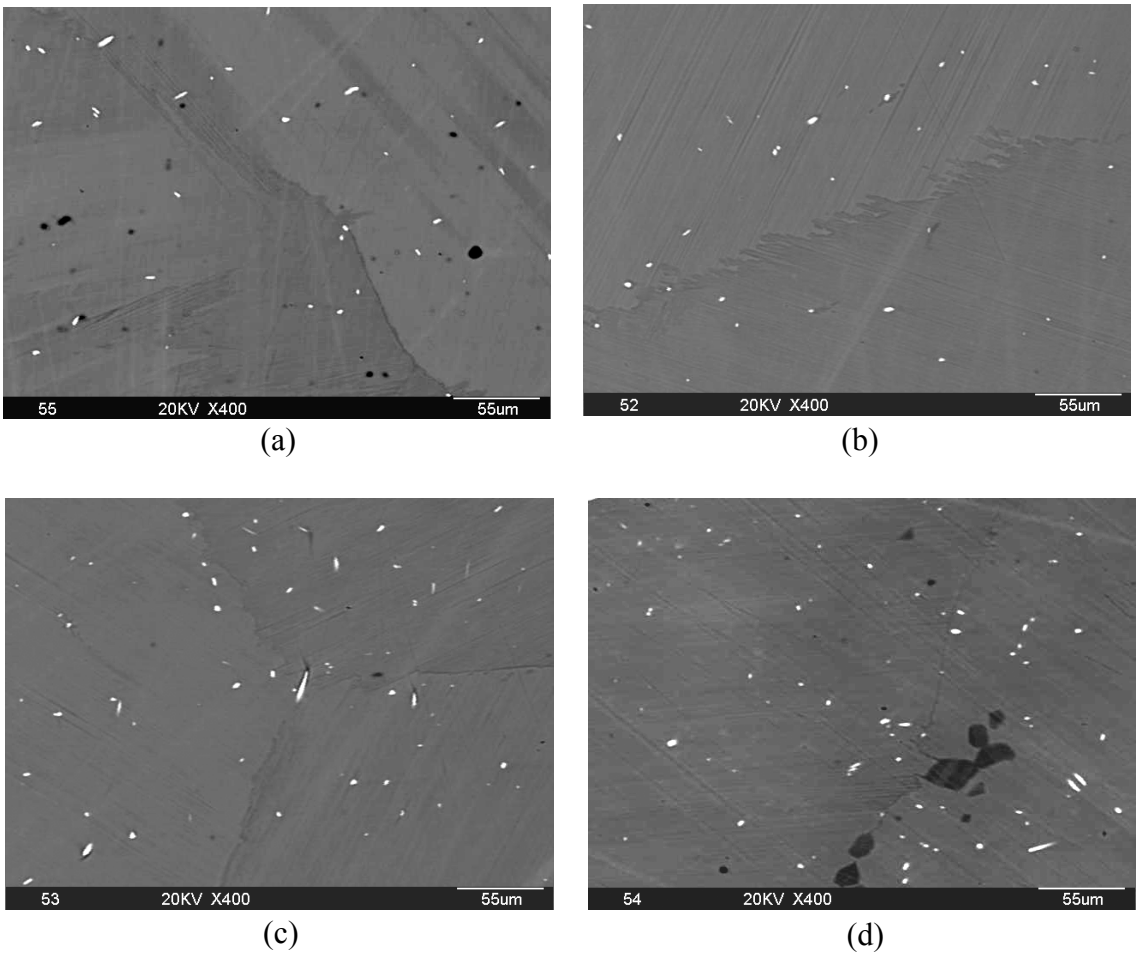

Figure 21 Microstructures of the Ti-Al-Nb-W-B alloys heat treated at 1,295^{0}C / 10 h, (a) Ti-45Al-7Nb-0.15B, (b) Ti-45Al-7Nb-0.15B-0.2W, (c) Ti-45Al-7Nb-0.15B-0.4W, and (d) Ti-45Al-7Nb-0.15B-0.7W

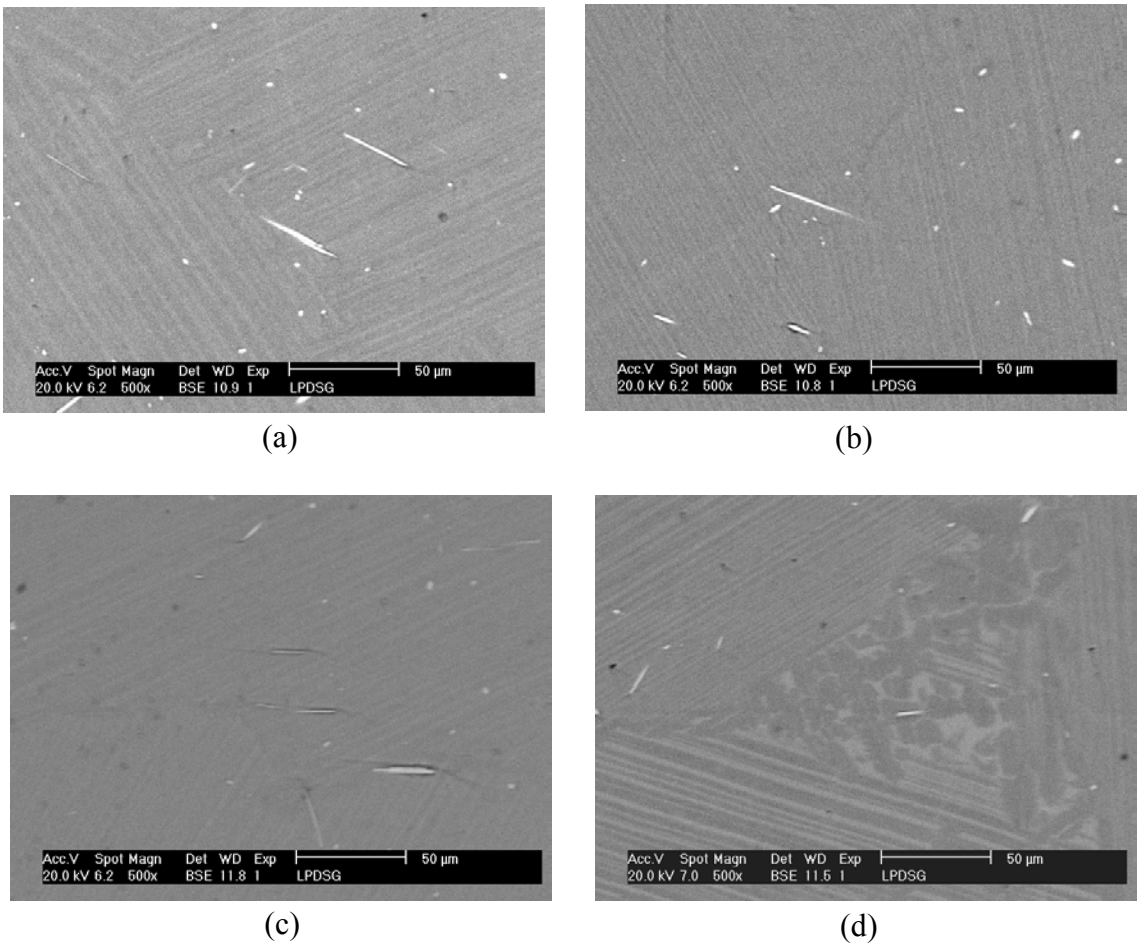

Figure 22 Microstructures of the Ti-Al-Nb-W-B alloys heat treated at 1,310^{0}C / 5 h, (a) Ti-45Al-7Nb-0.15, (b) Ti-45Al-7Nb-0.15B-0.2W, (c) Ti-45Al-7Nb-0.15B-0.4W, and (d) Ti-45Al-7Nb-0.15B-0.7W

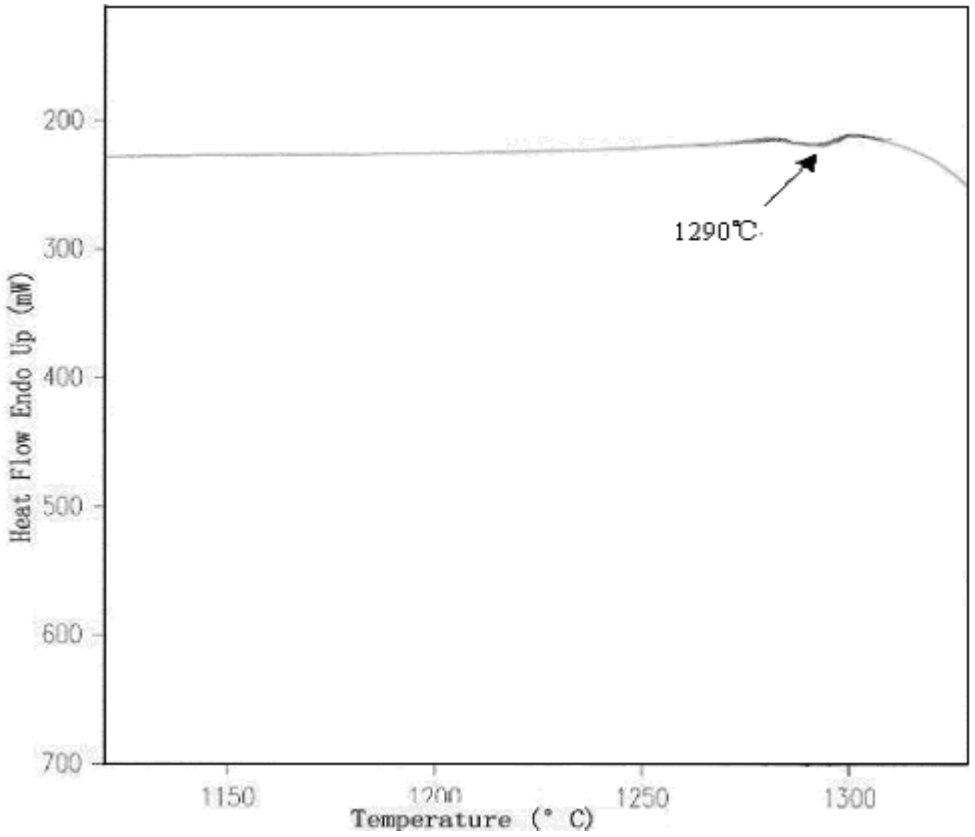

Figure 23 Differential-Thermal Analyses (DTA) of the Ti-45Al-7Nb-1.5B-0.4W alloy after HIPing and homogenization

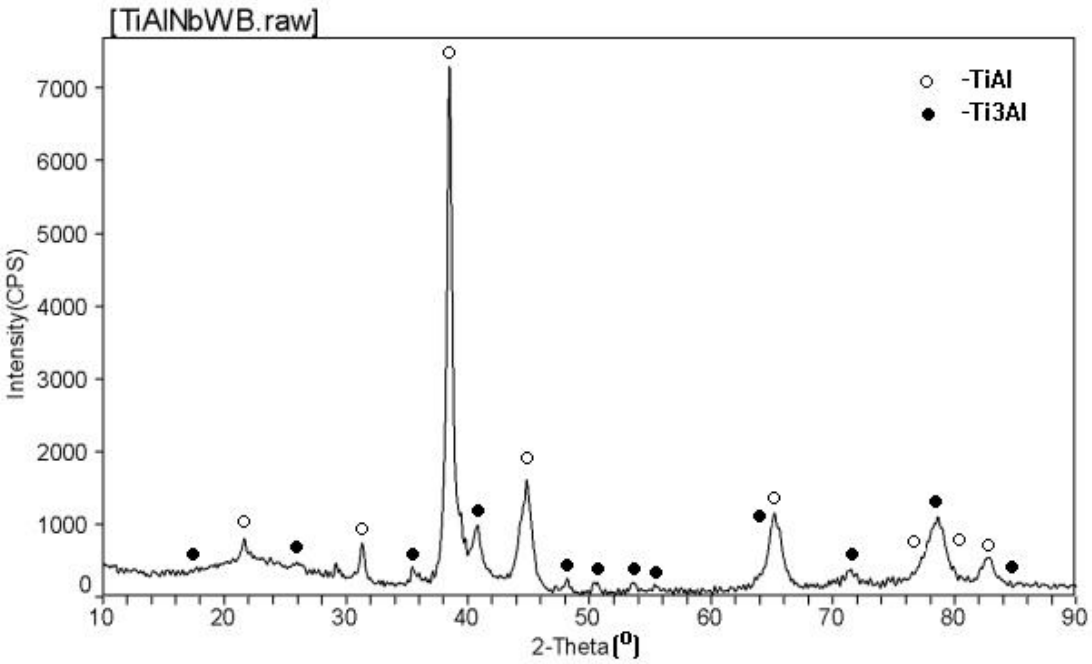

Figure 24 X-ray diffraction patterns of the Ti-45Al-7Nb-0.15B-0.7W alloy after HIPing and homogenization

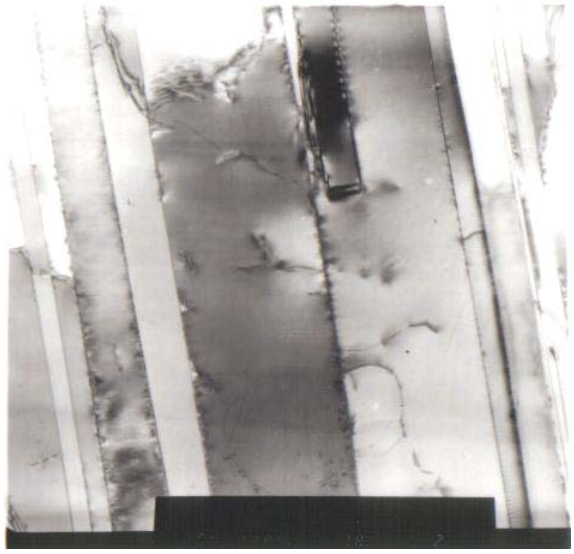

(a)

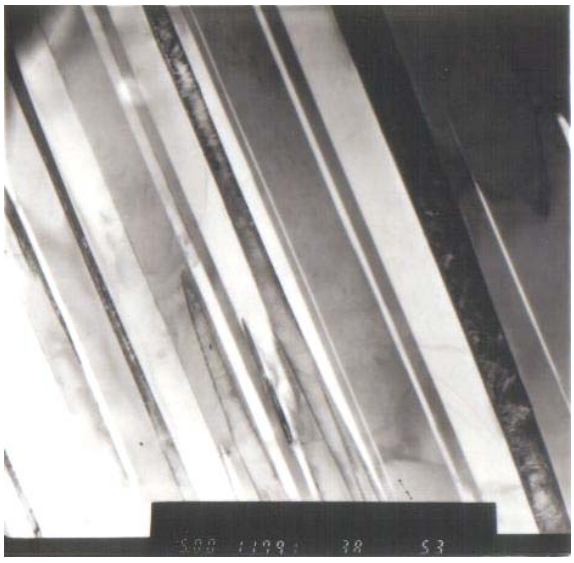

(b)

Figure 25 TEM analyses of the Ti-Al-Nb-W-B alloys after HIPing and homogenization, (a) Ti-45Al-7Nb-0.15B-0.2W, (b) Ti-45Al-7Nb-0.15B-0.4W, and (c) Ti-45Al-7Nb-0.15B-0.7W

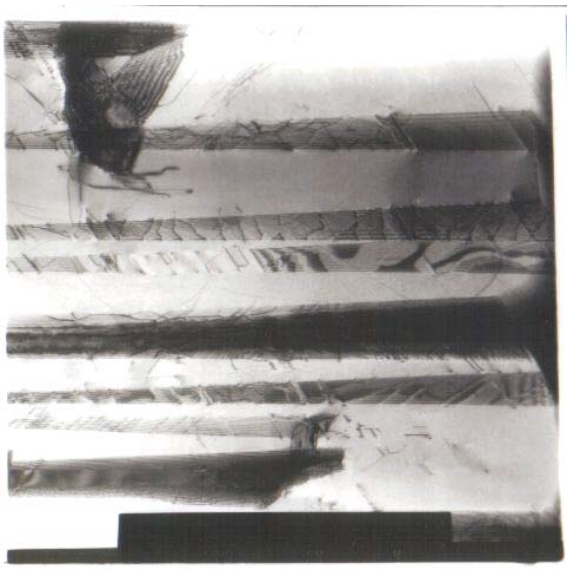

(c)

Figure 25 Continued

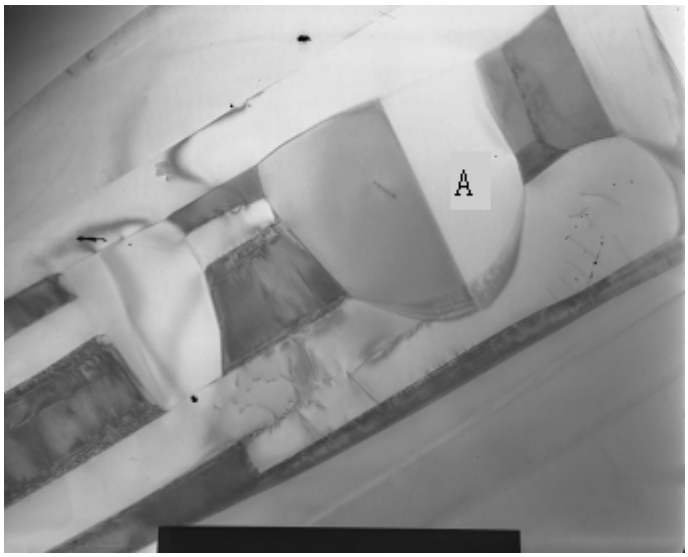

(a)

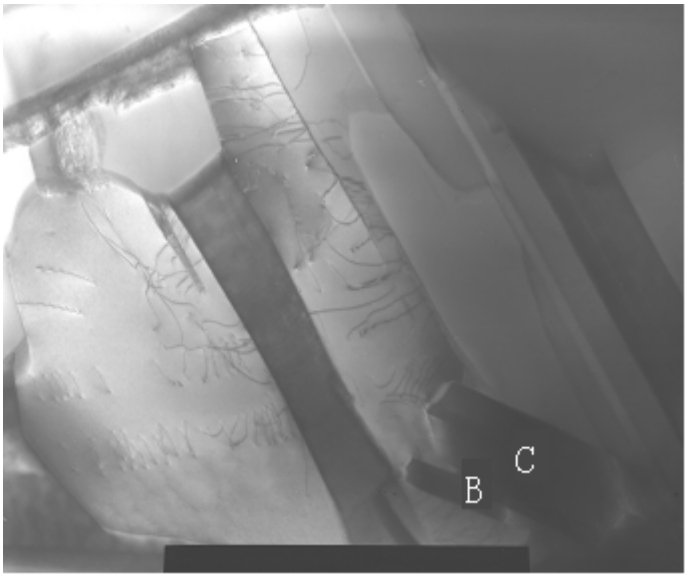

(b)

Figure 26 TEM analyses of the Ti-45Al-7Nb-0.15B-0.4W alloy after HIPing and homogenization, (a) γ-twin separated from the α_2/γ lamellae (shown in area A), (b) TiB_2 and γ-twin (shown in area B and area C)

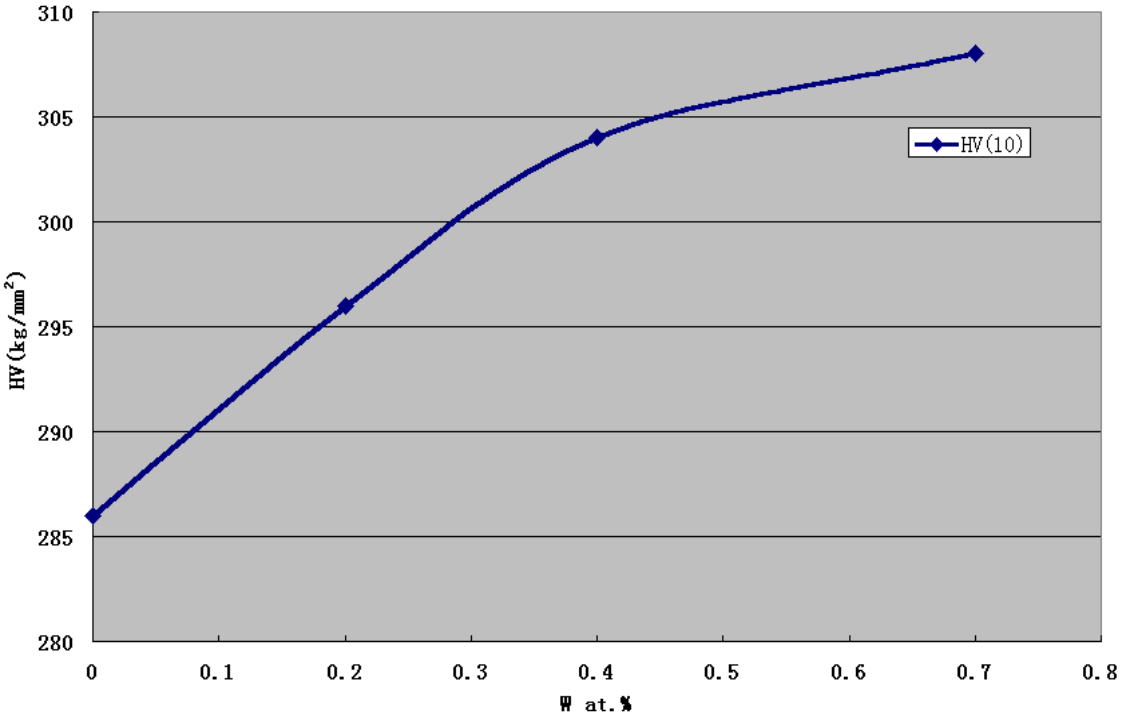

Figure 27 Effect of W content on the hardness of the Ti-Al-Nb-W-B alloys after heat treating at 1280^0C / 4 h

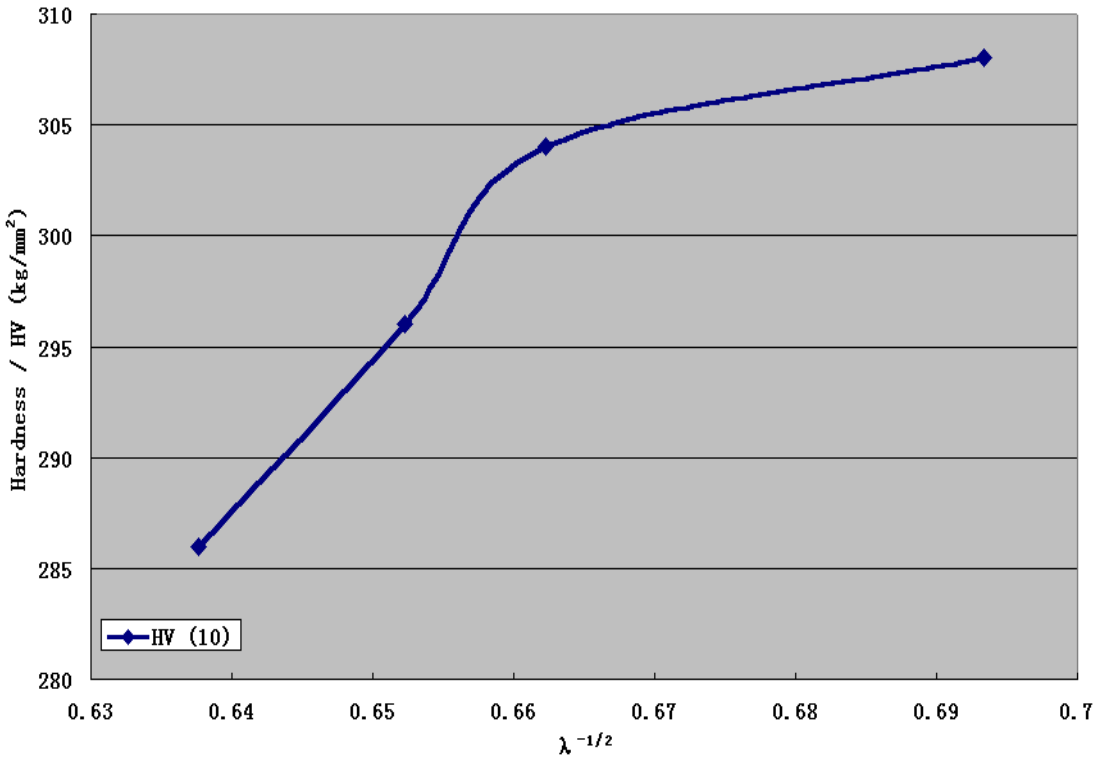

Figure 28 Effect of interlamellar spacing on the hardness of the Ti-Al-Nb-W-B alloys after heat treating at 1280^0C / 4 h

Vita

Lan Huang was born in Changsha, Hunan Province, People's Republic of China (PRC), on July 31, 1978. During September 1997 to June 2001, she pursued her undergraduate study at the *Hunan University*, and received her Bachelor degree majoring in Computer Science.

Lan came to the *University of Tennessee* in Knoxville and enrolled in the Master Program in Materials Science and Engineering Department in 2002. The Master degree will be received in August 2005.